

**BIOSENSING OF CARDIAC BIOMARKERS USING SINGLE POLYANINE  
NANOWIRES**

by

**Innam Lee**

B.S. in Petroleum and Resources Engineering, Seoul National University, 1998

M.S in Mechanical Design and Production Engineering, Seoul National University, 2002

M.S in Mechanical Engineering, Carnegie Mellon University, 2004

Submitted to the Graduate Faculty of  
Swanson School of Engineering in partial fulfillment  
of the requirements for the degree of  
Doctor of Philosophy

University of Pittsburgh

2012

UNIVERSITY OF PITTSBURGH  
SWANSON SCHOOL OF ENGINEERING

This dissertation was presented

by

Innam Lee

It was defended on

January 18, 2012

and approved by

William Stanchina, PhD, Professor, Department of Electrical and Computer Engineering

Hong Koo Kim, PhD, Professor, Department of Electrical and Computer Engineering

Kevin Chen, PhD, Associate Professor, Department of Electrical and Computer Engineering

Tracy Cui, PhD, Associate Professor, Department of Bioengineering

Dissertation Director: Minhee Yun, PhD, Associate Professor, Department of Electrical and

Computer Engineering

Copyright © by Innam Lee

2012

# **BIOSENSING OF CARDIAC BIOMARKERS USING SINGLE POLYANILINE NANOWIRES**

Innam Lee, PhD

University of Pittsburgh, 2012

In this thesis, we explore innovative methods of fabricating single polymer nanowires and applying the fabricated single polymer nanowires for biosensors. The fabrication of single polymer nanowire was carried out via electrochemical deposition growth method, which deposits ionized molecules in a pre-patterned nanochannel between two Au electrodes and forms a nanowire. For biosensing application, we employ polyaniline (PANI) in this research since it has advantages of biocompatibility, easy synthesis, and broad range of electrical conductivity. The single PANI nanowires-based biosensor show high sensitivity and good sensing reliability due to the high surface to volume ratio and single nanowires.

Using the fabricated single PANI nanowires, the biosensors were developed to detect cardiac biomarkers such as myoglobin (Myo), cardiac troponin I (cTnI), creatine kinase-MB (CK-MB), and B-type natriuretic peptide (BNP). The single PANI nanowires are functionalized by surface immobilization method that was developed in our laboratory using 1-ethyl-3-(3-dimethylaminopropyl) carbodiimide (EDC) and N-Hydroxysuccinimide (NHS) to attach monoclonal antibodies (mAbs) of biomarkers without pre-chemical or physical treatments. Lastly, microfluidic devices including channels and solution infusion/withdrawal system were integrated on the biosensor in order to develop an all-in-one biosensor. Our single PANI nanowire-based biosensor is unique in terms of the functionalization on specific area; the mAbs are immobilized on the only surface of PANI nanowires because PANI has superior

biocompatibility to mAbs unlike SiO<sub>2</sub> layer or Au electrodes. This advantage reduces functionalization steps comparing to inorganic nanowire biosensors and frees the interfered signals from non-nanowire areas. In addition, the microfluidic channel helps achieving stable electrical signals, high sensitivity, safe sample handling, and minimal damage of nanowire.

The integrated single PANI nanowire biosensors with microfluidic devices detect very low concentrations of Myo (100 pg/mL), cTnI (250 fg/mL), CK-MB (150 fg/mL), and BNP (50 fg/mL) with good specificity. The remarkable specificity value in cardiac biomarker sensing is over 10<sup>6</sup> fold, that the specificity value is defined as the ratio of [the highest concentration of non-specific protein showing ignorable or non-response signal] to [the lowest concentration of specific protein showing significant signal change], in the test of bovine serum albumin (BSA) or other cardiac markers. The single PANI nanowire biosensors have shown linear sensing profiles along different concentration from hundreds fg/mL to tens ng/mL depending on the mAbs of the specific biomarkers, and exhibit fast response in a few minutes satisfying reference values of Myo, cTnI, CK-MB, and BNP to diagnose heart failure and determine the patient's stage of disease.

## TABLE OF CONTENTS

<b>PREFACE.....</b>	<b>XV</b>
<b>1.0 INTRODUCTION .....</b>	<b>1</b>
<b>1.1 NANOMATERIALS .....</b>	<b>2</b>
<b>1.2 NANOWIRES AND CONDUCTING POLYMER .....</b>	<b>3</b>
<b>1.3 FABRICATIONS OF NANOWIRES .....</b>	<b>5</b>
<b>1.4 RESEARCH MOTIVATIONS AND GOALS .....</b>	<b>6</b>
<b>2.0 SINGLE POLYMER NANOWIRES .....</b>	<b>10</b>
<b>2.1 ELECTROCHEMICAL DEPOSITION GROWTH METHOD .....</b>	<b>11</b>
<b>2.1.1 Preparation of electrodes and nanochannels .....</b>	<b>11</b>
<b>2.1.2 Growth of the single polyaniline nanowires .....</b>	<b>13</b>
<b>2.2 RESULTS AND DISCUSSIONS.....</b>	<b>15</b>
<b>2.2.1 Physical properties of single polyaniline nanowires .....</b>	<b>15</b>
<b>2.2.2 Ring substitution and doping on polyaniline by acetone .....</b>	<b>20</b>
<b>2.2.3 Improvement of structure in polyaniline nanowires by the acetone wetting .....</b>	<b>21</b>
<b>2.3 SUMMARY .....</b>	<b>24</b>
<b>3.0 SINGLE MULTICOMPOSITE NANOWIRE .....</b>	<b>25</b>
<b>3.1 FABRICATION OF SINGLE MULTICOMPOSITE NANOWIRES .....</b>	<b>27</b>
<b>3.2 RESULTS AND DISCUSSIONS.....</b>	<b>30</b>
<b>3.2.1 Structure of single multicomposite nanowires .....</b>	<b>30</b>

3.2.2	Characterization of SMNW entrapped with ZnO NPs .....	32
3.2.3	Changes of electrical conductivity and elasticity .....	37
3.2.4	Enhancement of physical properties in single multicomposite nanowires	40
3.3	SUMMARY .....	42
4.0	PROOF OF CONCEPT FOR SINGLE POLYANILINE NANOWIRE BIOSENSOR DETECTING IMMUNOGLOBULIN-G.....	43
4.1	DEVELOPMENT OF SINGLE POLYANILINE NANOWIRE-BASED BIOSENSORS .....	45
4.1.1	Functionalization of single polyaniline nanowire .....	45
4.1.2	Preparation of microfluidic channel .....	47
4.1.3	Measurement of conductance change to sense target proteins.....	49
4.2	RESULTS AND DISCUSSIONS.....	52
4.2.1	Functionalization of polyaniline nanowires with IgG mAbs .....	53
4.2.2	Functionalization mechanism of polyaniline.....	58
4.2.3	Preliminary biosensing of Immunoglobulin G.....	61
4.3	SUMMARY .....	64
5.0	BIOSENSING OF CARDIAC BIOMARKERS.....	65
5.1	APPLICATIONS OF SINGLE POLYANILINE NANOWIRES .....	66
5.1.1	Detection of Myo, cTnI, CK-MB, and BNP .....	66
5.1.2	Single polyaniline nanowires FETs .....	66
5.2	RESULTS AND DISCUSSIONS.....	68
5.2.1	Biosensing performance to detect cardiac biomarkers .....	68
5.2.2	Effect of net surface charge in biosensing .....	79
5.2.3	Biosensing mechanism.....	82
5.2.4	FET behavior of single polyaniline nanowires.....	85
5.2.5	Analysis of nanowire biosensor sensitivity .....	91

<b>5.3</b>	<b>SUMMARY .....</b>	<b>95</b>
<b>6.0</b>	<b>CONCLUSION AND FUTURE WORKS .....</b>	<b>98</b>
	<b>APPENDIX A .....</b>	<b>102</b>
	<b>BIBLIOGRAPHY .....</b>	<b>107</b>

## LIST OF TABLES

Table 1. The calculated hole mobility and threshold voltage of single PANI nanowire FETs. Sample 1, 2, 3 and 4 is consistent with Figure 27 (a), (b), (c) and (d), respectively. ....	88
Table 2. Reference values and other research results of cardiac biomarkers .....	96

## LIST OF FIGURES

- Figure 1. Prepared electrodes on a 4" wafer and a nanochannel between two Au electrodes. (a) The 4" wafer includes 69 biosensor chips. In a single biosensor chip, four gate electrodes are located in the center. 16 pairs of electrodes surround the back gates as shown in an inset. (b) A nanochannel bridges the gap between two Au electrodes and guides the fabrication of single nanowire between each pair of electrodes. .... 12
- Figure 2. The steps of the electrochemical deposition growth method for the single nanowire fabrication. The PANI single nanowire is fabricated to deposit PANI electrochemically in the nanochannel by applied static current between two electrodes..... 14
- Figure 3. The current vs voltage measurements of the PANI nanowires at the pre- and post-acetone wetting processes. (a) The resistances before and after the acetone wetting are represented by dotted and solid lines and with symbols, respectively. (b) The percentage of resistance change is given according to the length of the PANI nanowires..... 16
- Figure 4. AFM image of a fabricated single PANI nanowire. (a) AFM stereoscopic image of a single nanowire after the acetone wetting. (b) The topology of the identical PANI nanowire shows the thickness of 131.32 nm and the width of 129 nm. Note that the bottom of the nanowire looks wider than the SEM image because of the drift of AFM tips. .... 18
- Figure 5. The multiple array of single PANI nanowires. (a) These nanowires show a dense structure and uniform dimension in the length of 3.3  $\mu\text{m}$  and the width of 130.89 nm. (b) The topology of the multiple PANI nanowires array by AFM shows very similar thickness of the fabricated nanowires. .... 19
- Figure 6. SEM images of single PANI nanowires. (a) The sparse structure of the PANI nanowire before the acetone wetting. (b) The denser structure of the PANI nanowire with the width of 139.6 nm after the acetone wetting. (c) The 5  $\mu\text{m}$  long and 160 nm wide PANI nanowire before the acetone wetting. (d) The identical PANI nanowire of (c) after the acetone wetting with the width of 141.1 nm and a resistance change of 37.15% with dendrite-free structure. (e) The 5  $\mu\text{m}$  long and 126.5 nm wide PANI

nanowire before the acetone wetting. (f) The identical nanowire of (e) with the width of 111.6 nm after the acetone wetting. .... 23

Figure 7. The fabrication and mechanical strength test of SMNW with ZnO NPs. (a) In the region of high voltage, the ionic aniline monomers and ZnO NPs deposit along the nanochannel. After growing, the SMNW bridges the gap between the two metal electrodes. The inset is the TEM image of SMNW. (b) The mechanical strength (elasticity) is measured on the nanowire by an AFM load test. In order to provide the space for deflection of the nanowire in the AFM load test, the SiO<sub>2</sub> layer under the nanowire was etched away by BOE. .... 28

Figure 8. Fabricated SMNWs with different ZnO NP concentrations. (a) Low resolution SEM image of 5 μm long SMNW, entrapped ZnO NPs with uniform dimension. (b) Highly magnified image of a 5 wt. % ZnO NP-entrapped PANI nanowire with height of 97 nm and width of 133 nm. Diameters of the observed particles are ranged from 33.90 to 35.39 nm. (c) 10 wt. % ZnO NP-entrapped PANI nanowire with the height of 108 nm and width of 110 nm. Diameters of the observed particles are 54.87 and 59.42 nm. (d) 20 wt. % ZnO NP-entrapped PANI nanowire with the height of 98 nm and the width of 80 to 110 nm. The agglomerated particles greatly changes surface morphology of the SMNW with taped shape. .... 31

Figure 9. EDS data and Raman spectrum for single PANI nanowires and single ZnO NP-entrapped PANI nanowires. (a) The SMNWs with ZnO NPs show clear peaks at Zn and a higher peak at O, which is resulted from the entrapment of ZnO NPs. The two different ZnO concentrations (black dashed line: 20 wt. %, red solid line: 5 wt. %) display different intensities of Zn. (b) The Raman spectrum identifies the materialization of doped PANI in a fabricated single nanowire. .... 33

Figure 10. HRTEM images of single PANI nanowire and SMNWs with different ZnO NP concentrations. (a) A single 10 wt. % ZnO NP-entrapped nanowire is extracted from the electrode and transferred to the TEM sample grid by a nanomanipulator. The SMNW was scratched laterally at the end of nanowire and detached. (b) A HRTEM image of single PANI nanowire: 0 wt. % ZnO NP concentration. ZnO NPs are absent in this single nanowire. Note the uniform width of 137.5 nm. (c) A HRTEM image of 5 wt. % ZnO NPs (width of 154 nm) and (d) A 10 wt. % ZnO NP-entrapped PANI nanowires (width of 113 nm). The diffraction pattern for each SMNW is shown in the corresponding inset. Note the ring patterns (PANI) and dots indicating randomly oriented crystalline structure (ZnO). (e) An 1 wt. % ZnO NP-entrapped PANI nanowire from applying a current of 900 nA in the growing condition. (f) A 2.5 wt. % ZnO NP-entrapped PANI nanowire from applying a current of 900 nA in the growing condition. The SMNWs of (e) and (f) show tightly agglomerated ZnO NPs inside the nanowire similar to the nanowire of (d). .... 36

Figure 11. Enhancement in physical properties of the SMNWs. Electrical conductivity (black solid line at 300 K) and elasticity (blue dash and double dot line) are measured for 0, 1, 2.5, 5, 10, and 20 wt. % ZnO NP. Note the dramatic increase in each from 2.5 to 10

wt. % ZnO NP concentration. The slopes of physical properties decrease after 10 wt. % ZnO NP, resulting from the saturation of ZnO NP entrapment.....	38
Figure 12. Development of the single PANI nanowire-based biosensors. (a) Preparation of a nanochannel using e-beam lithography between Au electrodes on Si/SiO <sub>2</sub> substrate. (b) Fabrication of a single PANI nanowire along the nanochannel from an ionized aniline solution. (c) The fabricated single PANI nanowire after removal of PMMA layer. (d) The functionalized single PANI nanowire with the mAbs via the surface immobilization process. ....	46
Figure 13. A single PANI nanowire-based biosensor integrated with a microfluidic channel. The functionalized nanowire with antibodies shows the change of conductance upon binding target proteins. Integration of a microfluidic channel regulates introduction of protein solution onto the nanowire active area only with the control of laminar flow. The microfluidic channel and flow injection prevent nanowire from breakage during biosensing and reduce non-specific binding on electrodes.....	48
Figure 14. Experimental set-ups and illustration of single PANI nanowire biosensor to detect cardiac biomarkers. (a) The experimental setup; the microfluidic channel is adhered on the nanowire biosensor and the nanowire biosensor chip is mounted on a probe station connecting to semiconductor analyzer and syringe pump with inlet and outlet. (b) The integrated biosensor system includes a printed circuit board, a chip carrier, and wire-bonded PANI nanowires-based biosensor with microfluidic device in an aluminum shield box. This system is connected to the semiconductor analyzer. (c) The conductance change in the single PANI nanowires-based biosensors is monitored. The injection of PBS (mark a), BSA (mark b), and cardiac biomarker (mark c) shows the different change of conductance.....	51
Figure 15. Surface immobilization with EDC/NHS and IgG mAbs on the PANI thin film. (a) The functionalized PANI thin film with IgG mAbs labeled by Texas Red fluorescent dyes. (b) The Comparison of the Raman spectra before functionalization and after functionalization of PANI thin film with IgG mAbs.....	54
Figure 16. Verification for surface immobilization of IgG mAbs on the single PANI nanowires. (a) The SEM image of the non-functionalized single PANI nanowire. (b) The SEM image of the functionalized single PANI nanowire with IgG mAbs. (c) The functionalized single PANI nanowire with IgG mAbs labeled by Texas Red fluorescent materials (in a circle). (d) The comparison of Raman spectra before and after functionalization of the single PANI nanowire with IgG mAbs. ....	56
Figure 17. Functionalization mechanisms of EDC/NHS and GA. (a) EDC/NHS with mAbs modifies –COOH at the end of mAbs and couples to –NH of PANI. (b) The symmetric structure of GA links –NH of PANI to –NH of aptamer. ....	60
Figure 18. IgG sensing on single PANI nanowire biosensors. (a) The measurement of conductance changes on a single non-functionalized PANI nanowire (a: PBS, b: BSA of 10 µg/mL, and c: IgG of 3.3 µg/mL). (b) The specificity tests of a functionalized	

single PANI nanowire with IgG mAbs (a: PBS, b: BSA of 50 ng/mL, and c: IgG of 33 ng/mL). (c) The detection of IgG on a single PANI nanowire biosensor (a: IgG of 5 ng/mL, b: IgG of 37 ng/mL, c: IgG of 54 ng/mL, d: IgG of 242 ng/mL, e: IgG of 368 ng/mL, f: IgG of 1.74  $\mu$ g/mL, g: IgG of 2.78  $\mu$ g/mL, and h: BSA of 5  $\mu$ g/mL). (d) The sensitivity of the single PANI nanowire biosensors with various concentrations of IgG mAbs (50, 100, and 200  $\mu$ g/mL)..... 63

Figure 19. Biosensing of cardiac biomarkers on the single PANI nanowires-based biosensors by measuring conductance change under the direct droplet measurement. (a) Detection of Myo (a: PBS, b: BSA of 500 ng/mL, and c: Myo of 1.4 ng/mL). (b) Detection of cTnI (a: PBS, b: Myo of 5 ng/mL, and c: cTn-I of 300 fg/mL) (c) Detection of CK-MB (a: PBS, b: BSA of 100 ng/mL, c: CK-MB of 300 pg/mL, and d: CK-MB of 2.5 pg/mL) (d) Detection of BNP (a: PBS, b: BSA of 100 ng/mL, c: BNP of 1 ng/mL, d: BNP of 10 ng/mL, and d: BNP of 100 ng/mL)..... 69

Figure 20. Biosensing for Myo and cTnI in the wide sensing ranges. (a) Detection of Myo on a single PANI nanowire biosensor (a: PBS, b: 5 ng/mL, c: 30 ng/mL, d: 50 ng/mL, e: 200 ng/mL, f: 350 ng/mL, and g: 2.5  $\mu$ g/mL). (b) Stepwise change of conductance to different concentration of cTnI (a: PBS, b: 5 pg/mL, c: 40 pg/mL, d: 300 pg/mL, e: 2 ng/mL)..... 70

Figure 21. Demonstration of ultra-high sensitivity and specificity of the single PANI nanowires-based biosensors integrated with microfluidic devices. (a) The detection of Myo using microfluidic channel shows good specificity to BSA and clear response to the low concentration of Myo. (a: PBS, b: BSA of 100 ng/mL, and c: Myo of 100 pg/mL) (b) Biosensing with microfluidic channel for detection of cTnI (a: PBS, b: BSA of 10 ng/mL, c: cTnI of 5 fg/mL, d: cTnI of 250 fg/mL, and e: cTnI of 20 pg/mL). (c) Biosensing with microfluidic channel for detection of CK-MB (a: PBS, b: BSA of 10 ng/mL, and c: CK-MB of 150 fg/mL). (d) Biosensing with microfluidic channel for detection of BNP (a: PBS, b: BSA of 100 ng/mL, c: BNP of 50 fg/mL, and d: BNP of 1 pg/mL)..... 72

Figure 22. Specificity test of nanowire biosensor in the presence of non-target proteins. (a) For the specificity test of nanowire biosensor for Myo. (a: PBS, b: cTnI of 1 ng/mL, c: Myo of 1 ng/mL, d: BNP of 1 ng/mL, e: Myo of 10 ng/mL, and f: CK-MB of 1 ng/mL). (b) For detection of cTnI (a: PBS, b: BSA of 1 ng/mL, c: cTnI of 500 fg/mL, d: PBS, e: Myo of 1 ng/mL, f: CK-MB of 1 ng/mL, g: BNP of 1 ng/mL, and h: cTnI of 1 ng/mL), the nanowire biosensor responds to only cTnI. (c) For detection of CK-MB (a: PBS, b: BSA of 1 ng/mL, c: BSA of 100 ng/mL, d: CK-MB of 25 pg/mL, e: PBS, f: Myo of 1 ng/mL, g: cTnI of 1 ng/mL, h: BNP of 1 ng/mL, and i: CK-MB of 1 ng/mL), the nanowire biosensor responds to only CK-MB. (d) For detection of BNP (a: PBS, b: BSA of 100 ng/mL, c: BNP of 1 ng/mL, d: BNP of 10 ng/mL, e: PBS, f: Myo of 1 ng/mL, g: cTnI of 1 ng/mL, h: CK-MB of 1 ng/mL, and i: BNP of 1 ng/mL), the nanowire biosensor responds to only BNP. .... 75

Figure 23. Optimization of sensing performance with various concentrations of Myo, cTnI, CK-MB, and BNP mAbs. (a) In order to optimize the condition of functionalization, the

sensitivities of the nanowire biosensors are compared in different mAbs. Myo mAbs of 100  $\mu\text{g/mL}$  showed better sensing performance than the mAbs of 200  $\mu\text{g/mL}$ . (b) cTnI mAbs of 200  $\mu\text{g/mL}$  presented the best linear sensing profile and highest sensitivity of the three different conditions of cTnI mAbs. (c) For CK-MB, CK-MB mAbs of 200  $\mu\text{g/mL}$  showed the best sensing profile without fluctuation in sensitivity. (d) For BNP, BNP mAbs of 100  $\mu\text{g/mL}$  provided higher sensitivity in a broader sensing range than the other conditions. .... 77

Figure 24. Tests of net surface charge effect on the functionalized PANI nanowires. (a) Decreased conductance on the nanowire biosensor during a sensing test with positively charged cTnI protein solutions (a: PBS of pH 5, b: 1 ng/mL, and c: 10 ng/mL). cTnI protein solutions were prepared with PBS of pH 5. (b) Comparison of sensitivity with different concentrations of cTnI detection. The nanowire biosensor shows significantly higher sensitivity according to higher concentration. The mark “a” on black solid line presents the injection of BSA (100 ng/mL). After the injection of BSA, cTnI of 300 fg/mL was injected to the biosensor. .... 80

Figure 25. An illustration of charge neutralization and re-distribution. The complex of charged proteins and mAbs induce the charge neutralization at the interface, and then charge re-distribution in the mAbs. Those re-distributed charge result in the net surface charge change on the nanowire. .... 84

Figure 26. A single PANI nanowire FET. The fabricated single PANI nanowire between two Au electrodes works as a channel of FET with a back gate. .... 85

Figure 27. The measured  $I_{SD} - V_{SD}$  from PANI nanowire FET. (a) The various  $V_G$  from -16 to 16 V shows slight change of  $I_{SD}$ . (b) The PANI nanowire FET is turned off at  $V_G$  of 0 V. (c) Changing  $V_G$  from -20 to 16 V, the PANI nanowire FET shows clear change of  $I_{SD}$ . (d) The data of PANI nanowire FET scanned by  $V_G$  from -20 to 20 V. This nanowire FET shows very high  $I_{SD}$  and significant change in scanned range of  $V_{SD}$ . 86

Figure 28. The schematic of an effective conductance area in a nanowire. The black solid line is the edge of nanowire. The green dotted line is the edge of the depleted area resulting from surface charge neutrality. The thick blue dotted line is the edge of the effective cross section area after applying  $V_G$ . + and - refer to the surface charge from molecules and immobile charges, respectively. .... 92

Figure 29. The general schemes of polyaniline, Leucoemeraldine and pernigraniline are fully reduced and oxidized forms, respectively. Emeraldine is consisted with reduced and oxidized forms. .... 103

Figure 30. The process of polymerization. Aniline monomer transfers into two different kinds of ionized aniline monomer. Ionized aniline monomers combine each other and form dimeric species. Then, polyaniline is synthesized. .... 104

Figure 31. Mechanism of oxidative electropolymerization of aniline. .... 106

## PREFACE

All of my researches including this thesis has been purposed to develop a single PANI nanowire-based biosensors to detect cardiac biomarkers. The single PANI nanowire biosensor was constructed via the nanowire fabrication, the functionalization of fabricated nanowire, and the conductance measurement of the nanowire using microfluidic device. In addition, the characterization of the nanowires and discussion of nanowire biosensing were carried out elaborately. However, those experiments, analysis, and discussions in my PhD thesis have received a lot of help from my advisor and colleagues. Especially, I express my eternal appreciation to my adviser, Dr. Minhee Yun. It was my privilege to do doctoral program under his guidance and support in cutting edge technology area Also, I thanks deeply to my dissertation committee, Dr. William Stanchina, Dr. Hong Koo Kim, Dr. Kevin Chen, and Dr. Tracy Cui for their taking time to serve on my committee and giving me invaluable comments and suggestions on this dissertation. I would like to thank my colleagues, Dr. Xiliang Luo, Dr. Yushi Hu, Dave Perello, Jiyong Huang, Dave Sanchez, and Yiwen Xu for their helps in my experiments and discussions. And, I would like to say thanks to all of my friends in Benedum Hall and Pittsbrugh. Finally, I appreciate to my parents and my younger sister in Korea. They have been patient and supporting me in my long journey of doctoral years with encouragements and love. They have raised me up with boundless support whenever I was in difficulty.

## 1.0 INTRODUCTION

The interests in health care system drive the development of various point-of-care systems to diagnose diseases such as diabetes, cancers, and cardiac diseases. The detection of glucose for diabetes is a representative commercialized point-of-care system, which is very useful to determine blood-sugar level at home. However, the diagnoses of other important diseases such as cancer or cardiac disease have not realized in home care systems, because they require the complicated processes to detect biomarkers. Therefore, many researchers have studied actively to develop biosensing system, which could be applied for cancer or cardiac disease, using various materials such as nanomaterials.

The development of nanomaterials over the last few decades has resulted in many applications such as the mechanical, electrical and biomedical engineering with nanowire, nanoparticle (NP), and carbon nanotube (CNT). The nanowire in particular has been improved dramatically due to large surface to volume ratio, low power consumption, and miniaturization of device. Therefore, the nanowire has been employed in the point-of-care system with the advantages of fast response, cost efficiency and mass-producibility using the semiconductor process. However, some limits remain with respect to the uniformity of production, biocompatibility of inorganic nanomaterials, and reliability of performance. In this research, the single polymer nanowires are presented to overcome those disadvantages and applied for the diagnosis of cardiac disease, which is one of the highest death causes in US and Europe.

## 1.1 NANOMATERIALS

The nanomaterials such as nanowire, NP, and CNT are attractive for various applications such as electrical device or biosensor due to their various physical properties of electrical conductivity, mechanical strength, light absorption, and biocompatibility. The nanowires of inorganic or organic materials have been studied in the diameter from a few tens to hundreds nanometer and the length of micrometer [1]. The fabricated nanowires have been applied for the diverse areas of display devices, mechanical parts, or medical diagnostic systems with the advantages of miniaturization, low power consumption, improved mechanical strength, and controllable electrical conductivity. The NPs, which is 0-dimensional structure of sphere in nanoscale, have been researches in optical and biological applications with the superiority of scattering and absorbing light. Using these properties, we could detect cancer cell with binding to healthy cells and cancerous cells [2, 3]. The CNT, which has two categories of single-walled CNT and multi-walled CNT, is determined in metallic or semiconducting by the direction of wrapping a one-atom-thick layer of graphite, called Graphene, into a seamless cylinder [4].

In the area of medical devices, nanowire, NP, CNT are competing to satisfy the requirement of label-free-detection, miniaturization, cost efficiency in mass production and easy development process. However, the low biocompatibility of CNT to biomolecules requires many steps of development process in a biosensor [5]. In addition, the inorganic NPs are limited to be constructed as a single electric device due to their 0-dimensional structure. Therefore, we consider the nanowire for a candidate of biosensing device, because the nanowire can be easily synthesized in uniform dimension and mass production. In addition, the organic nanowire has superior biocompatibility to realize cost efficiency in development process.

## 1.2 NANOWIRES AND CONDUCTING POLYMER

In the area of nanowire device applications, inorganic and organic nanowires have been developed with the functionalization of nanowires for advanced electrical devices such as gas or bio/chemical sensors [6]. For the high sensitive sensors, a hydrophilic conducting polymer is very attractive due to the good compatibility to biomolecules, the semiconducting electrical properties, and the outstanding design flexibility [7, 8]. Conducting polymers such as polyaniline (PANI) and polypyrrole (PPy) have been spotlighted as alternative materials for nanowire sensor applications due to their easily controllable synthesis and electrical properties similar to inorganic semiconductor devices [9]. Moreover, conducting polymers can be easily modified through reaction with some organic molecules for the expected designs in biosensing application [10-13]. The amine group on backbone in PANI enables to transfer various structure and link with other chemicals.

In the characteristics of PANI, amine group or hydrogen bonding in PANI provides improved physical properties through transferring to PANI derivatives by reacting with protonic or organic acids [14-16]. It is well known that protonic or organic acids create various PANI derivatives by the reaction on the benzene ring or on the nitrogen of its chain in macro or micro structure [14, 16]. In addition, a substitution in PANI using an acetone wetting results in a change of electrical and mechanical characteristics [12]. The behavior of the acetone wetting effects on the properties of PANI basically focused on polymer thin films or microfibers [15, 16]. Therefore, those diverse properties of PANI have driven various applications in different electrical device structures such as a field effect transistor (FET) and a diode.

In PANI FET sensors, PANI thin film FETs have been developed prolifically [17]. A PANI thin film is spread on two metal electrodes, which are a few microns distance from each

other on an insulating substrate. The electrode metals such as Au or Pt were employed according to the different work functions between the metal and PANI thin [18]. In PANI thin film FET testing, an applied gate voltage provides a change of drain current in the linear and saturation regions. The PANI thin film FET is normally on, i.e. threshold voltage is positive, generally observed to be around 5 V. Based on developments in polymer FET, the functionalized PANI thin film FET sensors show a change of electrical signal when exposed to gases, chemicals or biomolecules – indicating detection of targets such as gases, chemicals and biomolecules. In these days, the PANI nanowire or PANI multicomposite with NPs or CNTs have also been researched for highly advanced applications in electrical or biomedical devices [19-24]. In order to realize those researches, the conducting nanomaterials such as nanowire or nanoparticle were fabricated chemically or electrochemically using anodic aluminum oxide (AAO) template, nanoimprint lithography or chemical vapor deposition [25-27]. However, those fabrication methods require post-process to select a nanowire from a bundle of fabricated nanowires and build electrical device on the selected nanowire. In addition, many conducting polymer nanomaterials were researched with composites of CNT or inorganic nanowires [28, 29]. Those researches synthesized CNT or inorganic nanowires first, and then conducting polymers were coated electrochemically on the surface of fabricated CNT or nanowire. Those multicomposite conducting polymer nanowires have shown synergistic physical properties in electrical conductivity or mechanical strength. However, the yield ratio of conducting polymer nanowire application may be very low due to the intricate fabrication processes, the brittleness and relatively low melting temperature of conducting polymer. Therefore, it is motivated to fabricate single conducting polymer nanowire with high yield ratio and cost-effective process in my research.

### 1.3 FABRICATIONS OF NANOWIRES

The nanowires of semiconductors, metals, or conducting polymers have been developed in the various fabrication methods and post-processes in regards to their applications in biosensors, optoelectronic devices, and electrical devices for high density circuits [1, 30]. Those various nanowires have been fabricated using an anodic aluminum oxide template, chemical vapor deposition, and laser ablation [31-33]. However, current fabrication methods have drawbacks, including low throughput, limited addressability, and low controllability in large-scale integrated systems, because they are often synthesized in bundled nanowires. In order to remedy these defects, the nanowire fabrication method to grow a single nanowire between pre-patterned electrodes has been studied [33]. Addressable single nanowires composed of various metals or conducting polymers have been grown at micron or sub-micron width and several micrometer length in nanochannels between pre-deposited gold electrodes [34]. This fabrication method, called the electrochemical deposition growth method, is highly controllable, addressable, efficient, and attractive for large-scale integrated systems with various materials that can be electrochemically deposited. In addition, the electrochemical deposition growth method provides the uniformly sized nanowires by the designed nanochannels and pre-deposited electrodes. Therefore, the high yield ratio was realized in the fabrications of palladium (Pd), PANI, and PPy nanowires in our researches [33, 35].

## 1.4 RESEARCH MOTIVATIONS AND GOALS

The incidence of myocardial infarction, which is one of the highest mortality in US or Europe, increases in the elderly [36, 37]. Therefore, the diagnosis of cardiac disorder is very important, as well as its prevention. In myocardial infarction, myoglobin (Myo), cardiac troponin I (cTnI), creatine kinase MB (CK-MB), and b-type natriuretic peptide (BNP) have been demonstrated to be useful biomarkers in the diagnosis of myocardial infarction [36, 38, 39]. Among those cardiac markers, Myo is a basic protein to check at the onset of infarction [36, 40]. However, because it has cross-activity with the skeletal muscle pain, it is necessary to monitor the level of other proteins such as cTnI, CK-MB, and BNP in patients' serum for accurate, prompt and continuous diagnosis of myocardial infarction [37-39]. In the relationship of cardiac biomarkers to the muscle pain, cTnI is only related to the cardiac muscle pain [41]. CK-MB and BNP are useful to diagnose the heart failure in the case of reoccurrence and cardiac vascular disease, respectively [36, 39, 42]. For detecting clinically those cardiac biomarkers, the commercial assays for biomarkers have been developed using the type of immunoassay such as enzyme-linked immunosorbent assay (ELISA) [36]. The immunoassay method has presented good biosensing performance although requiring many process steps and time consuming for reaction between antibodies and enzymes [43]. The immunoassay method requires also several different primary and secondary antibodies to detect target proteins. For biosensing, those antibodies and target proteins bind together tightly and react to fluorescent measurement. In those processes, there may be non-specific physical adsorption on the surface of biosensor chip or to the antibodies due to the long process time such as a couple of ten minutes to hours. Although this immunoassay method is well established as a clinical biosensor to test human serum, it is limited to apply to home health care system due to different sensitivity depending on sample condition and special

detection system with the time consuming processing. Therefore, the new development of biosensor has been highly demanded satisfying the reliable biosensing performance and the portable size of biosensing device. Many research groups have studied various types of biosensor with micro- or nanomaterials.

The detection of these biomarkers has been researched using several methods. For examples, biosensing based on fluorescence has been applied for the detection of Myo, which was carried out to measure the fluorescent intensity from a sandwich immunoassay labeled with fluorescent dyes [42, 44, 45]. In addition, a surface plasmon resonance (SPR) biosensor, which measures SPR angle shift once target proteins are bound on specifically functionalized substrates, is one of the most popular biosensing methods to be employed for the various cardiac markers such as Myo, cTnI, and BNP [40, 46-48]. However, although the biosensors developed by the fluorescence or the SPR have shown improved performance in sensitivity and specificity, they are limited in terms of miniaturization and cost efficiency. They have the relatively lower sensitivity and specificity than nanomaterials (nanowire, NP, and CNT) based biosensors due to the high surface to volume ratio of nanomaterials [19, 21, 49].

Those nanomaterials provide outstanding physical properties such as various conductivity from semiconducting to metallic regions, which can be tuned by doping or synthesis methods, and fast carrier mobility to realize real-time sensing with a 0- or 1-dimensional structure [24, 50]. To date, these advantages of nanomaterials have been actively employed to develop biosensors using inorganic or organic materials [22, 51, 52]. In nanowire biosensing, Si nanowire sensor arrays have been shown to detect very low concentrations of cTnI measuring the conductance change of the nanowire biosensor [53]. However, the biosensing applications of inorganic nanomaterials require additional processes to improve bioaffinity to antibodies, which play a

major role in detecting target proteins. In contrast, organic nanomaterials such as PANI and PPy include the amine functional group to provide sites to link with antibodies [54-56]. The covalent bonds between PANI and antibodies enable direct measurement of physical changes in conductance, capacitance, or impedance on PANI when antibodies bind to target proteins [57, 58]. In addition, conducting polymers of PANI or PPy are appealing for electrical, mechanical, or biomedical applications due to their advantages in terms of tunable conductivity, mechanical flexibility, and exceptional bioaffinity [59]. All of these advantages of conducting polymers are driving the interest in conducting polymer nanowire for use in biosensing applications. PANI and PPy nanowires have been also used in organic nanowire FETs, light emission diodes, and biosensors [60-63]. These applications were established on a single nanowire selected from among bundled nanowires; however, the processes required to develop these applications consume much efforts and offer the lower production yield.

In order to overcome those limitations and to realize the diagnosis of heart failure using nanoscale biosensors, the single PANI nanowires-based biosensors by electrochemical deposition growth method were functionalized to detect Myo, cTnI, CK-MB, or BNP using surface immobilization of monoclonal antibodies (mAbs) and integrated with microfluidic devices in this research. The electrochemical deposition growth method for the fabrication of single nanowires makes it possible to skip the selection and the alignment of a nanowire, which are necessary in typical nanowire fabrication methods [35, 64]. In biosensing, the single PANI nanowire-based biosensor shows either an increase or decrease in conductance depending on the charge of the target proteins, when the target proteins are detected [65]. The conductance measurement in single PANI nanowire can show the different level of conductance change depending on the charge of detected target biomarker and facilitate the label-free-detection due

to the fast response in a few minutes with good specificity to respond to only target proteins, while conventional method like an immunoassay requires at least a few hours to incubate the complex of mAbs and targets [66]. In addition, the integration of microfluidic devices on the nanowire biosensors enables the accurate biosensing and the injection of biomarkers onto only the active area of PANI nanowire [67]. Therefore, the integrated single PANI nanowire-based biosensors have shown good sensitivity, specificity, and reliability in the detection of cardiac biomarkers in this research, and they show promise in the diagnosis of other diseases as well.

## 2.0 SINGLE POLYMER NANOWIRES

The electrochemical deposition growth method is a unique method to fabricate a site-specific single nanowire. This method employs the electrochemical deposition of ionized materials in a nanochannel between two Au electrodes, which are pre-patterned lithographically on a substrate. Therefore, the array of nanowires on designed locations and mass production of nanowires are possible with a high density chip for biosensing-, chemical-, or electrical-applications. In addition, this electrochemical deposition growth method economizes on the development processes of nanowire applications via the free-selection and alignment of nanowire. In our researches, the PANI, PANI multicomposite with ZnO NPs, PPy, and Pd were employed for single nanowire fabrication [35, 68].

The fabricated single nanowires were developed for gas sensors or biosensors depending on the characteristics of nanowire materials. Pd nanowires were developed for the hydrogen gas sensor and PANI or PPy nanowires have been investigated for the biosensor. A single multicomposite nanowire (SMNW) with entrapment of ZnO NPs into PANI was studied regarding materialization, electrical conductivity, and mechanical strength along the various concentrations of ZnO NPs. The development of the electrochemical deposition growth method has provided the cost effective nanowire chip, which act as the base for biosensors in this research.

## 2.1 ELECTROCHEMICAL DEPOSITION GROWTH METHOD

### 2.1.1 Preparation of electrodes and nanochannels

The pre-process of electrodes and nanochannels on a 4" wafer enables the mass production of single nanowires and the efficient development of nanowire applications unlike conventional nanowire fabrication methods such as vapor-phase synthesis or template-assisted growth. Those conventional methods synthesize bundled nanowires in a time and build up the application architecture on a selected nanowire from the bundled nanowires. In design of biosensor chips on a 4" wafer, 69 biosensor chips are arrayed and each chip can include maximum 16 nanowires in  $1 \times 1 \text{ cm}^2$  area as shown in Figure 1 (a). In a single chip, back gate electrodes were located on the center surrounded with 16 pairs of electrodes as shown in the inset of Figure 1 (a). A pair of electrodes works as electrodes to provide a static current in the fabrication of the single nanowire. In addition, those electrodes play the role of a source and drain with the pre-patterned back gate in a nanowire FET after the single nanowire is grown between the two electrodes. All of electrodes in a single chip are extended to pads for wire-bonding in a chip carrier.

The fabrication of single PANI nanowire started by preparing electrodes and nanochannels on a substrate of Si/SiO<sub>2</sub>, which SiO<sub>2</sub> is thermally grown on a p-type Si wafer of 1000 Å or 1500 Å. A positive photoresist (Shipley s1805) was spun on the substrate at 4000 rpm for 45 seconds by the thickness of 500 nm. The wafer with the photoresist was heated on a hot plate at 110 °C for 2 minutes for a soft bake. The substrate was then lithographically patterned through exposure to UV light for 13 seconds using a mask aligner (Q-4000-4, Neutronix/Quintel). The UV-exposed wafer was developed in an MF-351 developer diluted in a 4:1 mixture ratio with de-ionized water (18.2 MΩ) for 60 seconds. Then Ti/Au was deposited at

the thickness of 30/970 Å using an electron beam evaporation (VE-180, Thermionics). The metal deposition was lifted off using acetone in 45 °C for 20 minutes. Post lift-off process, nanochannels were patterned with the width of 100 nm and the length of 15 μm on the polymethyl methacrylate (PMMA, 950 K A4) bridging the gap between each pair of electrodes by an electron beam lithography (e-Line, Raith), as shown in Figure 1 (b). The 100 nm thick PMMA layer was coated at 5000 rpm for 50 seconds. In order to optimize the growing condition, the various PMMA thicknesses of 100 nm, 150 nm, and 200 nm were spin-coated by changing the spin-coating speed. Therefore, we could fabricate single PANI nanowires with different thicknesses.

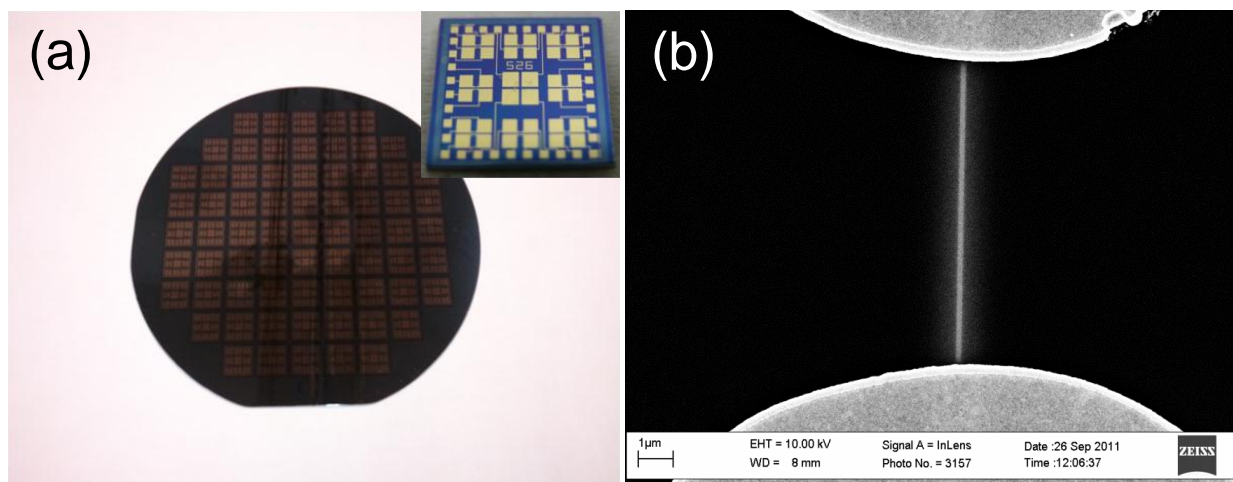


**Figure 1.** Prepared electrodes on a 4" wafer and a nanochannel between two Au electrodes. (a) The 4" wafer includes 69 biosensor chips. In a single biosensor chip, four gate electrodes are located in the center. 16 pairs of electrodes surround the back gates as shown in an inset. (b) A nanochannel bridges the gap between two Au electrodes and guides the fabrication of single nanowire between each pair of electrodes.

### 2.1.2 Growth of the single polyaniline nanowires

After preparation of the nanochannel and electrodes on the substrate, single inorganic or organic nanowires were grown along the patterned nanochannel by the electrochemical deposition growth method using ionic solutions. The electrodes provide electrons to deposit ions of solution from the cathode (anode) to the anode (cathode) applying a static current. For a single PANI nanowire, the static current between two electrodes activates the redox (reduction-oxidation) processes for the polymerization of aniline along the nanochannel. A semiconductor analyzer (B1500A, Agilent) was used to apply the static current through a probe station and monitored the voltage change between a pair of electrodes. When the nanowire is fabricated to connect two electrodes, the voltage drops from around 3 V to below 1 mV due to the conduction along the nanowire. In Figure 2, the steps of the electrochemical deposition growth method are shown from the preparation of nanochannel between two Au electrodes to the fabrication of PANI nanowire. In this research, 2 to 7  $\mu\text{m}$  long nanowires were successfully fabricated. The dimension of the nanowire can be determined by changing the nanochannel size, the thickness of PMMA layer and the distance between two electrodes in the electrochemical deposition growth method. In addition, the fabrication conditions of applied current or volume of ionic solution were optimized depending on the materials and structures of nanowires [35, 69].

The fabrication of single PANI nanowire was carried out through applying a static current in the range of 300 nA – 650 nA between two electrodes and across the nanochannel, which were all covered with ionic aniline solution (0.01M aniline in 0.1M HCl, 0.3  $\mu\text{L}$  – 0.5  $\mu\text{L}$ ). Ionized aniline monomers in the aniline solution were deposited inside the nanochannel, creating a polyaniline chain through the process of electrochemical oxidative polymerization (See Appendix A). When the single PANI nanowire was fabricated connecting two Au

electrodes, the monitored voltage dropped to sub-millivolt. After removing the residual aniline solution by an air blower, the sample with the PANI nanowires was immersed fully with agitating gently in acetone for 10 minutes and rinsed in de-ionized water to completely remove the PMMA coating. The side walls of fabricated single PANI nanowire can be exposed from the PMMA layer. Finally, the sample was dried by blowing softly nitrogen gas onto it to evaporate moisture. In order to characterize the morphologies and electrical conductivities of the PANI nanowires, the resistances of the PANI nanowires were measured using the semiconductor device analyzer (B1500A, Agilent) in the range of 0 to 20 mV. The morphologies of the PANI nanowires were characterized using an atomic force microscope (AFM, XE-100, PSIA) in the noncontact mode and a scanning electron microscopy (SEM, e-Line, Raith) with an accelerating voltage of 10 kV.

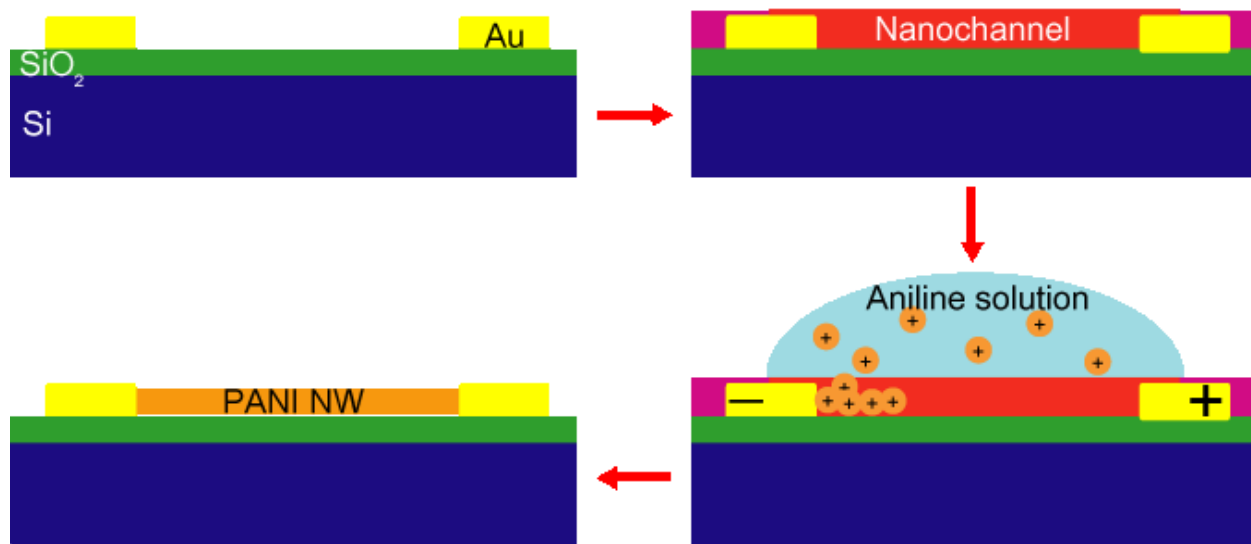


**Figure 2.** The steps of the electrochemical deposition growth method for the single nanowire fabrication. The PANI single nanowire is fabricated to deposit PANI electrochemically in the nanochannel by applied static current between two electrodes.

## 2.2 RESULTS AND DISCUSSIONS

### 2.2.1 Physical properties of single polyaniline nanowires

We measured the resistance of the single PANI nanowires from the I-V curve at the pre- and post-acetone wetting process to compare the resistance change. The measured resistances of the PANI nanowires are grouped in a range of  $430.94 \pm 51.5 \Omega$  depending on the structure of formation and the dimension of the nanowires before the acetone wetting. The resistances of the PANI nanowires after the acetone wetting were in the range of  $297.75 \pm 31.7 \Omega$ .

The resistance changes after the acetone wetting have smaller variation as compared to before the acetone wetting as shown in Figure 3 (a). The resistance changes along the different nanowires with the various length are plotted on the graph of the nanowire length vs the resistance change ratio in Figure 3 (b). The percentage in the resistance change of the PANI nanowires increased proportionally to the length of the nanowires, with grouping along a trend line. We can deduce that the resistance change after the acetone wetting was affected more in longer PANI nanowires than shorter ones, with the average resistance change being  $39.57 \pm 11.57\%$ .

In order to verify the improvement in the electrical conductivity of the PANI nanowires, the electrical resistivity of the PANI nanowires was compared with previously reported data. The calculated electrical resistivity was in the range of  $2.38 \pm 0.3 \times 10^{-4} \Omega\cdot\text{cm}$  in this work, and the reported minimum electrical resistivity of a 220  $\mu\text{m}$  diameter PANI microfiber was  $4.69 \times 10^{-4} \Omega\cdot\text{cm}$  [70]. The electrical resistivity of our PANI nanowire is smaller than the reported minimum value by  $50.64 \pm 6.39\%$ . This shows that the single PANI nanowires have the significantly higher electrical conductivity than the microstructure of PANI due to the fast carrier mobility in nanomaterials.

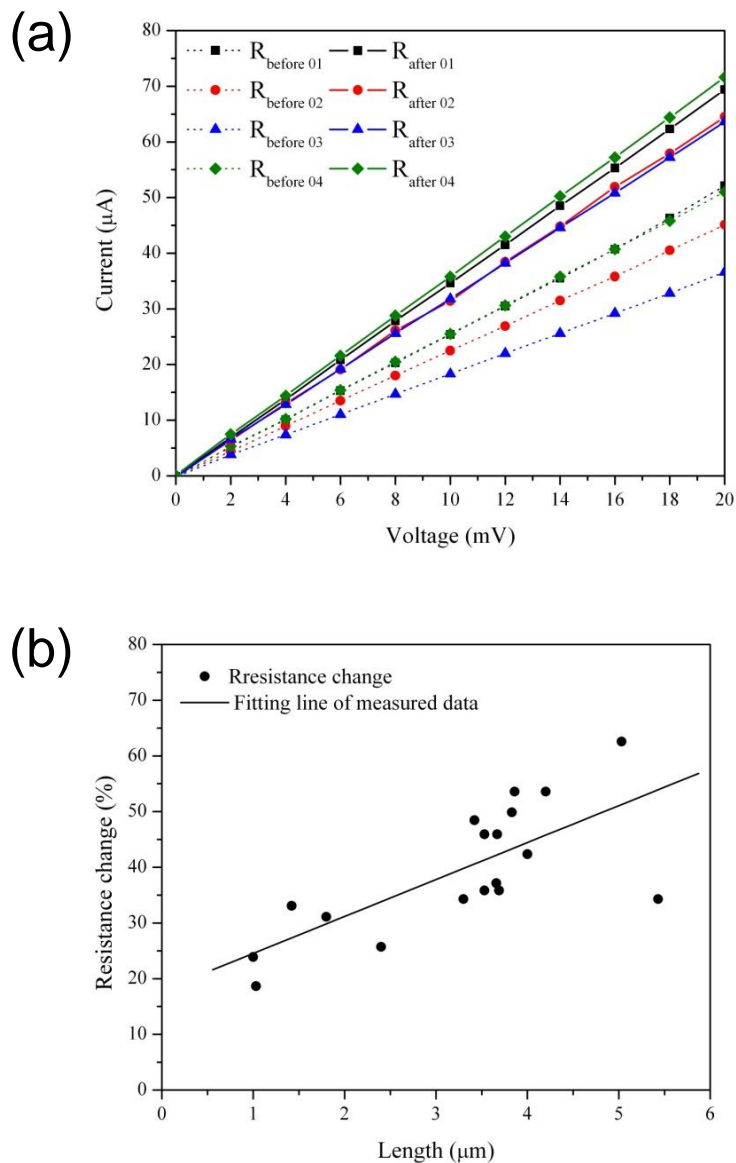


**Figure 3.** The current vs voltage measurements of the PANI nanowires at the pre- and post-acetone wetting processes. (a) The resistances before and after the acetone wetting are represented by dotted and solid lines and with symbols, respectively. (b) The percentage of resistance change is given according to the length of the PANI nanowires.

For the study of morphology, AFM images provide the stereo structure and roughness of the nanowire surfaces by supplying topology data as shown in Figure 4 (a) and (b). After the acetone wetting, the nanowire surface became smooth. The top and walls of the nanowire show uniform structure. The PANI nanowire within the 150 nm thick PMMA seems to demonstrate a stereoscopic structure and thickness in Figure 4 (a) and (b). The thickness of the PANI nanowire is determined by PMMA thickness after the acetone wetting process. We fabricated the PANI nanowire with the thickness of  $133.77 \pm 13.82$  nm and the width of  $133.17 \pm 13.01$  nm. The acetone wetting process regulates uniformly the dimension of width and thickness as previously mentioned. And, these measured data show that the PANI nanowires were fabricated uniformly corresponding to the dimensions of nanochannels. This demonstrates that not only a single addressable nanowire can be fabricated, but also a multiple array of nanowires is possible through the electrochemical deposition growth method. We exhibited a multiple array of the single PANI nanowires, which were fabricated on the substrate coated with 200 nm thick PMMA as shown in Figure 5 (a).

In the multiple array, the PANI nanowires show unified dimensions, with the length of 3.3  $\mu\text{m}$  and the width of 130.89 nm. In Figure 5 (b), the measured thickness of nanowires by AFM is 186.27 nm and 191.12 nm, respectively. On the bottom of the nanowires, the width of the nanowires was 465 nm due to the drift of the AFM cantilever beam. As shown in Figure 5, the multiple array of the single site-specific PANI nanowires can increase the density of nanowires on a single chip in applications such as the gas- or biosensors.

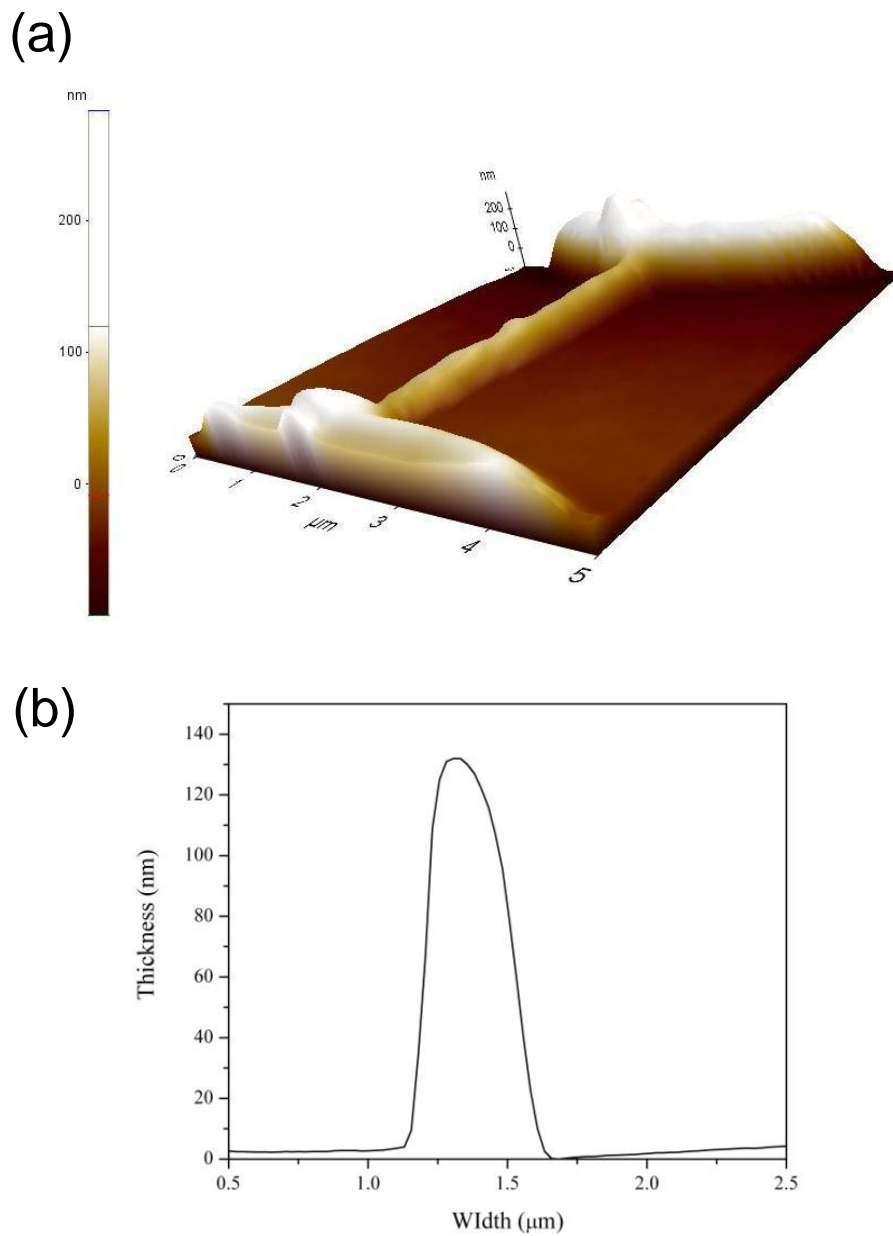


**Figure 4.** AFM image of a fabricated single PANI nanowire. (a) AFM stereoscopic image of a single nanowire after the acetone wetting. (b) The topology of the identical PANI nanowire shows the thickness of 131.32 nm and the width of 129 nm. Note that the bottom of the nanowire looks wider than the SEM image because of the drift of AFM tips.

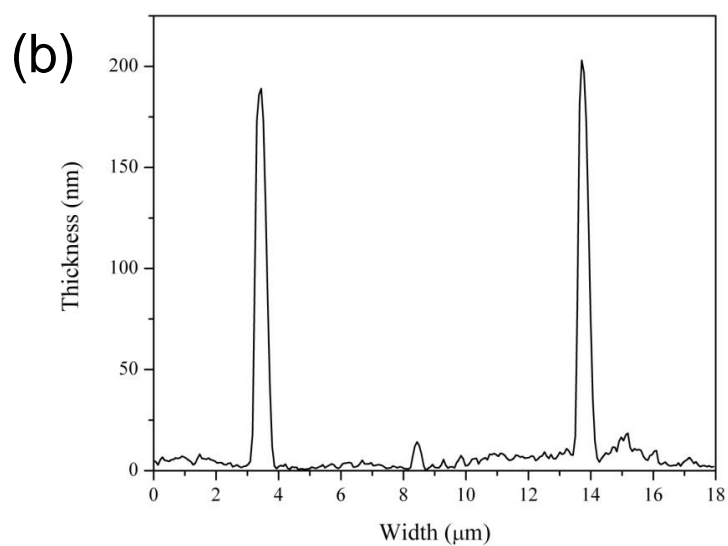
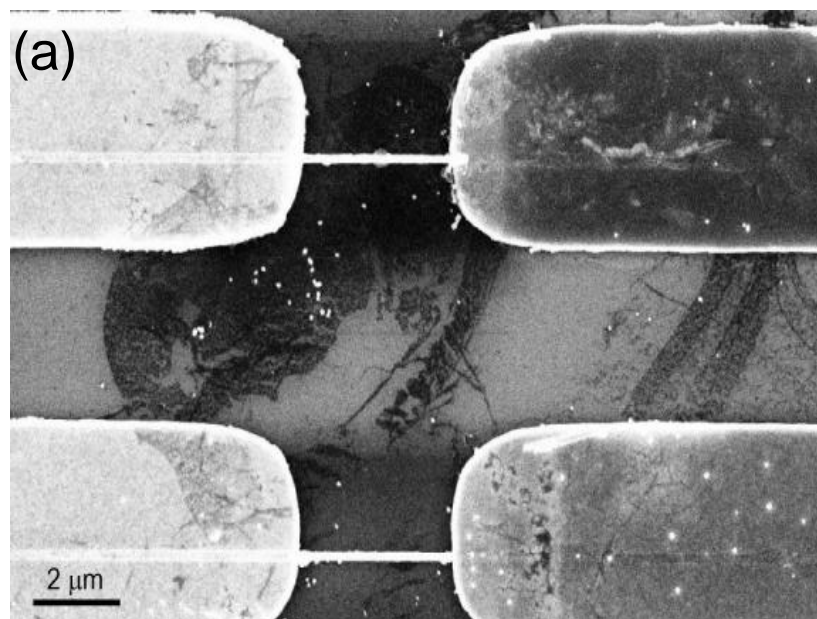


**Figure 5.** The multiple array of single PANI nanowires. (a) These nanowires show a dense structure and uniform dimension in the length of 3.3 μm and the width of 130.89 nm. (b) The topology of the multiple PANI nanowires array by AFM shows very similar thickness of the fabricated nanowires.

## 2.2.2 Ring substitution and doping on polyaniline by acetone

The PANI nanowire fabricated through the electrochemical oxidative polymerization takes one of the emeraldine forms according to the pH degree of aniline aqueous solution and the post-process in electropolymerization process [12]. The emeraldine form of PANI can be modified by soaking it in polar solvents such as acetone.

Acetone can cause a change in the electrical conductivity of PANI through creating derivatives of PANI [12]. Hydrogen atoms in a PANI chain can be substituted by  $-OCH_3$  or  $-OC_2H_5$  through the acetone wetting [12]. The substitution on PANI synthesizes hydrochloride salts of the polymer. In particular, the electrical conductivity of the PANI nanowire becomes improved since a solvent such as acetone diffuses into the PANI backbone through the formation of hydrochloride salt of PANI [12]. The structure of PANI is also shrunk by the coagulation of the polymer after the acetone wetting [16]. Similarly to acetone, solvents such as butyl acetate and methyl isobutyl ketone (MIBK) result in the shrink of PANI [16]. In the coagulation by acetone, the porosity in the PANI is decreased because the denser structure of the new PANI may have a partly crystalline structure [71, 72]. With respect to protonic acid doping, the PANI nanowire can be doped by the concentration of aniline or HCl in an aqueous solution [12, 73-75]. In the ionized aniline solution, 0.1 M HCl creates a lower pH than pH 3. In low pH aniline solutions, the surplus protonic acid of HCl reacts with PANI after polymerization. The PANI is protonated in non-redox doping with the surplus HCl [75]. The protonation of PANI changes electrical conductivity depending of degree of oxidation in PANI [71]. In addition, an acetone wetting of the PANI nanowires improved electrical conductivity in the microstructure as well as in the nanostructure of PANI [75, 76].

In our experimental data, the fabricated single PANI nanowires showed a dramatic decrease of resistance after the acetone wetting as shown in Figure 3. The resistances of the nanowires after the acetone wetting exhibited the smaller value and with the smaller deviation, than the nanowires before the acetone wetting, shown in Figure 3 (a). The resistance of longer nanowires can change more than that of the shorter ones, shown Figure 3 (b). The resistance change increases linearly according to the length of the nanowire. Those data support the idea that the acetone wetting process to remove PMMA layer after the nanowire fabrication can affect on the resistance of PANI nanowires through the ring substitution and coagulation, which is well known behavior in the macro- or microstructure of PANI.

### **2.2.3 Improvement of structure in polyaniline nanowires by the acetone wetting**

In order to verify the effects of acetone on the structure of PANI nanowires, we obtained SEM images of the PANI nanowires to compare the changes in structure at the pre- and post-acetone wetting processes, as shown in Figure 6. The nanowires show plane geometry and structural change. The less dense PANI nanowire before the acetone wetting is 139.6 nm wide and 3.7  $\mu\text{m}$  long as shown in Figure 6 (a). The structure of the PANI nanowires is modified to become denser after the acetone wetting as shown in Figure 6 (b). In Figure 6 (c) and (d), the shrunken structure is compared between two different single PANI nanowires. After the acetone wetting, the 5  $\mu\text{m}$  long PANI nanowire became thinner than before the acetone wetting with decreasing the resistance of the PANI nanowire by 37.15%. The width of the PANI nanowire changed from 160 to 141.1 nm. In Figure 6 (e) and (f), the over-deposited PANI nanowire above the nanochannel is cleaned and shrunken by the acetone wetting. The width of the nanowire decreased from 126.5 to 111.6 nm. The over-deposited PANI on the right-hand side of Figure 6

(e) was erased after the acetone wetting as shown in Figure 6 (f). The widths of single PANI nanowires were in the range of  $133.17 \pm 13.01$  nm according to the SEM images.

In the structure of PANI nanowires, the acetone wetting contributes to the PANI nanowire being dendrite-free and completely fitting in the nanochannel, with a lift-off effect on the over-deposited PANI along the channel as a result of cleaning off PMMA. The PANI nanowires after the acetone wetting have a standard deviation of less than 11% in resistance, thickness, and width. The coagulation, which resulted from the acetone wetting, provided a denser structure and significantly contracted width, as shown in Figure 6 (b), (d), and (f). Furthermore, the reproducibility of PANI nanowires was increased by the acetone wetting. As shown in Figure 5, the multiple array of the single PANI nanowires makes possible the buildup of a large-scale integrated system for bio- or chemical sensors with regularly aligned electrodes and nanowires.

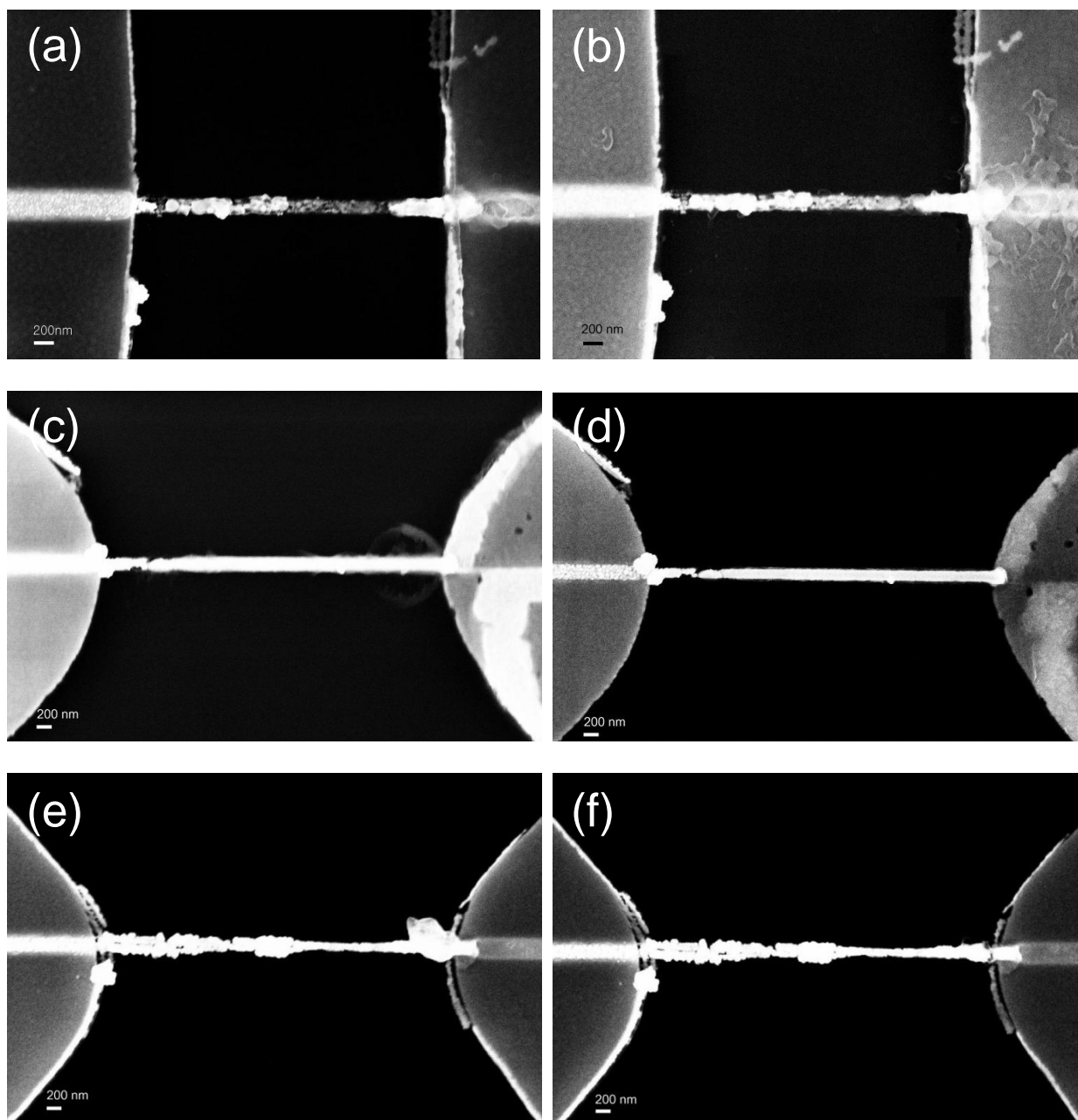


**Figure 6.** SEM images of single PANI nanowires. (a) The sparse structure of the PANI nanowire before the acetone wetting. (b) The denser structure of the PANI nanowire with the width of 139.6 nm after the acetone wetting. (c) The 5  $\mu\text{m}$  long and 160 nm wide PANI nanowire before the acetone wetting. (d) The identical PANI nanowire of (c) after the acetone wetting with the width of 141.1 nm and a resistance change of 37.15% with dendrite-free structure. (e) The 5  $\mu\text{m}$  long and 126.5 nm wide PANI nanowire before the acetone wetting. (f) The identical nanowire of (e) with the width of 111.6 nm after the acetone wetting.

## 2.3 SUMMARY

The improvements in the electrical conductivity and morphology of the single PANI nanowires, which were fabricated by the electrochemical deposition growth method with the acetone wetting, were demonstrated in my research. This electrochemical deposition growth method is an easy and effective method to fabricate site-specific, uniform, and reproducible nanowires bridged between two electrodes. The PANI nanowires showed a decrease in resistance and a dense structure after the acetone wetting. The resistance of our PANI nanowires was decreased by  $39.57 \pm 11.57\%$  after the acetone wetting. The coagulation and ring substitution in PANI nanowires by the acetone wetting caused changes in physical properties such as electrical conductivity, material structure, and surface configuration. Those controlled physical properties of the PANI nanowires could make them useful in applications such as biosensors due to the feasibility of uniform single nanowire between a pair of electrodes.

The above properties guarantee that the PANI nanowires can be used as reliable sensors with constant performance. This improvement in the PANI nanowire means that nanowire can be employed for use as bio- or chemical sensors, which require high sensitivity, selectivity, reproducibility, and reliability.

### 3.0 SINGLE MULTICOMPOSITE NANOWIRE

Multicomposite materials have been researched in order to improve vastly physical and chemical properties from single composite materials. In nanomaterials areas, nano-multicomposite materials have been also developed to apply for electrical, biomedical, and mechanical engineering applications with the excellent electrical conductivity and mechanical strength as a result of reactions between the composites in synthesis [77, 78]. The nano-multicomposite materials are typically produced as a mixture of CNT, Graphene or NP using an organic material such as a conducting polymer [79-82]. These composite materials are intriguing because each individual component's complementary nature in the mixture acts synergistically to improve physical and chemical properties [83-85]. For example, CNT-polymer multicomposites synthesized by *in situ* polymerization, which are studied in thin film and nanowire structures, have shown the improved electrical conductivity, photoluminescence, and mechanical strength [23, 86-89]. Likewise, bundled CNT-PPy nanowires fabricated from AAO templates via cyclic voltammetry demonstrate the higher electrical conductivity than PPy nanowires [28, 29]. In the case of CNT-PPy composites, the end result displays a metallic character, whereas PPy nanowires serve as semiconductors. Other inorganic nanowire-polymer composites of ZnO, RuO<sub>2</sub>, and Ag with PANI or PPy demonstrate the varying electrical conductivity according to synthesis types (*in situ* or *ex situ* polymerization) and as a function of the mix composition [90].

These nano-multicomposite nanowires are fabricated in bundles via the various methods such as the AAO template method, electrochemical deposition, and electrospinning [28, 29, 88-90]

In this research, we suggest a newly developed method for the fabrication and characterization of single multicomposite nanowires (SMNWs) based on the electrochemical deposition growth method. The entrapment of ZnO NPs in a nanowire can provide an innovative method to develop effectively a nanowire biosensor. If the functionalized ZnO NPs for biosensing were located in a nanowire exposing bioreceptor such as antibody out of the nanowire surface, the nanowire biosensor could be developed easily. In addition, the fabricated single ZnO NPs-entrapped PANI nanowires using the electrochemical deposition growth method showed the improved mechanical strength and electrical conductivity dependent on ZnO NP concentration (1, 2.5, 5, 10, and 20 wt. %) when compared to pure single PANI nanowires. The growth of SMNWs is similar to that of single conducting polymer nanowires, except that ZnO NPs are attracted to the nanochannel via an electric field applied from the electrodes, while *in situ* polymerization of PANI occurs simultaneously. ZnO NPs were chosen because of their controllable conductivity, wide-bandgap and optical transparency, all of which make them useful for various applications [91-93]. PANI was the polymer of choice because of its excellent bioaffinity, cost efficiency, environmental stability, and ease of synthesis [94]. Through modulation of ZnO NPs and PANI components, the goals of this research are to create a synergistic compound with tailorable physical characteristics and a new noble material which can be utilized for the effective functionalization of nanowires. If the surface immobilized NPs with antibodies or aptamer were mixed in the ionic aniline solution, the functionalized nanowire would be established in a simple process in the future research.

### 3.1 FABRICATION OF SINGLE MULTICOMPOSITE NANOWIRES

The SMNWs with ZnO NPs were also synthesized using the electrochemical deposition growth method with aniline solutions (0.01 M aniline in 0.1 M HCl) containing ZnO NPs (1 wt. %; 2.5 wt. %; 5 wt. %; 10 wt. %; and 20 wt. %, Alfa Aesar). The solutions were sonicated for 60 to 90 minutes to disperse the NPs in the solution homogeneously before growing nanowires. During sonication, the temperature of the solution was kept below 50 °C to prevent the high-temperature agglomeration of the NPs. After the sonication, 0.4  $\mu$ L solution was dropped over a nanochannel while a static current of 500 nA to 800 nA was applied between two metal electrodes. The fabrication of SMNWs follows the steps of the electrochemical deposition growth method explained in chapter 2.1. Similar to the fabrication of single PANI nanowire, the ionized aniline solution including ZnO NPs deposits multicomposite material inside of a nanochannel monitoring the change of voltage between two electrodes from around 3.5 V to close 0 V as shown in Figure 7 (a).

The morphology of the fabricated SMNWs was studied using an SEM and AFM in non-contact mode. Energy dispersive X-ray spectroscopy (EDS, XL-30, Philips) and Raman Spectroscopy (inVia, Renishaw) were utilized to reveal the elemental composition of the nanowires and validate our claim of ZnO NP entrapment in the nanowires. High resolution transmission electron microscope (HRTEM, JEM 2100F, JEOL) images were obtained, with SMNW samples extracted by the etching with a Focused Ion Beam (FIB, Nova 200 NanoLab, FEI) and nanomanipulator (F100 Nanomanipulator, Zyvex). In this process, SMNWs spanning two electrodes were detached by laterally scratching the surface with the nanomanipulator and transferring the loosely bound nanowire to a TEM grid. HRTEM was carried out with an acceleration voltage of 200 kV and a camera constant of 25 cm.

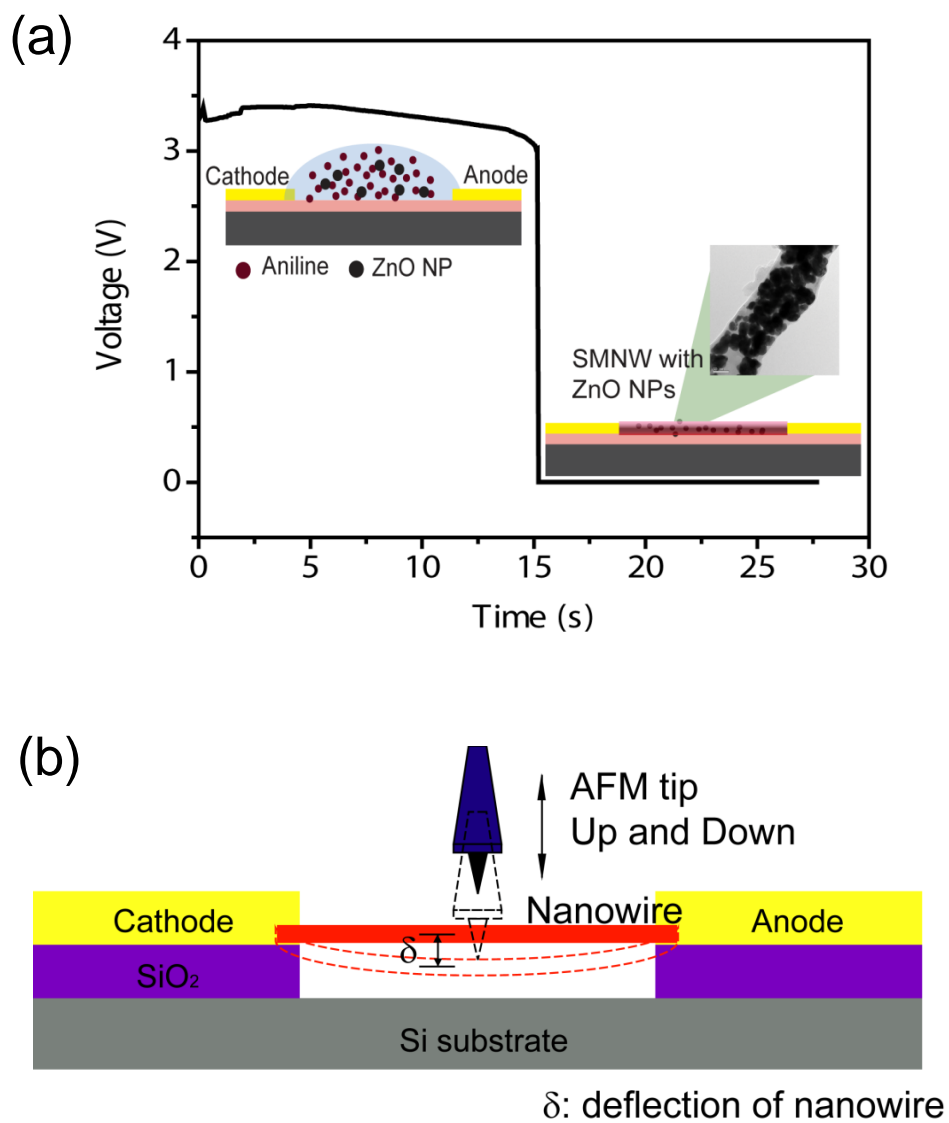


**Figure 7.** The fabrication and mechanical strength test of SMNW with ZnO NPs. (a) In the region of high voltage, the ionic aniline monomers and ZnO NPs deposit along the nanochannel. After growing, the SMNW bridges the gap between the two metal electrodes. The inset is the TEM image of SMNW. (b) The mechanical strength (elasticity) is measured on the nanowire by an AFM load test. In order to provide the space for deflection of the nanowire in the AFM load test, the SiO<sub>2</sub> layer under the nanowire was etched away by BOE.

The HRTEM images were utilized to confirm the internal structure of the SMNWs and the entrapment of ZnO NPs related to different conditions of fabrication such as the applied static current and the weight concentration of ZnO NP. The electrical conductivity and elasticity of the SMNWs were measured by a semiconductor device analyzer and force-displacement (FD) measurement from AFM, respectively. Electrical conductivity was calculated from the measured I-V curve with dimensions of the nanowires. The force of 5 nN used in the AFM FD measurements was applied in the center of the nanowire with both ends supported, as shown in Figure 7 (b). The freestanding structure of SMNW was constructed via etching SiO<sub>2</sub> with using buffered oxide etchant (BOE).

## 3.2 RESULTS AND DISCUSSIONS

### 3.2.1 Structure of single multicomposite nanowires

The fabrication of SMNWs involves using the electrochemical deposition growth method described in chapter 2.1. In Figure 8, the fabricated SMNWs are 5  $\mu\text{m}$  in length and uniform in dimension. Specifically, these SMNWs have a very uniform width of 108 to 133 nm and a height of 97 to 112 nm, measured using both SEM and AFM. Figure 8 (a) shows that the uniform structure of the SMNW is comparable to that of the single PANI nanowire demonstrated in previous chapter. Highly magnified images of the SMNWs for 5, 10, and 20 wt. % of ZnO NP concentrations are shown in Figure 8 (b), (c), and (d), respectively. In these SEM images, some observed contrast spots on the SMNWs are assumed to be ZnO NPs with a diameter of 30 to 60 nm. This range is consistent with the 20 to 70 nm range listed in the datasheet from Alfa Aesar. The 5 wt. % ZnO NPs SMNW shows a uniform width of 133 nm and smooth topography in Figure 8 (b). The observed particles were 33.90 and 35.39 nm in diameter, respectively (measured with an SEM). The 10 wt. % ZnO NP-entrapped PANI nanowire displays a regular width of 117 nm and a greater number of ZnO NPs than the 5 wt. % ZnO NP concentration, as might be expected, in Figure 8 (c). The 20 wt. % ZnO NP-entrapped PANI nanowire displays widths varying from 80 to 110 nm in Figure 8 (d). Increases in the density of the NPs and changes in the surface morphology of the SMNWs are clear when comparing Figure 8 (b) and (c). In the insets of Figure 8 (b), (c), and (d), the AFM line scans show height variation from 98 to 112 nm along the nanowire. As the ZnO NP concentration increased, the NPs aggregated tightly in SMNW, and the structure of SMNW was affected. Thus, the ZnO NP concentration clearly affects the morphology of the SMNWs, as demonstrated in the SEM images.

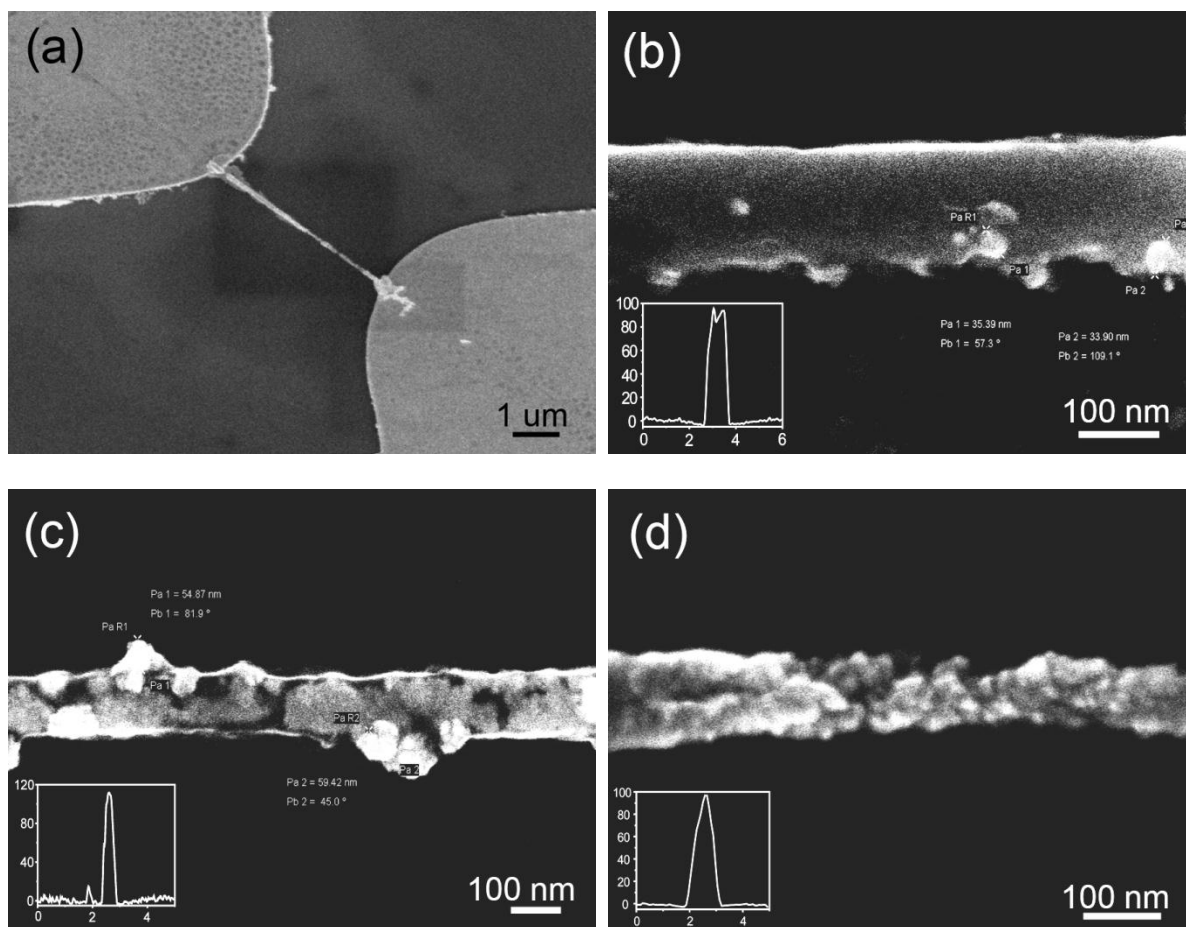


**Figure 8.** Fabricated SMNWs with different ZnO NP concentrations. (a) Low resolution SEM image of 5  $\mu\text{m}$  long SMNW, entrapped ZnO NPs with uniform dimension. (b) Highly magnified image of a 5 wt. % ZnO NP-entrapped PANI nanowire with height of 97 nm and width of 133 nm. Diameters of the observed particles are ranged from 33.90 to 35.39 nm. (c) 10 wt. % ZnO NP-entrapped PANI nanowire with the height of 108 nm and width of 110 nm. Diameters of the observed particles are 54.87 and 59.42 nm. (d) 20 wt. % ZnO NP-entrapped PANI nanowire with the height of 98 nm and the width of 80 to 110 nm. The agglomerated particles greatly changes surface morphology of the SMNW with taped shape.

### 3.2.2 Characterization of SMNW entrapped with ZnO NPs

To further characterize that the contrast spots are indeed ZnO NPs, we investigated the composition of nanowires with EDS and Raman Spectroscopy, as shown in Figure 9. The EDS data in Figure 9 (a) shows a variation in peaks corresponding to element used: C, O, Si, or Zn. C, Si, and O are from the PANI and the SiO<sub>2</sub>/Si substrate, respectively. Clear peaks in the SMNWs for the element Zn as compared to this element in the single PANI nanowires are visible. Other evidence for ZnO NP entrapment is the increased oxygen peaks in the SMNW as compared to images for the single PANI. However, the different ZnO NP concentration and specific distribution of ZnO NPs in the SMNWs might have resulted in different Zn and O intensities in the EDS scanning data.

The Raman spectrum in Figure 9 (b) shows that the fabricated single nanowire materializes with the doped PANI presenting the peaks on 1590 cm<sup>-1</sup> (C=C bonding), 1480 cm<sup>-1</sup> (C=N bonding), 1431 cm<sup>-1</sup> (C-C stretching), 1220 cm<sup>-1</sup> (C-N stretching), 1165 cm<sup>-1</sup> (in-plane C-H bending), 840 cm<sup>-1</sup> (Amine deform), 779 cm<sup>-1</sup> (Ring deform), and 750 cm<sup>-1</sup> (Imine deform) [95]. Therefore, it is clear that our electrochemical deposition growth method works to electropolymerize aniline for fabrication of SMNW. The SMNW with ZnO NPs could develop another innovative method to functionalize nanowires using entrapment of NPs, which are surface immobilized with bioreceptor such as antibody.

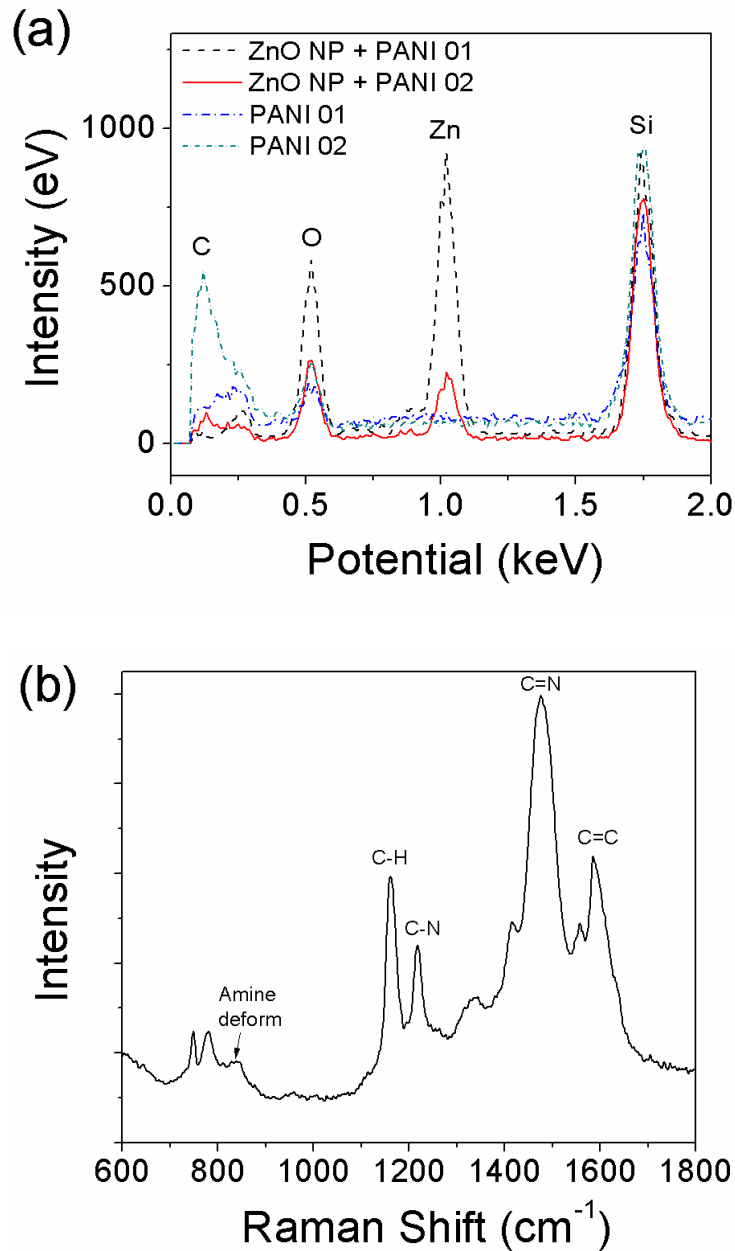


**Figure 9.** EDS data and Raman spectrum for single PANI nanowires and single ZnO NP-entrapped PANI nanowires. (a) The SMNWs with ZnO NPs show clear peaks at Zn and a higher peak at O, which is resulted from the entrapment of ZnO NPs. The two different ZnO concentrations (black dashed line: 20 wt. %, red solid line: 5 wt. %) display different intensities of Zn. (b) The Raman spectrum identifies the materialization of doped PANI in a fabricated single nanowire.

For an in-depth examination of the ZnO NP entrapment, a TEM was utilized. Specifically, the HRTEM was utilized to find the diffraction pattern of individual nanowires. Figure 10 (a) shows a 10 wt. % ZnO NP-entrapped PANI nanowire between electrodes, lifted off prior to placement on a TEM grid using an FIB and a nanomanipulator. Other HRTEM images for 0, 5, and 10 wt. % ZnO NP-entrapped PANI nanowires are shown in Figure 10 (b), (c), and (d), respectively. Additionally, the SMNWs (1 and 2.5 wt. % ZnO NP concentration) created under different growing conditions are demonstrated in Figure 10 (e) and (f). From these HRTEM images, entrapped ZnO NPs approximately 30 to 60 nm in diameter were observed, while the reference single PANI nanowire (0 wt. % ZnO NP) shows a very uniform structure and a width of 137.5 nm without ZnO NPs in Figure 10 (b).

For the SMNW, a few interesting effects can be observed. The ZnO NPs are distributed almost randomly and display differing degrees of aggregation, which can be seen in Figure 10 (c) and (d). A comparison of two different ZnO NP concentrations shows increased agglomeration of the 10 wt. % when compared with the 5 wt. %. From these images, we observed that in low ZnO NP concentrations, the entrapped ZnO NPs disperse almost randomly within the nanowire core structure during the *in situ* polymerization process, with signs of agglomeration occurring. As the ZnO NP concentration increase, the ZnO NPs formed a continuous structure inside of the SMNW – similar to an amorphous ZnO nanowire - as shown in Figure 10 (d). Images taken for the SMNWs with the concentration higher than 10 wt. % showed little difference in the nanowire morphology as a result of saturation at 10 wt. %, revealing that this is the point at which the saturation of ZnO NP entrapment occurs in the SMNW structure. The inset in Figure 10 (c) displays the ring diffraction patterns for each SMNW. These diffraction patterns can be attributed to the random orientation of the ZnO NPs as well as the polycrystalline structure of

PANI. The x-ray diffraction pattern of the entrapped ZnO grown via electrochemical deposition was observed at room temperature. The observed diffraction patterns were (113), (002), (111), and (220) in all directions as shown in Figure 10 (c). The diffraction pattern of (002) identifies ZnO in the SMNW. Other patterns represent Si, SiO<sub>2</sub>, and Au, which originate in the substrate of Si/SiO<sub>2</sub> and Au electrodes.

The entrapment of ZnO NPs in the SMNW is also dependent on the amount of current used in the fabrication of the nanowire (See Figure 10 (e) and (f)). The SMNWs of the 1 and 2.5 wt. % ZnO NP were fabricated in the condition 900 nA current, which is the higher current than the current (600 nA) applied to the SMNWs in Figure 10 (c) and (d). The higher applied current in the fabrication of the nanowire induced a stronger electrical field inside the nanochannel, which resulted in more ZnO NPs being attracted to the nanochannel. As shown in the HRTEM images Figure 10 (e) and (f), for the SMNWs, the different growing condition of high current shows the feasibility of tuning entrapment of ZnO NPs in low concentrations of ZnO NPs (1 and 2.5 wt. %). The HRTEM images of SMNWs verify the entrapment of ZnO NPs and the controlled entrapment depending on the fabrication condition such as ZnO NP concentrations and an applied static current. For biosensing application of those SMNWs, the further optimal entrapment condition of functionalized ZnO NPs will be required maximizing biosensing sensitivity and reliability in the NP concentrations and growing condition.

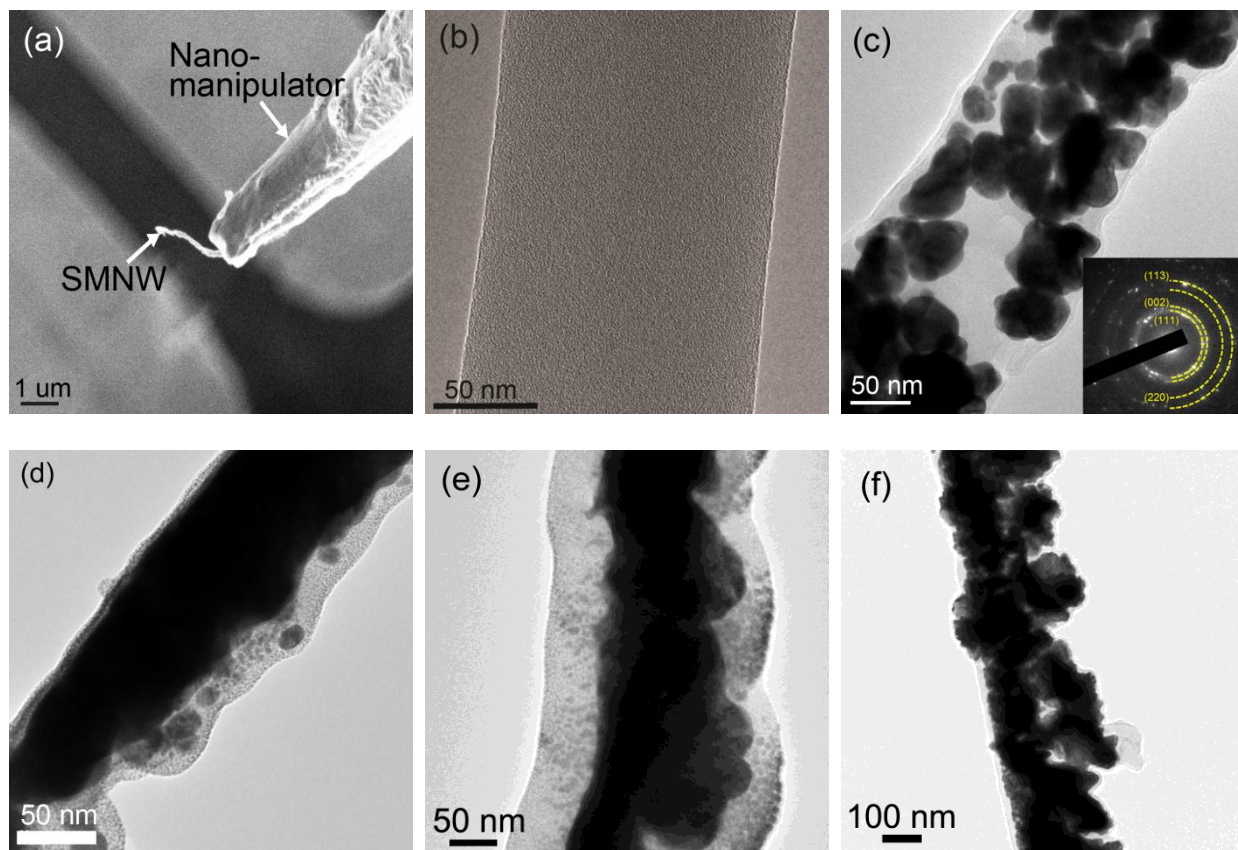


**Figure 10.** HRTEM images of single PANI nanowire and SMNWs with different ZnO NP concentrations. (a) A single 10 wt. % ZnO NP-entrapped nanowire is extracted from the electrode and transferred to the TEM sample grid by a nanomanipulator. The SMNW was scratched laterally at the end of nanowire and detached. (b) A HRTEM image of single PANI nanowire: 0 wt. % ZnO NP concentration. ZnO NPs are absent in this single nanowire. Note the uniform width of 137.5 nm. (c) A HRTEM image of 5 wt. % ZnO NPs (width of 154 nm) and (d) A 10 wt. % ZnO NP-entrapped PANI nanowires (width of 113 nm). The diffraction pattern for each SMNW is shown in the corresponding inset. Note the ring patterns (PANI) and dots indicating randomly oriented crystalline structure (ZnO). (e) An 1 wt. % ZnO NP-entrapped PANI nanowire from applying a current of 900 nA in the growing condition. (f) A 2.5 wt. % ZnO NP-entrapped PANI nanowire from applying a current of 900 nA in the growing condition. The SMNWs of (e) and (f) show tightly agglomerated ZnO NPs inside the nanowire similar to the nanowire of (d).

### 3.2.3 Changes of electrical conductivity and elasticity

The electrical and mechanical properties of SMNWs were measured in the nanowires fabricated under the same growing condition (600 nA current). First, the I-V measurements of SMNWs with the various concentrations were taken and compared with the measurements of single PANI nanowires. Figure 11 displays the results when plotting electrical conductivities as a function of the ZnO NP concentration. Electrical conductivities at 300 K were calculated from the I-V curves and the dimensions of the nanowire (from SEM and AFM measurements). The SMNWs clearly show increased electrical conductivity compared with the single PANI nanowire. The single PANI nanowire electrical conductivity is  $3.30 \pm 0.03 \times 10^2 \text{ S}\cdot\text{cm}^{-1}$ . The electrical conductivity of ZnO NPs-entrapped PANI nanowires (300 K), on the other hand, varied from  $3.58 \pm 0.03 \times 10^2$  to  $1.05 \pm 0.21 \times 10^2 \text{ S}\cdot\text{cm}^{-1}$  in Figure 11. Electrical conductivity demonstrated increases linearly with the increased ZnO NP concentration, but the increase in electrical conductivity slowed down in the range of concentrations higher than 10 wt. %, with the data trend showing logarithmically increasing behavior.

To study the load strength of the nanowires, elasticity was measured taking an AFM FD measurement. The insulating layer below the nanowire was first removed using a BOE. For the FD measurement, the deflection of the nanowires was obtained by pushing down and up at the center of the nanowires with a load of 5 nN. For the calculations, the free standing nanowire was assumed to be supported at both ends. The deflection of the nanowire was measured from the FD measurement curve. Young's modulus of the nanowires was then calculated using the deflection of nanowire and applied force by the AFM.

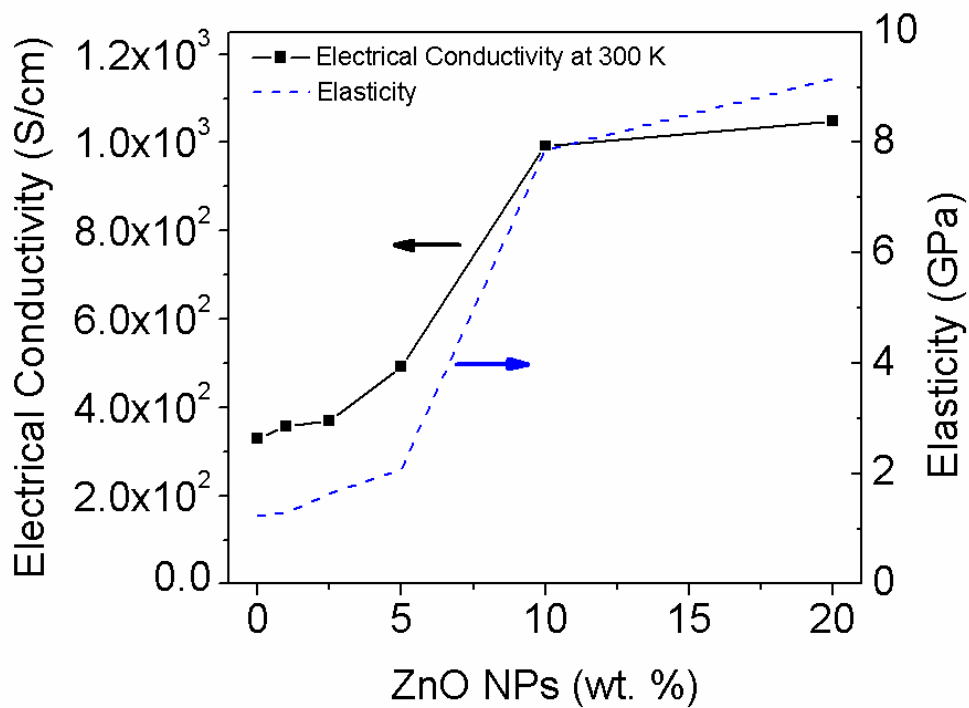


**Figure 11.** Enhancement in physical properties of the SMNWs. Electrical conductivity (black solid line at 300 K) and elasticity (blue dash and double dot line) are measured for 0, 1, 2.5, 5, 10, and 20 wt. % ZnO NP. Note the dramatic increase in each from 2.5 to 10 wt. % ZnO NP concentration. The slopes of physical properties decrease after 10 wt. % ZnO NP, resulting from the saturation of ZnO NP entrapment.

Figure 11 shows the results of these calculations. Young's modulus for the SMNW is distinctly larger than that of the single PANI nanowire. The elasticity of the single PANI nanowire ranged from 1.24 to 3.46 GPa, depending on the shape of the nanowire – in keeping with the 2 to 3 GPa elasticity of PANI microfiber found in other researches [16]. From 1 to 5 wt. % ZnO NP concentrations, the ZnO NP-entrapped PANI nanowires have a Young's modulus measurement similar to the single PANI nanowire, with a modulus of 1.3 and 2.1 GPa, respectively. This can be attributed to the dominance of the PANI in terms of volume of the nanowire, since those concentrations do not form a continuous link that could increase stiffness of the nanowire. Subsequent measurements of SMNWs with 10 and 20 wt. % have a modulus estimated to be 7 and 9 GPa, respectively as shown in Figure 11. The limited increase here is caused by the saturation of ZnO NPs. Although much lower than quoted values of the ZnO nanowire Young's modulus [96], it should be noted that the SMNW contains only entrapped ZnO NPs and its elasticity is not comparable to single-crystal ZnO nanowire measurements. When all the results are plotted, Young's modulus changes logarithmically with ZnO NP concentrations. We suggest that this improvement of elasticity in the SMNWs is caused by the reaction between PANI and ZnO NPs from *in situ* polymerization [97, 98]. The elasticity of SMNW shows a saturation behavior similar to the electrical conductivity in the high ZnO NP concentration of 10 wt. %.

### 3.2.4 Enhancement of physical properties in single multicomposite nanowires

The enhanced electrical conductivity may be the result of various mechanisms. It could be a result of a structural change in the SMNW and the reaction between the ZnO NP and the PANI as noted elsewhere [90, 97, 98]. In pure single PANI nanowires, electrical conductivity is defined by electron transfer along the backbone of PANI [16, 70, 99]. On the other hand, the SMNW may provide multiple electron pathways through both the PANI and ZnO NPs, which may cause the increased conductivity [100]. In addition, the internal structures of SMNWs have the various patterns as observed in the HRTEM images. Qualitatively, when comparing the fraction of entrapped ZnO NPs, PANI would be a dominant conducting material for below 5 wt. %. Contrastively, the continuous ZnO NP structure in over 10 wt. % may be dominant for an electron transfer pathway as observed in Figure 10 (d). The presence of this continuous ZnO structure explains why the increase of electrical conductivity begins to slow down at certain concentrations. In the saturation of ZnO NP entrapment in the SMNWs, the continuous structure of ZnO NPs as shown in Figure 10 (d), like ZnO nanowire, provides an electron pathway for electrons to move about freely in the SMNW [70, 100]. The improvement of electron transfer in the nano-multicomposite thin films via *in situ* polymerization of PANI with ZnO NPs has also been previously reported [97, 98, 100]. In addition, the saturation behavior in regard to electrical conductivity is well known in macro- or micro-multicomposite materials [100, 101]. Between 5 and 10 wt. %, we can only surmise that the mechanism of electron transfer consists of a mix of two pathways, which are dominant electron transfers in PANI or continuous ZnO structure, indicating a strong dependence on the random placement of the ZnO NP during the growth.

For the developed SMNWs, we assume the dominant mechanism of electrical conductivity is a mixture of hopping and tunneling, depending on the different structures of ZnO

NP entrapment as shown in Figure 10 and Figure 11. The dispersed ZnO NPs are spaced less than 10 nm apart, indicating that tunneling may be dominant – especially for the SMNWs developed at higher applied electric fields as shown in Figure 10 (c). However, PANI may be a superior electron path way due to the random distribution of ZnO NPs in the SMNWs of lower ZnO NPs than 5 wt. % concentration [102].

### 3.3 SUMMARY

The SMNW with ZnO NPs, a new novel material, was fabricated using the electrochemical deposition growth method. The entrapment of ZnO NP inside the nanowire was validated by use of an SEM, EDS, and HRTEM. Additionally, when the electrical conductivity and elasticity of the SMNWs were varied in a logarithmic fashion by varying the ZnO NP concentrations in the electrochemical growth aniline solution, variations in electrical conductivity and elasticity of SMNW displayed the saturation behavior in accordance with the ZnO NP concentrations.

The HRTEM images and characterization revealed the different levels of ZnO NP entrapments in SMNWs and the different effects of ZnO NP concentration on its physical properties. In the higher concentration than 10 wt. %, the ZnO NP entrapment resulted in hardly any change in physical properties of electrical conductivity and elasticity. Note, however, that we suggest a logarithmic relationship for the ZnO NPs wt. % to aniline monomer in the growing solution and not the concentration inside the SMNW – a very stark difference. The nature of this relationship might have to do with some activation energy for NPs successfully polymerizing into the nanowire during growth. From our results, it seems that the appropriate ZnO NP concentration, between 5 wt. % and 10 wt. %, provides regularly dispersed entrapment of functionalized ZnO NPs in the SMNW. Based on the advantages of PANI and ZnO NPs in bioaffinity and electrical conductivity, we suggest that this development of SMNWs shows the feasibility of ZnO NPs entrapment and the enhancement of physical properties than pure materials [103]. This method of SMNW fabrication will be applicable for a biosensor or electrical devices with further researches.

#### **4.0 PROOF OF CONCEPT FOR SINGLE POLYANILINE NANOWIRE BIOSENSOR DETECTING IMMUNOGLOBULIN-G**

Biosensors based on nanomaterials have been developed using nanowires or CNTs, presenting a fast detection time, miniaturization of device, and high sensitivity. The development of biosensor based on nanomaterials is mainly composed of the fabrication of nanomaterial and functionalization of the fabricated nanomaterial. In our research, it was presented that the single PANI nanowire and SMNW with ZnO NPs were successfully fabricated using the electrochemical deposition growth method. Those single nanowires showed the advantages of uniform dimension, high density of electrical device in unit area, and cost-efficiency in mass production. Our single PANI nanowire realizes the speedy development process reducing many tedious development processes such as selection and alignment of a nanowire from bundles. In addition, the employment of PANI for nanowire fabrication provides another advantage in the functionalization of fabricated nanowire.

For the functionalization of nanowire, the immobilization of mAbs on the nanowire surface is required to realize dense immobilization and correct orientation of mAbs for high sensitivity and good sensing reliability. Therefore, various functionalization methods such as surface immobilization or physical adsorption have been studied on nanowires [104]. However, the surface immobilization on inorganic nanowire often requires multiple chemical or physical treatments due to inorganic nanowire's low reactivity to biomolecules [105]. In this regard,

organic nanowires such as PANI and PPy are more promising candidate materials for biosensor applications. Unlike the inorganic nanowire, the organic nanowire can be functionalized relatively easily as the tunability of the doping ratio in PANI and PPy provides sufficient functional groups such as the amine groups to biomolecules [59]. Therefore, we employed the single PANI nanowire in order to develop a nanowire biosensor due to the advantages of good electrical conductivity, ease of synthesis, environmental stability, and biocompatibility [106].

In this research, we present a functionalized single PANI nanowire biosensor to detect immunoglobulin G (IgG) and cardiac biomarkers such as Myo, cTnI, CK-MB, and BNP. The single PANI nanowire-based biosensors employ the advantages of conductometric biosensing: fast detection, good specificity, and high sensitivity induced through the conductance change of nanowire without tedious processes such as sample preparation, separation, or signal filtering process required in other biosensing types such as immunoassay biosensors and amperometric biosensors [107, 108]. The single PANI nanowires were functionalized to detect target biomolecules using 1-ethyl-3-(3-dimethylaminopropyl) carbodiimide (EDC) and N-hydroxysuccinimide (NHS) with specific mAbs [109]. In the functionalization, EDC/NHS makes covalent bonds between PANI and mAbs providing the high density of immobilized mAbs on the surface of PANI nanowires and controlling the orientation of mAbs. The single PANI nanowire-based biosensors showed the high sensitivity with a very low detection limit and the good sensing linearity in response to broad concentration ranges of target proteins such as IgG and cardiac biomarkers. This method represents a novel, robust, and simple way to establish a single PANI nanowire biosensor with reliable sensing performance, cost-efficient development process, and feasibility of application to other biosensing targets. The same mechanism could be applied to different conducting polymer nanowires and various sensing targets.

## 4.1 DEVELOPMENT OF SINGLE POLYANILINE NANOWIRE-BASED BIOSENSORS

### 4.1.1 Functionalization of single polyaniline nanowire

The functionalization of single fabricated PANI nanowire is facilitated by the immobilization of mAbs on the nanowire surface using EDC, NHS, and mAbs. In advance of the functionalization, the single PANI nanowires were soaked in HCl of 0.1 M for 10 min, increasing the doped ratio on the amine functional group of PANI for the high dense immobilization of mAbs. This method involves coupling mAbs to the single PANI nanowire through a covalent bonding. A mixture solution of EDC/NHS (0.2/0.2 M) with the mAbs of target proteins was dropped on the top of the single PANI nanowires and kept for 3 hours at room temperature in a dark area. Then, the single PANI nanowires were washed using a phosphate buffer saline (PBS, 1×, pH 7.4) and de-ionized water to eliminate un-immobilized mAbs on the nanowires, SiO<sub>2</sub> layer, and Au electrodes. The various concentrations of mAbs with 50 µg/mL, 100 µg/mL, and 200 µg/mL were tested for the optimal functionalization in order to obtain a biosensor with a higher sensitivity and a linear sensing profile. The covalently coupled mAbs on the single PANI nanowire play a role to detect the target proteins and induce the conductance change in the single PANI nanowire after the target proteins are bound to the mAbs. After surface immobilization, the single PANI nanowires were then soaked in a high concentration BSA (2 mg/mL) for 30 minutes to block the non-specific protein's interaction on the nanowire surface. The processes from the nanowire fabrication to the developed single PANI nanowire-based biosensors are illustrated in Figure 12.

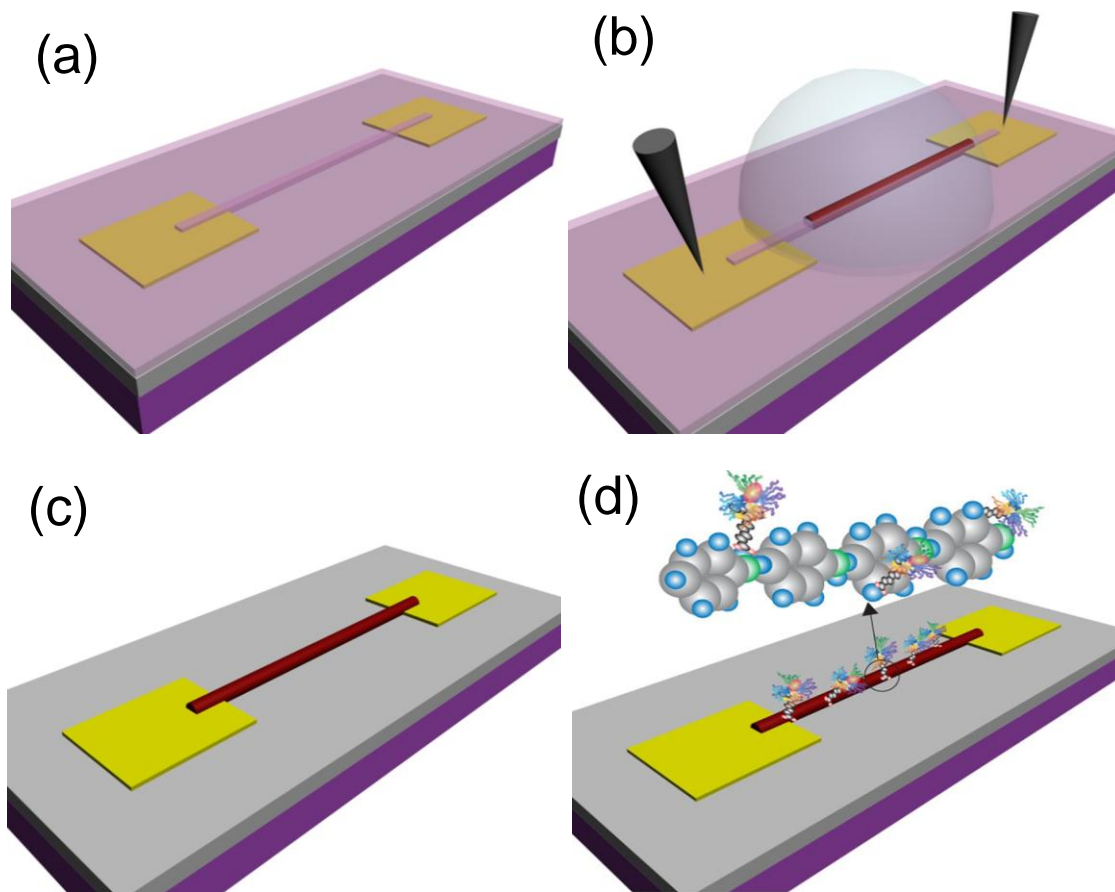


**Figure 12.** Development of the single PANI nanowire-based biosensors. (a) Preparation of a nanochannel using e-beam lithography between Au electrodes on Si/SiO<sub>2</sub> substrate. (b) Fabrication of a single PANI nanowire along the nanochannel from an ionized aniline solution. (c) The fabricated single PANI nanowire after removal of PMMA layer. (d) The functionalized single PANI nanowire with the mAbs via the surface immobilization process.

To test the capability of our PANI nanowire biosensor in the detection of various cardiac biomarkers at lower cost, we first employed IgG mAbs to sense IgG proteins. In order to verify the surface immobilization of IgG mAbs on the single PANI nanowire, the Texas Red labeled IgG mAbs were functionalized on the single PANI nanowires, and those nanowires were imaged under a fluorescence microscope (Axioskop 2 MAT, Carl Zeiss) using a camera (AxioCamMRC5, Carl Zeiss) attached to the scope and the software of AxioVision Rel 4.2. Additionally, SEM and Raman spectroscopy were used to study changes in surface morphology and chemical structure on the nanowires before and after the functionalization, respectively.

#### **4.1.2 Preparation of microfluidic channel**

The microfluidic channel was fabricated using polydimethylsiloxane (PDMS, Sylgard 184, Dow Corning Corp.) and negative photoresist (SU-8 2050, MicroChem Corp.). The designed mold for the microfluidic channel was lithographically patterned and developed on a 4" Si/SiO<sub>2</sub> wafer with a 100 μm thick negative photoresist. The prepared PDMS was poured on the mold of the microfluidic channel and cured in an oven at 80 °C for 45 minutes. The microfluidic channel of PDMS was adhered on a nanowire biosensor chip with O<sub>2</sub> plasma treatment (250 mT, 30 W, 30 seconds). The functionalized PANI nanowires were covered by a bioshielding mask to protect them from the direct bombardment of ions in the plasma condition. The single PANI nanowires-based biosensor integrated with the microfluidic channels were tested by infusing PBS, BSA, or target protein solutions by a syringe pump. The flow rate of injections was set at 0.03 mL/min to keep a laminar flow in the micro-tube and microfluidic channel to avoid breakage of the nanowire or fluctuant signal in the conductance measurement from a turbulent flow. The concept of a nanowire biosensor with a microfluidic channel is depicted in Figure 13.

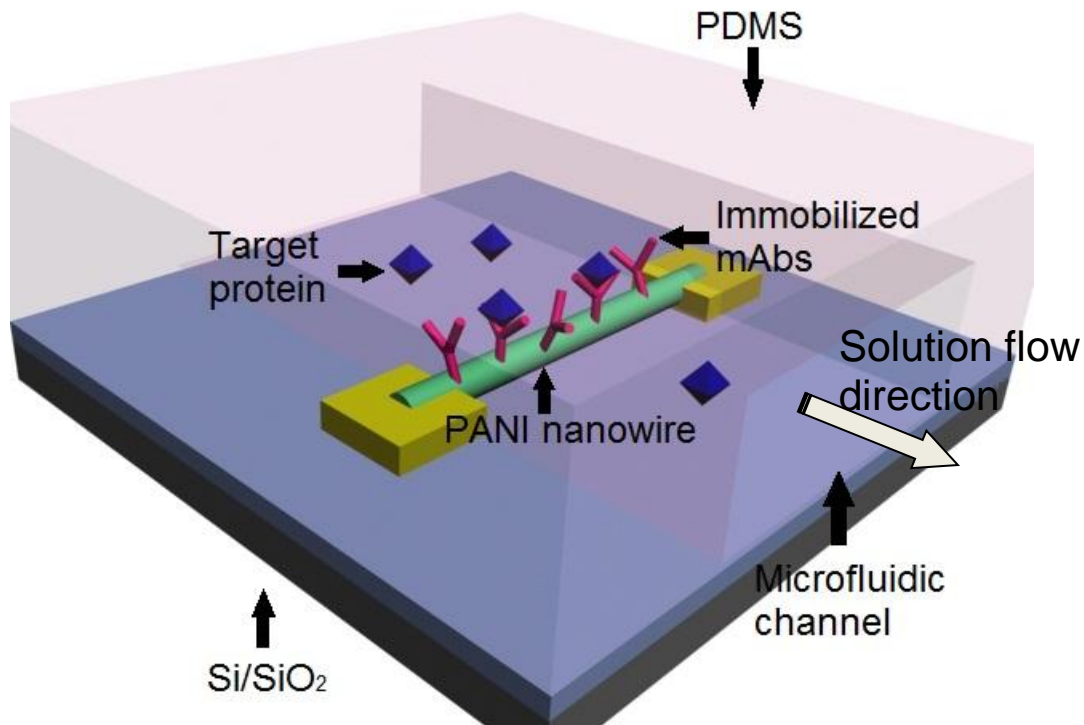


**Figure 13.** A single PANI nanowire-based biosensor integrated with a microfluidic channel. The functionalized nanowire with antibodies shows the change of conductance upon binding target proteins. Integration of a microfluidic channel regulates introduction of protein solution onto the nanowire active area only with the control of laminar flow. The microfluidic channel and flow injection prevent nanowire from breakage during biosensing and reduce non-specific binding on electrodes.

The solutions of PBS, BSA, or target protein flowed through the microfluidic channel to avoid spread and leakage of flow to electrodes. After the integration of the microfluidic channel on the single PANI nanowire biosensor, the semiconductor analyzer connected to the nanowire biosensor for conductance measurement using a probe station or wire-bonded chip, where the nanowire biosensor was mounted on, and the probes were then connected to the electrodes extended from both ends of a nanowire. The injection and withdrawal of the solutions were carried out using syringe pump controller, syringe pump, and micro tube connecting between microfluidic channel and syringe.

#### **4.1.3 Measurement of conductance change to sense target proteins**

The functionalized single PANI nanowires were used to detect target proteins of IgG or cardiac biomarkers in a broad range from a single fg/mL to a single  $\mu\text{g/mL}$  by measuring the conductance change at room temperature ( $23 \pm 2$  °C). The bio-activity of an antigen or antibody is dependent on the temperature. But, it is ignorable that the biosensing is carried out in the small variance of temperature like  $\pm 2$  °C [110]. For experimental setup, the biosensing on the functionalized single PANI nanowires-based biosensors were carried out three different ways of direct droplet on the nanowire, employment of microfluidic device with a probe station, and integrated biosensor system without a probe station.

The direct droplet way is to measure the nanowire conductance change without microfluidic device. The conductance measurement was carried out from a nanowire biosensor covered by a droplet of solution. This measurement showed physical fluctuant signals from dropping a solution on the nanowire. The employment of microfluidic device is to mount the single PANI nanowires-based biosensors, which is connected to a microfluidic device, on a

probe station as shown in Figure 14 (a). In order to inject PBS or target protein solutions such as IgG, BSA or cardiac biomarkers, a micro-tube is connected from an inlet of the microfluidic channel to the syringe pump. Another micro-tube is connected with the other end of the microfluidic channel as an outlet to withdraw PBS or target protein solutions as shown in the inset of Figure 14 (a). The integrated biosensor system was built using a microfluidic device, a printed circuit board, rotary switches, a chip carrier, a chip carrier connector, triaxial cable connectors, and an aluminum shield box as shown in Figure 14 (b). The image of wire-bonded PANI nanowires with microfluidic device was indicated by arrow from Figure 14 (b). The single PANI nanowires-based biosensors were wire-bonded between electrode pads and pads of chip carrier. This integrated system is expected to reduce sensing noise due to direct connection between nanowires and semiconductor analyzer. The all measurements were carried out applying a static current of 50 nA – 50  $\mu$ A, depending on the conductivity of the functionalized PANI nanowires, with a sampling ratio of 2 Hz. In addition, the single nS scale of semiconductor analyzer makes possible the high sensitivity of nanowire biosensor to detect very small change of conductance in biosensing. In conductometric biosensing on a single PANI nanowire, first, a baseline of conductance was obtained by flowing PBS solution (mark a) as shown in Figure 14 (c). Once the conductance was stabilized in 300 sec after injection of PBS solution into the microfluidic channel, the high concentration of BSA (mark b) was applied for the test of specificity in the nanowire biosensor. When the solution reaches the PANI nanowire and fills out the microfluidic channel, the conductance of nanowire shows little change from the baseline of conductance, indicating that the PANI nanowire biosensor shows good specificity not to respond to non-specific proteins. However, the injection of the target biomarker (mark c) shows clear

change of conductance value by the binding of mAbs with target biomarkers as depicted in an inset of Figure 14 (c).

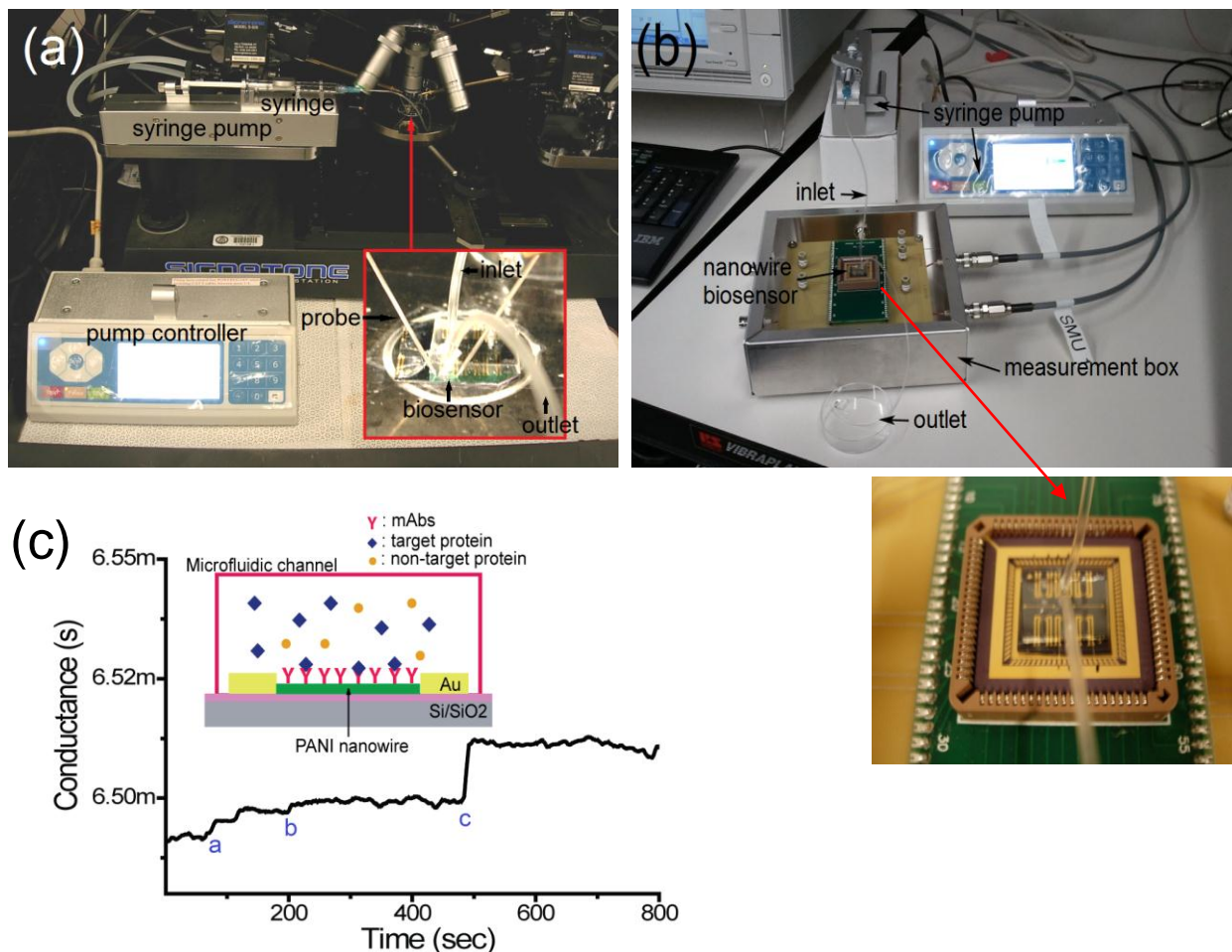


**Figure 14.** Experimental set-ups and illustration of single PANI nanowire biosensor to detect cardiac biomarkers. (a) The experimental setup; the microfluidic channel is adhered on the nanowire biosensor and the nanowire biosensor chip is mounted on a probe station connecting to semiconductor analyzer and syringe pump with inlet and outlet. (b) The integrated biosensor system includes a printed circuit board, a chip carrier, and wire-bonded PANI nanowires-based biosensor with microfluidic device in an aluminum shield box. This system is connected to the semiconductor analyzer. (c) The conductance change in the single PANI nanowires-based biosensors is monitored. The injection of PBS (mark a), BSA (mark b), and cardiac biomarker (mark c) shows the different change of conductance.

## 4.2 RESULTS AND DISCUSSIONS

The functionalization of the PANI nanowire affects the performance of a nanowire biosensor according to the density and orientation of immobilized mAbs [111, 112]. The density and orientation of immobilized mAbs on the surface of nanowire may show different results for sensitivity, sensing linearity, and specificity [113]. Therefore, it is important to decide a suitable method to functionalize nanowire which takes the nanowire materials into account. Generally, the two main categories of functionalization methods are physical immobilization and covalent immobilization. The physical immobilization method attaches mAbs on the nanowire surface via intermolecular forces such as ionic bonds or hydrophobic-polar interactions [112]. Though the functionalization can be easily carried out using this method without a chemical or physical treatment on the nanowire surface, this method has the drawbacks such as the random orientation of mAbs and weak attachment of immobilized mAbs, since each biomolecule tends to minimize the repulsive interaction with a substrate and previously adsorbed biomolecules. On the other hand, the covalent immobilization provides precise immobilization of mAbs on selected areas to form a chemical chain between the ends of the mAbs and the exposed functional groups on the nanowire surface. This covalent immobilization method requires more processing to couple the mAbs and the nanowire. However, it provides the strong immobilization of the mAbs and allows controlling the orientation of the immobilized mAbs. Therefore, the surface immobilization method using EDC/NHS, one type of the covalent immobilization, has often been employed for the functionalization of PANI nanowire and is employed in this study [114, 115].

### 4.2.1 Functionalization of polyaniline nanowires with IgG mAbs

In order to verify the functionalization of the single PANI nanowire, several techniques such as SEM, fluorescence observation, and Raman spectroscopy were used in this research. First, the functionalization of PANI with IgG mAbs was tested on PANI thin films due to scanning of fluorescence observation and Raman spectroscopy in the large area of thin film. The functionalized PANI thin film with fluorescently labeled IgG mAbs could be observed under a fluorescence microscope, as shown in Figure 15 (a). Use of the fluorescent dyes tagged on IgG mAbs is an effective way to identify the firmly immobilized mAbs on expected areas such as PANI thin film or nanowires. The fluorescent dots are evenly distributed on the PANI thin film surface, indicating that the mAbs were successfully immobilized on the PANI thin films.

The Raman spectroscopy on the thin film shows the difference between non-surface immobilized PANI thin film and functionalized PANI thin film as shown in Figure 15 (b). The functionalized PANI thin film has the different peaks at  $1240\text{ cm}^{-1}$  and  $1638\text{ cm}^{-1}$  from the Raman spectrum for the non-functionalized PANI thin film. Hence the comparison of Raman spectra clearly shows the change of chemical structure on the functionalized PANI thin film with IgG mAbs. The detail analysis will be explained in the functionalization of single PANI nanowires.

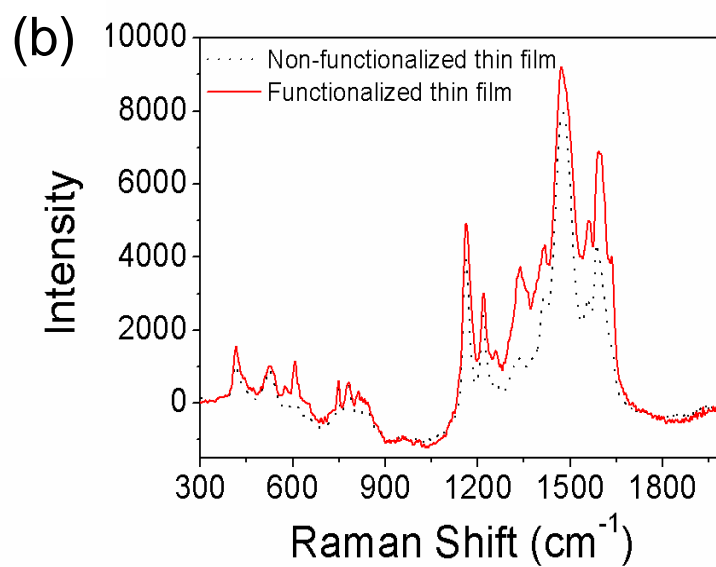
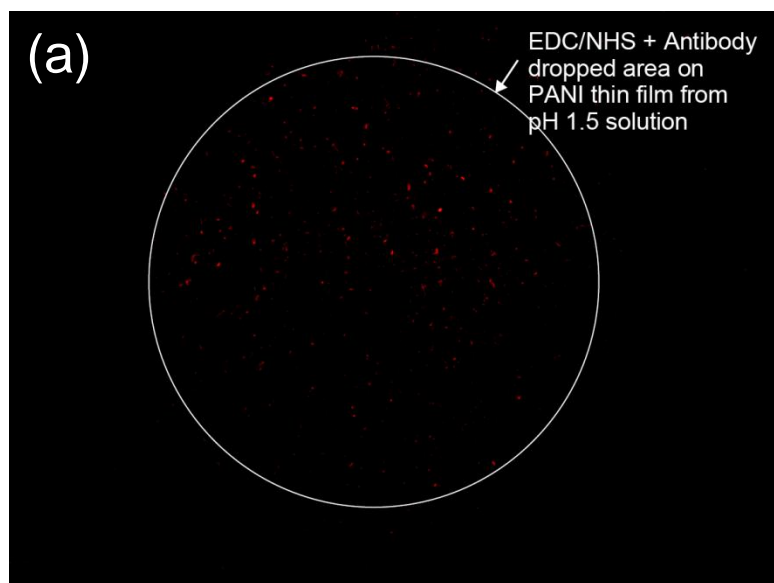


**Figure 15.** Surface immobilization with EDC/NHS and IgG mAbs on the PANI thin film. (a) The functionalized PANI thin film with IgG mAbs labeled by Texas Red fluorescent dyes. (b) The Comparison of the Raman spectra before functionalization and after functionalization of PANI thin film with IgG mAbs.

Furthermore, SEM images in Figure 16 compare the surface changes before and after the functionalization of single PANI nanowire. The non-functionalized single PANI nanowire shows a width of 105.4 nm with a smooth and clean surface as shown in Figure 16 (a). In Figure 16 (b), some particles on the nanowire after functionalization are clearly presented. Those particles were measured from 10 to 15 nm in diameter, and the surface of the functionalized single PANI nanowire became rougher than that of the non-functionalized one. In the functionalization of nanowire, several washing processes with PBS and de-ionized water eliminate un-immobilized mAbs on the nanowire surface, Au electrodes, and SiO<sub>2</sub> layer. Based on these observations in Figure 16 (b), the size of the particles is consistent with the average size of antibodies [116, 117]. Therefore, we conjecture that the immobilization of mAbs with EDC/NHS solution makes strong covalent bonds between PANI nanowire and mAbs from the observed nanowire surface change through the washing process of functionalization, discussed also in other research [118, 119]. For the further verification of the surface immobilization, various methods such as the characterization of chemical bonds and the observation of labeled immobilized antibodies with fluorescent materials or nanoparticles has been employed [120, 121]. In our experiments, the surface immobilization method of mAbs has been verified with fluorophore-tagged mAbs and Raman spectroscopy [65, 122].

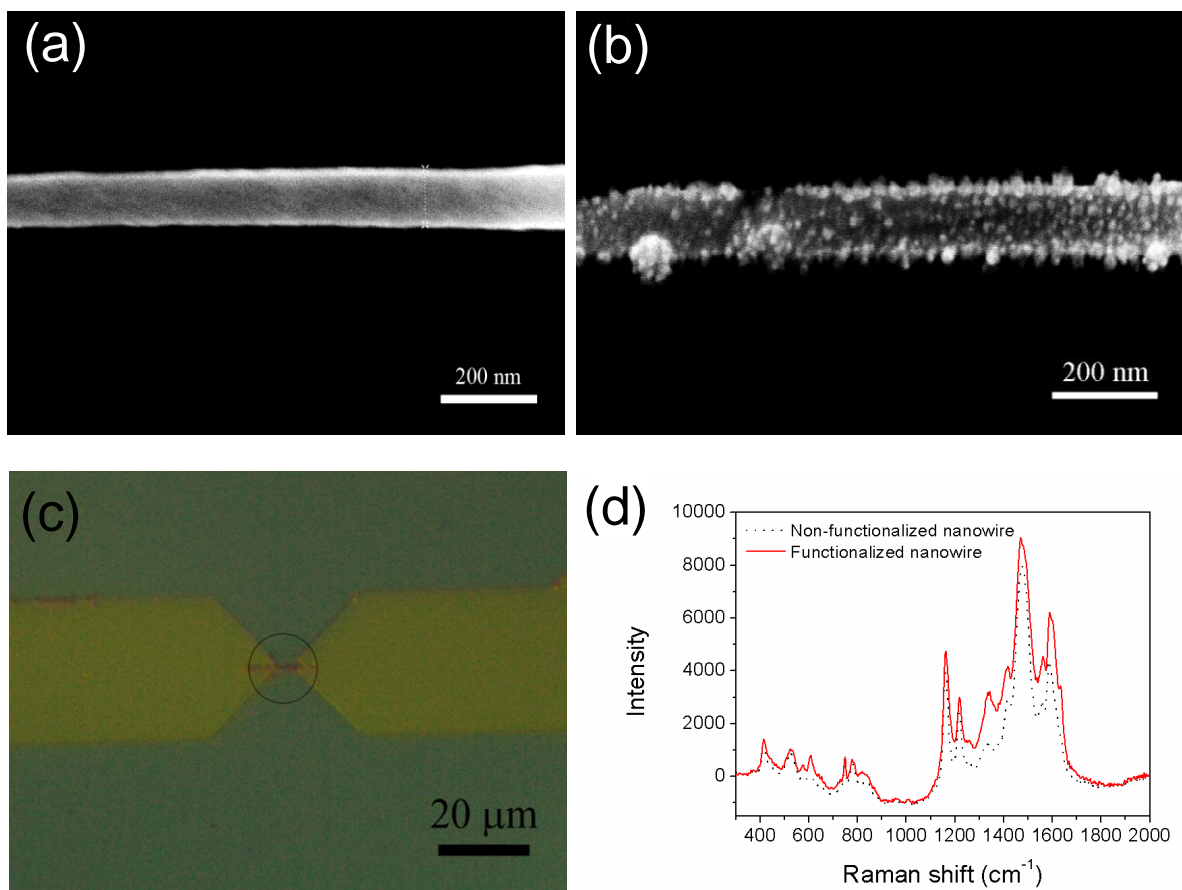


**Figure 16.** Verification for surface immobilization of IgG mAbs on the single PANI nanowires. (a) The SEM image of the non-functionalized single PANI nanowire. (b) The SEM image of the functionalized single PANI nanowire with IgG mAbs. (c) The functionalized single PANI nanowire with IgG mAbs labeled by Texas Red fluorescent materials (in a circle). (d) The comparison of Raman spectra before and after functionalization of the single PANI nanowire with IgG mAbs.

Fluorescence microscopy and Raman spectroscopy were used to characterize the functionalized single PANI nanowires with IgG mAbs. As shown in Figure 16 (c), red fluorescence is only seen on the region of the single PANI nanowire between the electrodes, being emitted from the fluorescent dyes on the IgG mAbs that were immobilized on the nanowire surface via the functionalization process. The agglomeration of IgG mAbs on the nanowire surface makes the tiny fluorescent emission visible via UV microscopy. In addition, the fluorescence of IgG mAbs were not observed other un-expected areas of Au electrodes or SiO<sub>2</sub> layer. Therefore, the surface immobilization of EDC/NHS works on the only PANI as observed in Figure 16 (c).

Raman spectra before and after the functionalization of the single PANI nanowires are compared in Figure 16 (d). The Raman spectrum of the non-functionalized PANI nanowire has typical peaks of doped PANI on 1590 cm<sup>-1</sup> (C=C bonding), 1480 cm<sup>-1</sup> (C=N bonding), 1431 cm<sup>-1</sup> (C-C stretching), 1220 cm<sup>-1</sup> (C-N stretching), 1165 cm<sup>-1</sup> (in-plane C-H bending), 840 cm<sup>-1</sup> (Amine deform), 779 cm<sup>-1</sup> (Ring deform), and 750 cm<sup>-1</sup> (Imine deform) [95]. The Raman spectroscopy of the PANI nanowire after the functionalization presents new peaks at 1638 cm<sup>-1</sup> and 1240 cm<sup>-1</sup>, which represent the chemical structure of Amide I (1638 cm<sup>-1</sup>) and Amide III (1240 cm<sup>-1</sup>) in IgG mAbs [123]. However, the Amide III band of IgG mAbs at 1240 cm<sup>-1</sup> in the single PANI nanowire has a relatively weak peak due to the strong intensity of Raman spectrum from the single PANI nanowire at 1220 cm<sup>-1</sup> after the functionalization. These characterizations confirmed the successful immobilization of IgG mAbs on the single PANI nanowire. Therefore, in this research, we have developed a successful functionalization method with EDC/NHS to utilize a single PANI nanowire biosensor for the detection of IgG or cardiac biomarkers.

#### 4.2.2 Functionalization mechanism of polyaniline

The amine functional group in PANI is compatible with biomolecules due to the possibility of electrostatic interactions between PANI and biomolecules. Therefore, many research groups have developed physical immobilization without any assist from cross-linker such as EDC/NHS and glutaraldehyde (GA) [124]. However, the covalent immobilization method has been employed more frequently than the physical immobilization due to random orientation and distribution of immobilized mAbs. In order to solve the random orientation of immobilized mAbs, various covalent immobilization methods such as the surface immobilization have been researched [125, 126]. The surface immobilization methods for conducting polymers of PANI and PPy have been developed using EDC/NHS or GA [127, 128]. EDC/NHS or GA provides cross-linkages between the conducting polymers and bioreceptors such as mAbs or aptamer. The cross-linker can be chosen along the different chemical structure of functional groups in the conducting polymer and the end of mAbs. In this research, the PANI nanowire has a doped structure, as verified in Raman spectroscopy of Figure 9 and Figure 16. The amine functional group in the doped PANI can be easily modified to couple with mAbs via a cross-linker such as EDC/NHS or GA [111, 114]. The selective covalent bonds between the functional groups at the nanowire surface and bioreceptor provide the suitable orientation of immobilized bioreceptors by the appropriate selection of cross-linker. It will be elucidated the functionalization mechanism of PANI nanowire using EDC/NHS with comparing the function of GA.

At the end of biomolecules, there are different kinds of the functional groups such as  $\text{-NH}_2$ ,  $\text{-SH}$ ,  $\text{-COOH}$ , or  $\text{-OH}$ . Each different cross-linker such as EDC/NHS or GA has different reactivity with functional groups depending on the concentration of the cross-linker, the order of the treatment process, or the environmental condition [124]. EDC/NHS, which is employed in

the functionalization of single PANI nanowire, is generally known to modify the  $\text{-COOH}$  in mAbs, then to connect the modified  $\text{-COOH}$  to the  $\text{-NH}$  of PANI. These reactions are illustrated in Figure 17 (a). The EDC/NHS solution with mAbs provides good orientation of the immobilized mAbs and strong covalent bonding [129]. However, it is difficult for EDC/NHS without mAbs to functionalize PANI for immobilization of mAbs due to the absence of a  $\text{-COOH}$  on PANI. In addition, the individual treatment process of EDC and NHS on PANI instead of mixture of EDC/NHS with antibodies does not help to modify  $\text{-COOH}$  for the immobilization of mAbs on PANI. If there is no introduction of NHS, the modified  $\text{-COOH}$  by EDC will make the EDC return to its original structure due to the instability of the modified  $\text{-COOH}$  group. Therefore, the mixture of EDC/NHS with mAbs makes a stable structure of modified  $\text{-COOH}$  group, and the concentration of EDC/NHS was optimized to tune the ratio between both concentrations [114]. In the case of tuning the mixture ratio in EDC/NHS, when either EDC or NHS has the higher concentration than the other, EDC/NHS modification makes a byproduct formation not to link between mAbs and EDC/NHS. In other research, the mixture of EDC/NHS with 1:1 ratio provided an optimal condition for the immobilization of mAbs [114].

Another surface immobilization involves employing GA to modify the  $\text{-NH}$  on PANI [111, 118]. The symmetric structure of GA links its  $\text{-COH}$  group to the  $\text{-NH}$  of PANI, as shown in Figure 17 (b). Then, the other end of GA links to the amine functional group of a biomolecule such as aptamer. On the other hand, the mAbs have basically a  $\text{-COOH}$  on the bottom of mAbs and  $\text{-NH}_2$  on the top of mAbs, as shown Figure 17 (a). Therefore, the employment of GA in surface immobilization may reduce the immobilization of mAbs and result in low sensitivity due to the linkage between the top of mAbs and the amine functional group in PANI. In this research, the EDC/NHS solution with mAbs provides strong covalent bonding between mAbs and PANI,

as verified in the fluorescence observation, SEM, and comparison of Raman spectra as presented in chapter 4.2.1 .

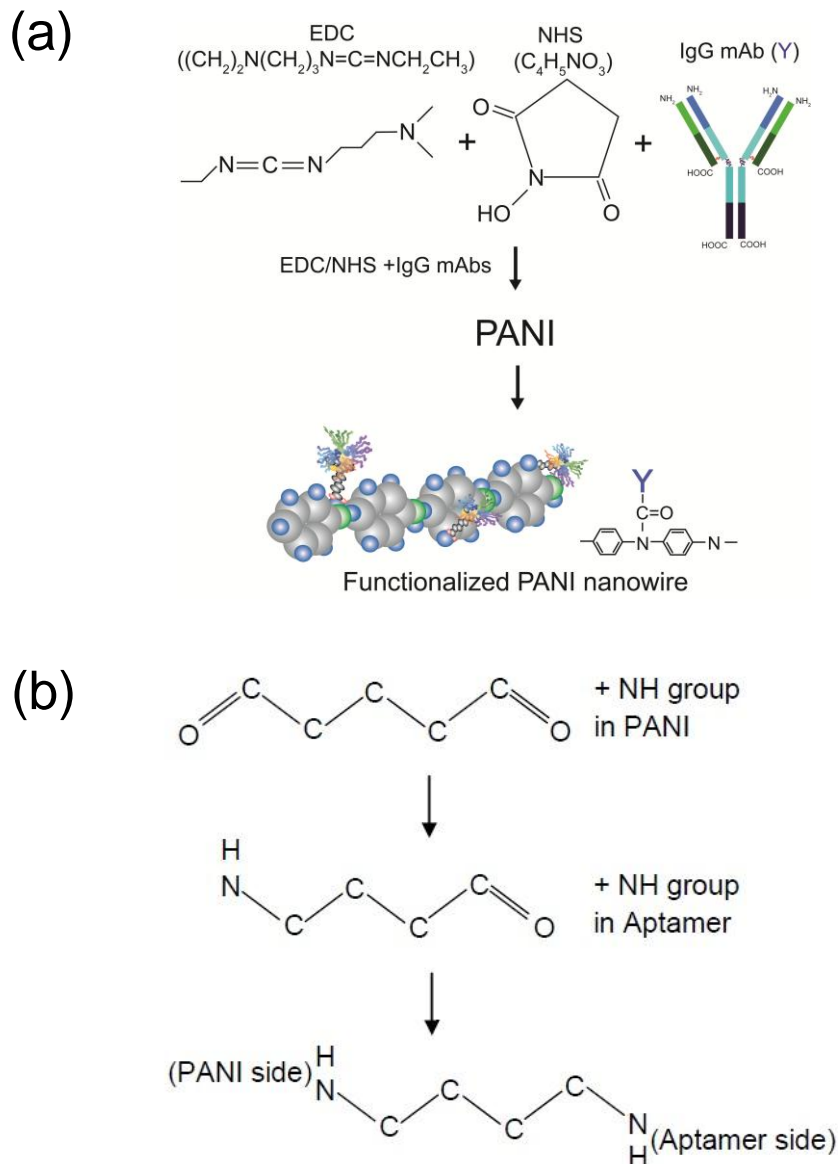


**Figure 17.** Functionalization mechanisms of EDC/NHS and GA. (a) EDC/NHS with mAbs modifies –COOH at the end of mAbs and couples to –NH of PANI. (b) The symmetric structure of GA links –NH of PANI to –NH of aptamer.

### 4.2.3 Preliminary biosensing of Immunoglobulin G

In order to confirm the functionality of single PANI nanowire biosensors, various tests were carried out on the non-functionalized and functionalized PANI nanowires for IgG detections as shown in Figure 18. The non-functionalized PANI nanowire shows no changes of conductance to PBS (pH 7.4), BSA (10  $\mu\text{g/mL}$ ), and IgG, which indicates a non-response to PBS and proteins, indicating the non-sensitivity of the non-functionalized PANI nanowire, as shown in Figure 18 (a). Figure 18 (b) shows the increasing conductance from the functionalized single PANI nanowire with IgG mAbs; the conductance increases with the injection of PBS due to the surface charge change induced from the net electrical charge of IgG mAbs. As can be seen from Figure 18 (b), there is no response to an injected BSA (50  $\text{ng/mL}$ ) and a distinct response to IgG (33  $\text{ng/mL}$ ), showing a good specificity of the biosensor to IgG. In Figure 18 (c), in sensing different concentrations of IgG, the functionalized single PANI nanowire with IgG mAbs of 100  $\mu\text{g/mL}$  shows stepwise changes along different concentrations of IgG, detecting the lowest level for the IgG of 5  $\text{ng/mL}$  and exhibiting no response to the BSA of 5  $\mu\text{g/mL}$ . These all sensing of IgG on single PANI nanowires were carried out by the direct droplet measurement, which is to measure the conductance change after dropping protein solutions on the nanowire.

We further investigated the effects of various IgG mAb concentrations (50  $\mu\text{g/mL}$ , 100  $\mu\text{g/mL}$ , and 200  $\mu\text{g/mL}$ ) for the sensitivity of functionalized single PANI nanowire in addition to the optimization of functionalization condition as plotted in Figure 18 (d), with a  $\Delta\text{G}/\text{G}_0$  ( $\Delta\text{G}$ : absolute value of conductance change,  $\text{G}_0$ : initial conductance in PBS) scale for the sensitivity and a log scale for IgG concentration. The sensitivity of IgG biosensing is varied from 0 to 4; it means that the conductance change can increase maximum four times from initial conductance value of single PANI nanowire in PBS solution. From the result, the single PANI nanowire

biosensor using IgG mAbs of 50  $\mu\text{g/mL}$  shows  $\sim 0.4$  change at the low IgG concentration (10  $\text{ng/mL}$ ). However, the sensitivity saturates at  $\sim 0.5$  as soon as high IgG concentration (300  $\text{ng/mL}$  – 2  $\mu\text{g/mL}$ ) is reached. On the other hand, we observed that when using IgG mAbs of 100  $\mu\text{g/mL}$ , the single PANI nanowire shows noticeable changes along a wide range of IgG concentrations (3  $\text{ng/mL}$  – 3  $\mu\text{g/mL}$ ); better than the sensitivity under the functionalization condition with IgG mAbs of 50  $\mu\text{g/mL}$ . Additionally, the conductance change was as high as the sensitivity of 3.0, which is the conductance increase from the initial conductance value by three times, at the highest IgG concentration (3  $\mu\text{g/mL}$ ). The single PANI nanowire biosensor using IgG mAbs of 200  $\mu\text{g/mL}$ , on the other hand, had relatively low sensitivity and showed only a small difference at the low concentration range (5  $\text{ng/mL}$  – 100  $\text{ng/mL}$ ) and high concentration range (100  $\text{ng/mL}$  – 3  $\mu\text{g/mL}$ ) of IgG. Based on this observation, we conclude that the immobilization with IgG mAbs of 100  $\mu\text{g/mL}$  provides the most effective number of the immobilized mAbs on the PANI nanowire surface, avoiding the insufficiency of detection with IgG mAbs of 50  $\mu\text{g/mL}$  or the insensitivity that might be caused by the agglomeration of mAbs from the excessive immobilization with IgG mAbs of 200  $\mu\text{g/mL}$ . Therefore, the optimal functionalization condition of the single PANI nanowire biosensor for IgG detection is IgG mAbs of 100  $\mu\text{g/mL}$  with demonstrating the high sensitivity and the good sensing linearity from a single  $\text{ng/mL}$  up to a  $\mu\text{g/mL}$  scale. Therefore, this proof-of-concept work done with IgG could be applied for the single PANI nanowire-based biosensors in the practical applications for the detection of cardiac biomarkers such as for Myo, cTnI, CK-MB, and BNP sensing, which are important biomarkers for the cardiac disease diagnosis.

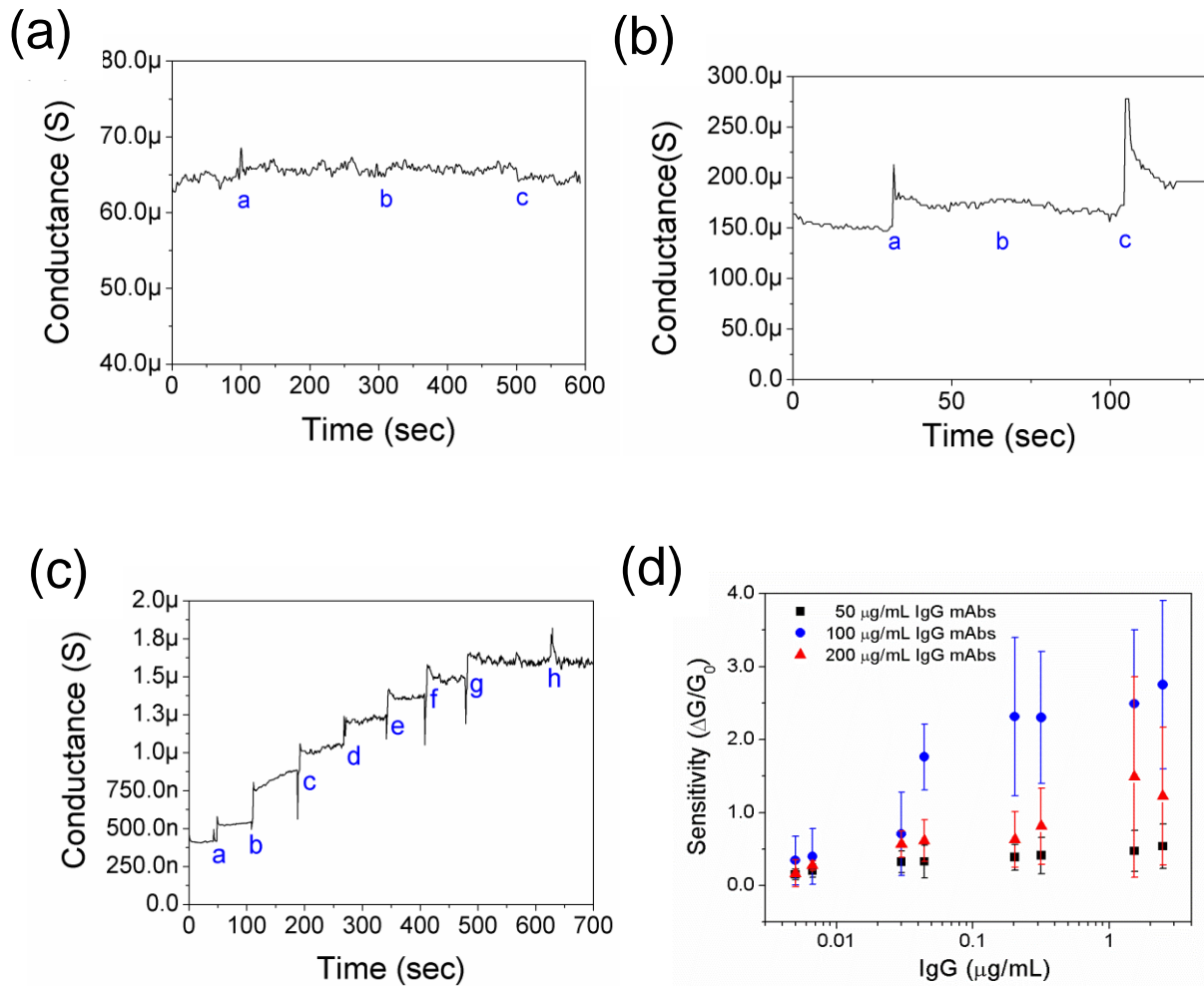


**Figure 18.** IgG sensing on single PANI nanowire biosensors. (a) The measurement of conductance changes on a single non-functionalized PANI nanowire (a: PBS, b: BSA of 10  $\mu$ g/mL, and c: IgG of 3.3  $\mu$ g/mL). (b) The specificity tests of a functionalized single PANI nanowire with IgG mAbs (a: PBS, b: BSA of 50 ng/mL, and c: IgG of 33 ng/mL). (c) The detection of IgG on a single PANI nanowire biosensor (a: IgG of 5 ng/mL, b: IgG of 37 ng/mL, c: IgG of 54 ng/mL, d: IgG of 242 ng/mL, e: IgG of 368 ng/mL, f: IgG of 1.74  $\mu$ g/mL, g: IgG of 2.78  $\mu$ g/mL, and h: BSA of 5  $\mu$ g/mL). (d) The sensitivity of the single PANI nanowire biosensors with various concentrations of IgG mAbs (50, 100, and 200  $\mu$ g/mL).

### 4.3 SUMMARY

The development of the single PANI nanowire biosensor in this research includes the surface immobilization of mAbs and measurement of conductance change in the functionalized single PANI nanowires. The single PANI nanowire biosensors, which were prepared through the electrochemical deposition growth method and surface immobilization of mAbs, show the high addressability for mass-production and dimensional uniformity for performance reliability. In addition, the surface immobilization on PANI alleviates the necessity of pre-treatment on a sample including nanowires for increasing bio-compatibility as well as a passivation layer to prohibit non-specific binding of biomolecules. We employ this development process of the single PANI nanowire biosensor, which was verified in the IgG biosensing, for the detection of cardiac biomarkers, and they show promise in the diagnosis of other diseases as well. The single PANI nanowire-based biosensors testing with IgG demonstrates the feasibility of point-of-care systems with high sensitivity, cost efficiency, and fast response for the detection of cardiac biomarkers.

## 5.0 BIOSENSING OF CARDIAC BIOMARKERS

The proof-of-concept studies in the functionalization of single PANI nanowires and IgG biosensing are applied for the detection of cardiac biomarkers such as Myo, cTnI, CK-MB, and BNP in this work. The single PANI nanowire-based biosensors for cardiac biomarkers detection were tested with the various concentrations of target biomarkers and non-target proteins. When the immobilized mAbs on the nanowire bind target proteins, the single PANI nanowires show either an increase or decrease of conductance depending on the charge of the target proteins and types of nanowires. The charged complexes of mAbs and target proteins induce major carrier accumulation or depletion in the nanowires. While conventional methods like immunoassay require at least a few hours to incubate the complex of mAbs and antigens [66], the conductance measurement requires only a few minutes and can realize the label free detection. In addition, integrating the microfluidic channels on the nanowire biosensors allows us to sense more accurately with showing very low detection limits and inject protein solutions at a slow flow rate onto only the active area of the PANI nanowire [67]. In this chapter, the detection of Myo, cTnI, CK-MB, and BNP are presented the ultra-high sensitivity to target proteins, linear sensing profile in the wide range of target proteins' concentration, and good specificity to detect only target proteins. The successful biosensing on the single PANI nanowire biosensors can be applied for the diagnosis of other biomarkers in the future and provide preliminary research to realize point-of-care system with label free detection.

## **5.1 APPLICATIONS OF SINGLE POLYANILINE NANOWIRES**

### **5.1.1 Detection of Myo, cTnI, CK-MB, and BNP**

Myo, cTnI, CK-MB, and BNP are considerably selected as biomarkers for the diagnosis of myocardial infarction [36, 38, 39]. Among these cardiac markers, Myo is a basic protein to check at the onset of infarction [36, 40]. However, it has the cross-activity with skeletal muscle pain. Therefore, it is necessary to monitor the level of other proteins such as cTnI, CK-MB, and BNP in patients' serum for the accurate, prompt and continuous diagnosis of myocardial infarction [37-39]. cTnI is only specific to cardiac muscles and never found in a healthy people [41]. CK-MB and BNP are related to recurrence of myocardial infarction and cardiac vascular disease, respectively. Therefore, the detection of cTnI, CK-MB, or BNP is valuable for people who suffer from heart failure [37, 39]. In this research, we present the detection of Myo, cTnI, CK-MB, and BNP using the single PANI nanowire-based biosensors, satisfying the requirements for the diagnosis of heart failure from very low concentration of target biomarkers to high concentration with good biosensing specificity.

### **5.1.2 Single polyaniline nanowires FETs**

The development of prompt diagnostic system has been demanded strongly with high sensitivity, portability, easy operation and cost efficiency. Considering the conventional biosensors, the most of them have limitations to realize the portability with miniaturization and the cost efficiency in manufacturing process or detecting targets. However, the conductometric measurement using nanowires or CNT shows the high yield in mass production with semiconductor process,

miniaturization with high density of nanowires or CNTs, and easy operation in measurement of conductance change. Therefore, the nanowire or CNT biosensor have been studied enthusiastically showing the enhanced sensing performance and the realization of miniaturization [19]. However, the drawbacks of selection and alignment of single nanowire or CNT have disturbed the high density of biosensor in small area. Another issue in nanomaterial-based biosensor is irregular sensing reliability from different size of nanomaterials. For good sensing reliability in nanomaterials biosensor, the nanomaterials such as nanowire or CNT should show the uniform doping concentration, carrier mobility, and dimension from an established fabrication method. Therefore, the development of nanowire FET is useful to reveal those physical properties of the single PANI nanowire and analyze quantitatively the nanowire biosensing for the further research.

The physical properties of nanowire can be determined measuring FET characteristics. The scanning of  $I_{\text{Drain}}$  vs  $V_{\text{Drain}}$  and  $I_{\text{Drain}}$  vs  $V_{\text{Gate}}$  from nanowire FETs reveals the doping concentration and carrier mobility of nanowire. Those physical properties of nanowire can be tuned in the fabrication method of nanowire or post-treatment on the fabricated nanowire depending on the purpose of applications [130]. In the conductometric biosensing of nanowire FET, the modulation of conductance helps to improve biosensing sensitivity with the additional control of conductive area in nanowire. In addition, the switching mode of nanowire FET is useful to increase the signal to noise (S/N) ratio at the very low concentration of target biomarkers holding in the subthreshold regime of nanowire FET [131]. Those advantages of nanowire FET can help to improve the biosensing reliability, analyze the physical properties of nanowire, and enhance the sensitivity and S/N ratio. Therefore, the single PANI nanowire FETs were studied with a back gate on the fabricated single PANI nanowire.

## 5.2 RESULTS AND DISCUSSIONS

### 5.2.1 Biosensing performance to detect cardiac biomarkers

For the detection of cardiac biomarkers, the mAbs of each cardiac biomarker (Myo, cTnI, CK-MB, and BNP) were immobilized on the single PANI nanowires using the same method introduced in the detection of IgG. The conductance changes in the single PANI nanowire biosensor for the detection of Myo, cTnI, CK-MB, and BNP were measured in the solutions of PBS, BSA, and cardiac biomarkers as shown in Figure 19. Those biosensing tests were carried out by the direct droplet measurement. In Figure 19 (a), the single PANI nanowire biosensor, functionalized with the mAbs of Myo, showed no response to a high concentration of BSA (500 ng/mL) but a clear conductance change in Myo (1.4 ng/mL), demonstrating the good specificity and high sensitivity to Myo. The Myo solution in PBS (pH 7.4) had a weak negative charge due to its pI value of 6.85 [132]. Therefore, the Myo proteins captured by the mAbs led to a negative surface charge on the p-type nanowire, which results in the increase of conductance as shown in Figure 19 (a). Other cardiac biomarkers of cTnI, CK-MB, and BNP, which have pI values of 5.2 ~ 6.5, were detected on the single PANI nanowires functionalized with each mAbs as shown in Figure 19 (b), (c), and (d), respectively [133, 134]. All detections of cardiac biomarkers had good specificity not to respond to BSA or other biomarkers and good sensitivity to show clear conductance changes. Furthermore, the developed biosensors provide a fast response time of a few seconds after applying a droplet of target protein solutions. However, the continuous detections of cardiac biomarkers in same nanowire consume the immobilized mAbs on the nanowire surface binding with target biomolecules. The conductance changes became smaller

(mark d and e) than first detection (mark c) of cardiac biomarkers as shown in Figure 19 (c) and (d).

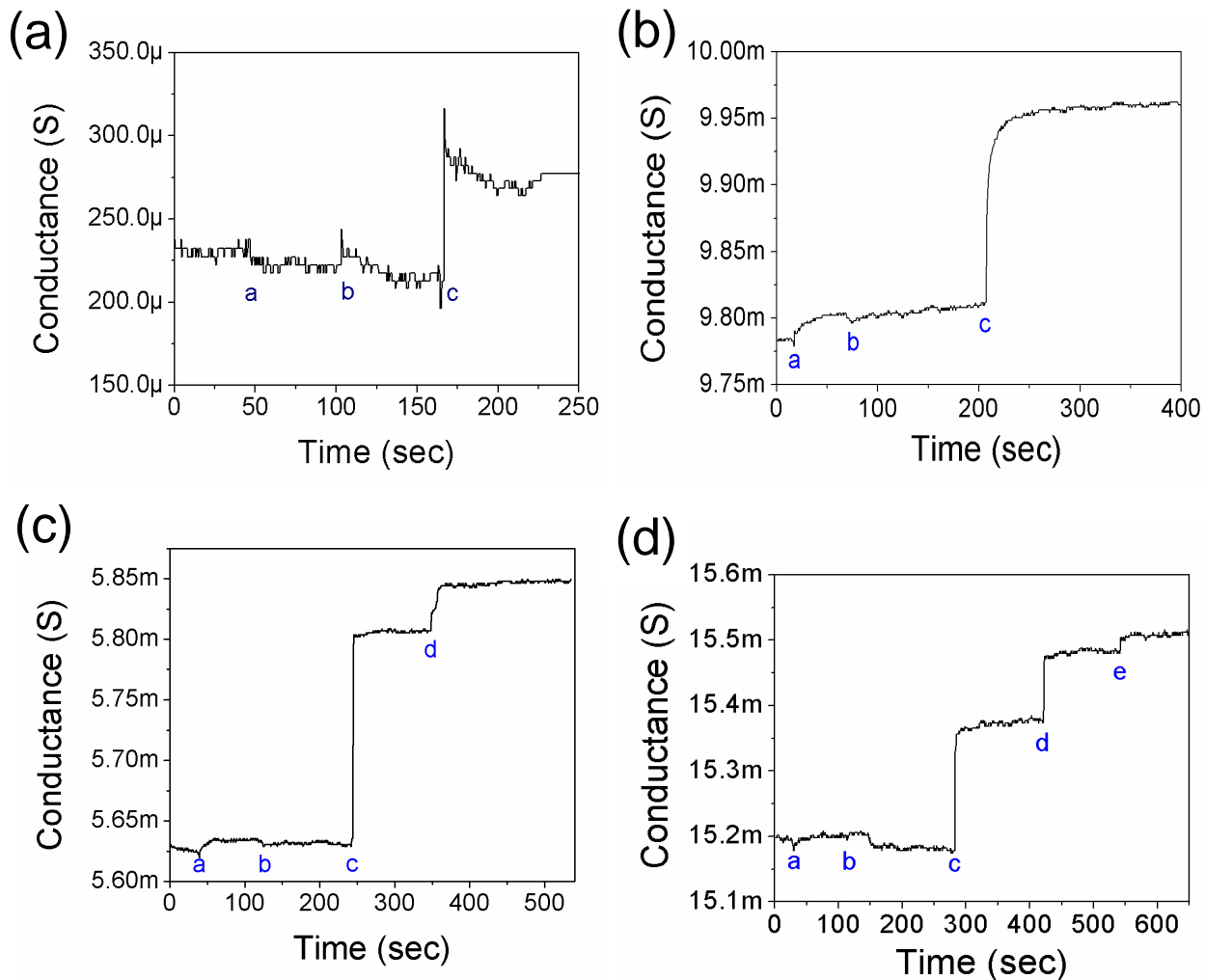


**Figure 19.** Biosensing of cardiac biomarkers on the single PANI nanowires-based biosensors by measuring conductance change under the direct droplet measurement. (a) Detection of Myo (a: PBS, b: BSA of 500 ng/mL, and c: Myo of 1.4 ng/mL). (b) Detection of cTnI (a: PBS, b: Myo of 5 ng/mL, and c: cTn-I of 300 fg/mL) (c) Detection of CK-MB (a: PBS, b: BSA of 100 ng/mL, c: CK-MB of 300 pg/mL, and d: CK-MB of 2.5 pg/mL) (d) Detection of BNP (a: PBS, b: BSA of 100 ng/mL, c: BNP of 1 ng/mL, d: BNP of 10 ng/mL, and d: BNP of 100 ng/mL)

In the biosensing of cardiac biomarkers, it is crucial that a biosensor has a broad range of detection for the diagnosis of heart disease. In order to investigate the sensing performance of the single PANI nanowire biosensors, various concentrations of Myo (5 ng/mL – 2.5  $\mu$ g/mL) and cTnI (5 pg/mL – 2 ng/mL) proteins were introduced to the single PANI nanowire biosensor as shown in Figure 20. In Figure 20 (a), the detection of Myo in the broad range of concentration shows step wise changes to the increased concentration of Myo. Similarly, the nanowire biosensor shows noticeable conductance changes along the different concentration of cTnI from the baseline of conductance in PBS (mark a) as demonstrated in Figure 20 (b). However, the continuous biosensing in the same nanowire reduces bioactivity of the immobilized mAbs and shows small step change in the high concentration (cTnI of 2 ng/mL). In the detection of CK-MB and BNP, the continuous biosensing on the nanowire shows also saturation behavior increasing the concentrations of target proteins.

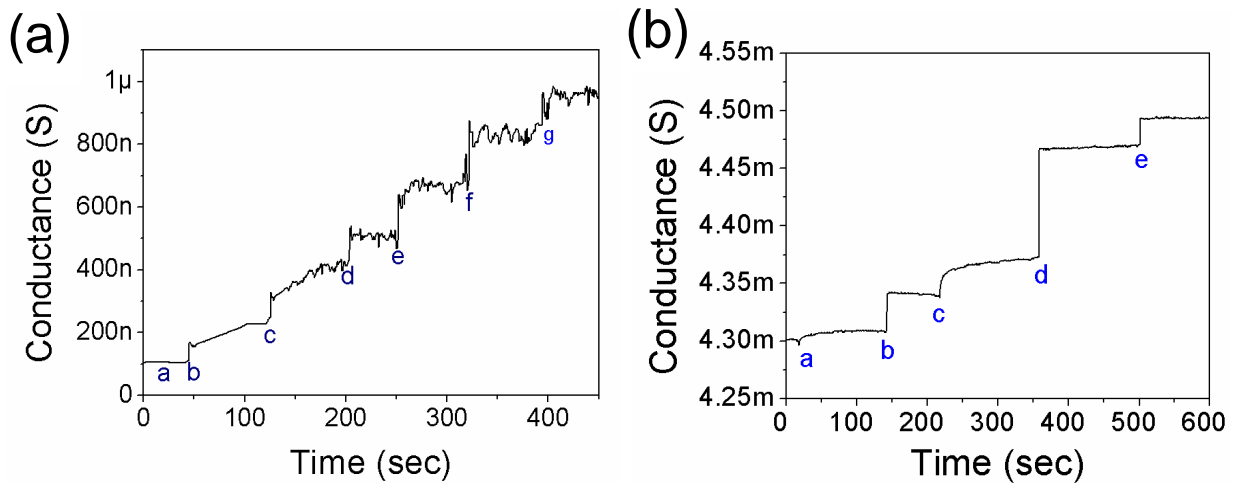


**Figure 20.** Biosensing for Myo and cTnI in the wide sensing ranges. (a) Detection of Myo on a single PANI nanowire biosensor (a: PBS, b: 5 ng/mL, c: 30 ng/mL, d: 50 ng/mL, e: 200 ng/mL, f: 350 ng/mL, and g: 2.5  $\mu$ g/mL). (b) Stepwise change of conductance to different concentration of cTnI (a: PBS, b: 5 pg/mL, c: 40 pg/mL, d: 300 pg/mL, e: 2 ng/mL).

In addition, the direct droplet measurement may result in the fluctuating signals due to physical drops on the nanowires as shown in Figure 19 and Figure 20. Therefore, it is required to integrate microfluidic devices with the single PANI nanowires after the functionalization. The integration of microfluidic channel assists accurate and reliable biosensing by directing flow of the solution only onto the active area of the single PANI nanowire, showing the smooth change of conductance and minimizing damage of nanowire with slow flow rate. The lowest detections of Myo, cTnI, CK-MB, and BNP were obtained at 100 pg/mL, 250 fg/mL, 150 fg/mL, and 50 fg/mL as demonstrated in Figure 21.

The detection of Myo with a microfluidic channel showed 100 pg/mL with the good specificity not to respond for BSA of 100 ng/mL in Figure 21 (a). This detection limit of Myo supported with the microfluidic channel is much lower than our previous result of 1.4 ng/mL and shows ultra-high specificity to BSA of 100 ng/mL [65]. For cTnI, CK-MB, and BNP, the single PANI nanowires-based biosensors had high specificity for BSA of 10 – 100 ng/mL with the ultra-high sensitivity as shown in Figure 21 (b), (c), and (d), respectively. In these tests, the specificity values, where specificity value is defined as the ratio of [highest concentration of non-specific protein showing ignorable or non-response signal] to [lowest concentration of specific protein showing significant signal change], were calculated in the range from  $1 \times 10^4$  fold in the Myo detection to  $2 \times 10^6$  fold in the BNP detection (cTnI:  $4 \times 10^5$  fold and CK-MB:  $6.7 \times 10^5$  fold). These detections of cardiac biomarkers were measured in the specific proteins without non-specific proteins; to do biosensing of cardiac biomarkers after flowing non-specific protein solution into microfluidic channels. In order to apply for practical diagnosis, it is necessary to verify sensing performance in the presence of BSA or non-target cardiac biomarkers.

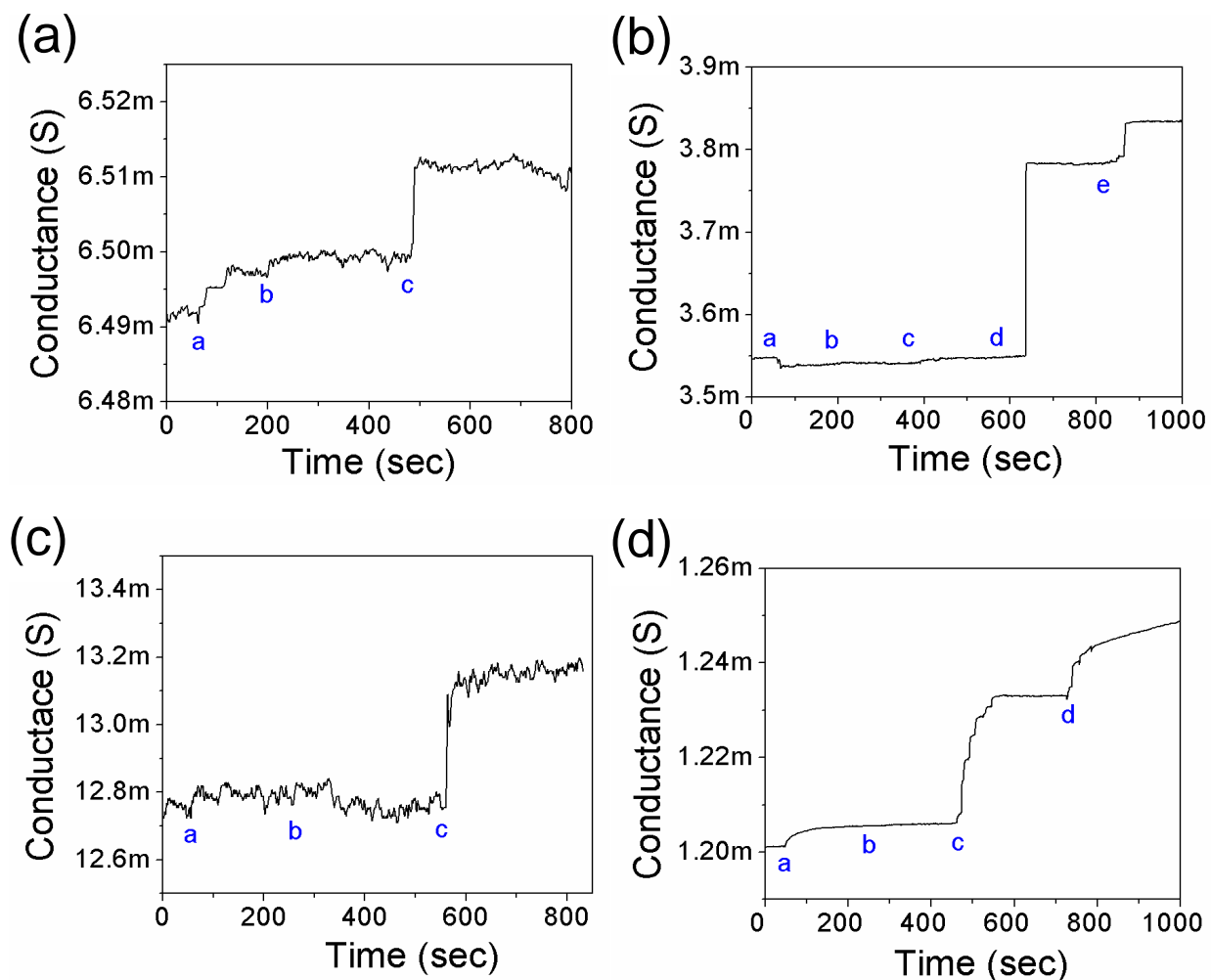


**Figure 21.** Demonstration of ultra-high sensitivity and specificity of the single PANI nanowires-based biosensors integrated with microfluidic devices. (a) The detection of Myo using microfluidic channel shows good specificity to BSA and clear response to the low concentration of Myo. (a: PBS, b: BSA of 100 ng/mL, and c: Myo of 100 pg/mL) (b) Biosensing with microfluidic channel for detection of cTnI (a: PBS, b: BSA of 10 ng/mL, c: cTnI of 5 fg/mL, d: cTnI of 250 fg/mL, and e: cTnI of 20 pg/mL). (c) Biosensing with microfluidic channel for detection of CK-MB (a: PBS, b: BSA of 10 ng/mL, and c: CK-MB of 150 fg/mL). (d) Biosensing with microfluidic channel for detection of BNP (a: PBS, b: BSA of 100 ng/mL, c: BNP of 50 fg/mL, and d: BNP of 1 pg/mL)

The presence of non-target proteins may interfere with the sensing performance due to the screening or physical absorption of non-target proteins. The detections of cardiac biomarkers with BSA may provide similar conditions to the practical diagnosis, because serum albumin is one of the most abundant proteins in human serum. On the other hand, the biosensing with other cardiac biomarkers shows functionality to detect only specific target proteins depending on the immobilized mAbs. Those biosensing of cardiac biomarkers for Myo, cTnI, CK-MB, and BNP with non-target proteins are demonstrated using the direct droplet way as shown in Figure 22 (a), (b), (c), and (d), respectively. For the detection of Myo, the other cardiac biomarkers of cTnI, CK-MB, and BNP were tested alternately on the nanowire with Myo. The single PANI nanowire-based biosensors responded to only Myo (mark c and e) with the non-responses to other cardiac biomarkers (mark b, d and f). For cTnI, CK-MB, and BNP, each nanowire biosensor was tested with BSA of 1 – 100 ng/mL followed by each target proteins showing significant conductance change (black solid line) as shown in Figure 22 (b), (c), and (d), respectively. The nanowire biosensors were tested with the addition of other cardiac biomarkers (red dash line) and show good specificity to detect only the target biomarkers. In the presence of non-target proteins, the nanowire biosensors have around  $1 \times 10^3 - 1 \times 10^6$  fold specificity values, which are lower than the specificity values in the test with the integrated microfluidic devices but acceptable for biosensing application. Non-specific binding of non-target proteins is restrained by the blocking process on the surface of nanowire after functionalization process. The concentration of BSA blocking solution (2 mg/mL) was considered to cover only the unoccupied area by mAbs without losing biosensing activity [135]. Therefore, the developed single PANI nanowire biosensors showed the feasibility of detection of cardiac biomarkers in the condition of target biomolecules with high concentration of non-target biomolecules together and satisfied the

requirements as a biosensor such as good specificity and high sensitivity. The sensitivity of single PANI nanowire biosensor means the percentage conductance change from initial conductance value in PBS solution multiplying 100 to sensitivity value. For example, if the sensitivity is 0.05, the conductance value increase or decrease from the initial conductance value by 5%.

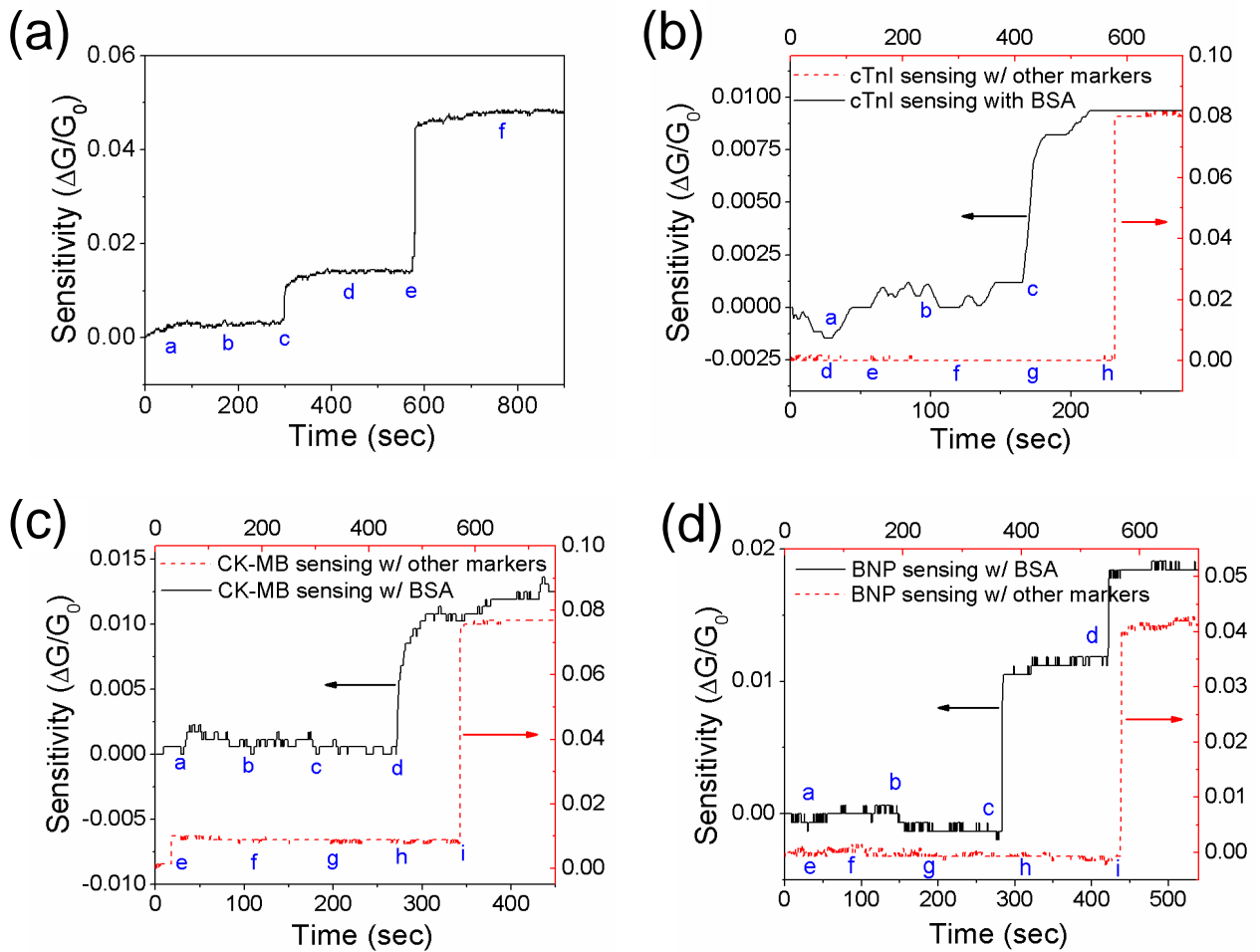


**Figure 22.** Specificity test of nanowire biosensor in the presence of non-target proteins. (a) For the specificity test of nanowire biosensor for Myo. (a: PBS, b: cTnI of 1 ng/mL, c: Myo of 1 ng/mL, d: BNP of 1 ng/mL, e: Myo of 10 ng/mL, and f: CK-MB of 1 ng/mL). (b) For detection of cTnI (a: PBS, b: BSA of 1 ng/mL, c: cTnI of 500 fg/mL, d: PBS, e: Myo of 1 ng/mL, f: CK-MB of 1 ng/mL, g: BNP of 1 ng/mL, and h: cTnI of 1 ng/mL), the nanowire biosensor responds to only cTnI. (c) For detection of CK-MB (a: PBS, b: BSA of 1 ng/mL, c: BSA of 100 ng/mL, d: CK-MB of 25 pg/mL, e: PBS, f: Myo of 1 ng/mL, g: cTnI of 1 ng/mL, h: BNP of 1 ng/mL, and i: CK-MB of 1 ng/mL), the nanowire biosensor responds to only CK-MB. (d) For detection of BNP (a: PBS, b: BSA of 100 ng/mL, c: BNP of 1 ng/mL, d: BNP of 10 ng/mL, e: PBS, f: Myo of 1 ng/mL, g: cTnI of 1 ng/mL, h: CK-MB of 1 ng/mL, and i: BNP of 1 ng/mL), the nanowire biosensor responds to only BNP.

The sensing performance of nanowire biosensor such as cost efficiency, sensitivity, and sensing reproducibility may be maximized by finding the optimum conditions of functionalization (concentrations of 50, 100, and 200  $\mu\text{g/mL}$  for each mAbs) as shown in Figure 23 . Similar to the optimal functionalization condition in the IgG PANI nanowire biosensor, the different concentrations of Myo mAbs (100  $\mu\text{g/mL}$  and 200  $\mu\text{g/mL}$ ) were studied to obtain an optimal condition of the single PANI nanowire biosensor for the Myo detection, shown in Figure 23 (a). The single PANI nanowire biosensors using Myo mAbs of 100  $\mu\text{g/mL}$  showed the higher sensitivity and better sensing linearity in the detection range of Myo proteins (1.4  $\text{ng/mL}$  – 2.5  $\mu\text{g/mL}$ ) than the nanowire biosensor using Myo mAbs of 200  $\mu\text{g/mL}$ . The biosensing tests were carried out at least 3 times from different nanowires at each concentration for avoiding the issue of sensitivity loss due to multiple biosensing in a same nanowire. In order to find optimal conditions with various mAb concentrations, we investigated the various conditions of surface immobilization satisfying sensing performance and realize cost-down in development of nanowire biosensor. In cTnI mAbs of 50 and 100  $\mu\text{g/mL}$ , the sensitivities of nanowire biosensors remain at around the level of 0.02 and 0.05 over cTnI of 30  $\text{pg/mL}$  as shown in Figure 23 (b). For cTnI sensing, the functionalization using mAbs of 200  $\mu\text{g/mL}$  showed the highest sensitivity and broadest sensing range from 300  $\text{fg/mL}$  to 3  $\text{ng/mL}$ . Standard deviations in the condition of 200  $\mu\text{g/mL}$  are much smaller than other conditions indicating the best reproducibility. Similar to the test of cTnI, the optimizations of surface immobilization for CK-MB mAbs and BNP mAbs were carried out as shown in Figure 23 (c) and (d), respectively. CK-MB of 200  $\mu\text{g/mL}$  shows the relatively smaller deviation and more linearly increased sensitivity than other concentrations of CK-MB mAbs. BNP of 100  $\mu\text{g/mL}$  shows linearly increased sensitivity along the broad range

of BNP concentrations from 50 fg/mL to 3 ng/mL. However, the deviation in that condition is greater than for BNP mAbs (50  $\mu\text{g/mL}$  and 200  $\mu\text{g/mL}$ ) as shown in Figure 23 (d).

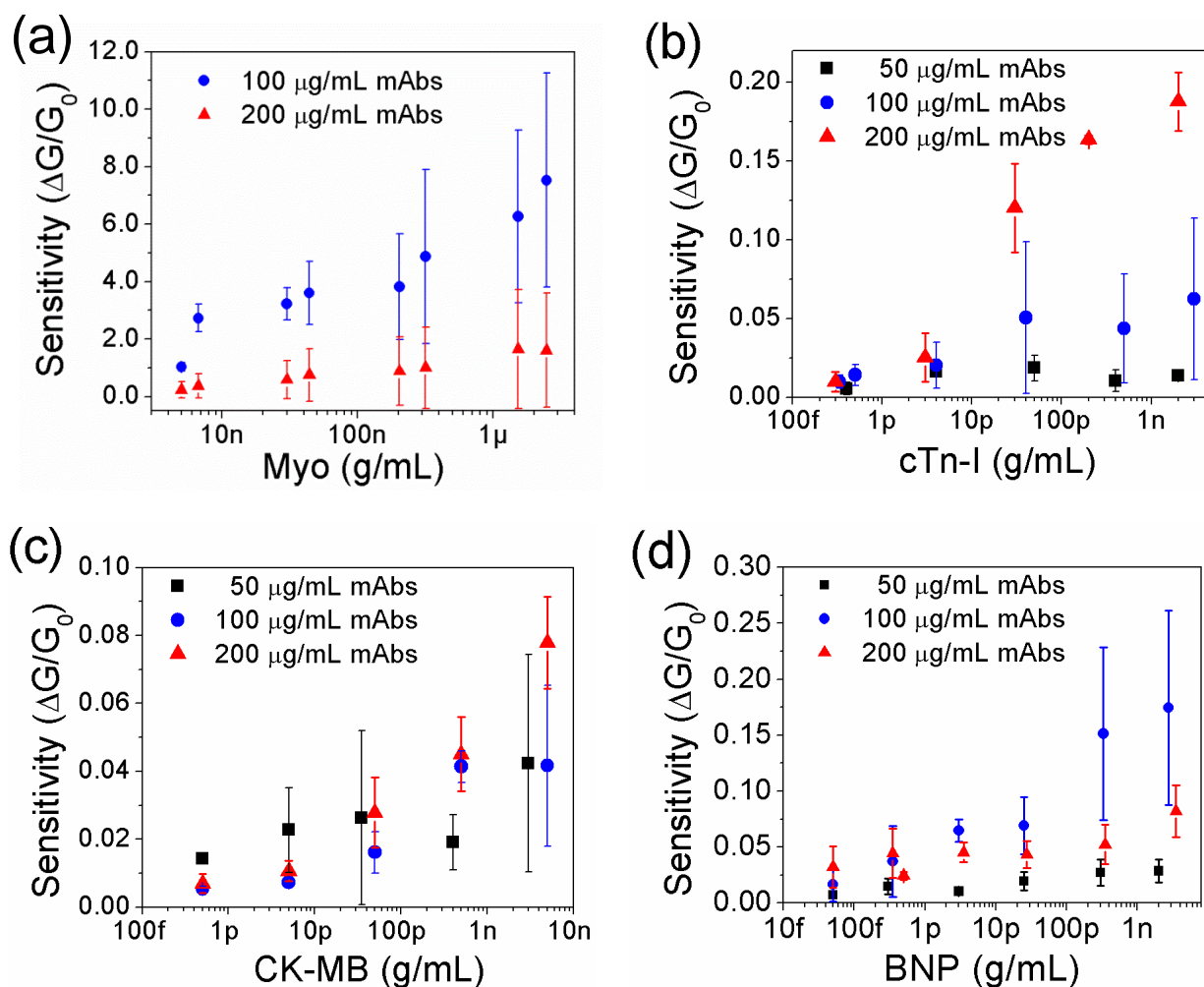


**Figure 23.** Optimization of sensing performance with various concentrations of Myo, cTnI, CK-MB, and BNP mAbs. (a) In order to optimize the condition of functionalization, the sensitivities of the nanowire biosensors are compared in different mAbs mAbs. Myo mAbs of 100  $\mu\text{g/mL}$  showed better sensing performance than the mAbs of 200  $\mu\text{g/mL}$ . (b) cTnI mAbs of 200  $\mu\text{g/mL}$  presented the best linear sensing profile and highest sensitivity of the three different conditions of cTnI mAbs. (c) For CK-MB, CK-MB mAbs of 200  $\mu\text{g/mL}$  showed the best sensing profile without fluctuation in sensitivity. (d) For BNP, BNP mAbs of 100  $\mu\text{g/mL}$  provided higher sensitivity in a broader sensing range than the other conditions.

The various results from the optimization of functionalization may be caused by the size of mAbs, uniformity of the immobilized mAbs per unit area and orientation of the immobilized mAbs [136]. Considering the concentration of mAbs, if an insufficient amount of mAbs on PANI nanowire were provided, the low conduction change could result from the small net surface charge. On the other hand, if the high concentration of mAbs were employed, the plentiful active binding sites on the surface of nanowire could improve sensing linearity and sensitivity. However, excessively immobilized mAbs in the functionalization of nanowire may crosslink together between primary amines and carboxylic groups of mAbs. This reaction results in less active binding site and low sensitivity [137]. In Figure 23, the low concentrations (50  $\mu\text{g/mL}$ , marked as solid black square) of each mAbs show the competitive sensitivity in the range from 50  $\text{fg/mL}$  scale to 5  $\text{pg/mL}$  scale. However, the sensitivities of the nanowire biosensors with mAbs of 50  $\mu\text{g/mL}$  are very poor and show the saturation behavior in high concentrations of target biomarkers. In those biosensing regions, the small numbers of binding site from immobilized mAbs result in the weak net surface charge to the single PANI nanowires for the detection in the high concentration of target biomarkers. The high concentrations of mAbs (100 or 200  $\mu\text{g/mL}$ ) have shown relatively higher sensitivity and linear sensing profile than the mAbs of 50  $\mu\text{g/mL}$  in this research. Therefore, the plentiful binding site on the functionalized nanowire is an important condition for realizing high performance biosensor. However, the advantages of single PANI nanowire biosensors will lose the cost efficiency of the surface immobilization, if concentrations greater than mAbs of 200  $\mu\text{g/mL}$  are employed. For the different optimal functionalization conditions such as Myo mAbs of 100  $\mu\text{g/mL}$ , cTnI mAbs of 200  $\mu\text{g/mL}$ , CK-MB mAbs of 200  $\mu\text{g/mL}$ , and BNP mAbs of 100  $\mu\text{g/mL}$ , the different size and types of mAbs may result in the different sensitivities and sensing.

### 5.2.2 Effect of net surface charge in biosensing

The single PANI nanowire-based biosensors for the detection of cardiac biomarkers demonstrated the high sensitivity, fast detection, and good sensing reproducibility using conductometric biosensing. The conductometric measurement has the advantages of not requiring reference electrode and extremely low power consumption [20, 138]. During the biosensing, the increase of conductance is mainly caused by the charge carrier accumulation on p-type PANI nanowire through binding of the charged target proteins to the immobilized mAbs on the PANI nanowire surface.

The charge of target protein solutions is determined by the isoelectric point (pI) values of the proteins and the pH value of buffer solution such as PBS. For example, if the pI value of target protein is higher than pH value of buffer solution, the target protein in the buffer solution has positive charge. It is generally known that Myo, cTnI, and CK-MB have pIs of 7.2, 5.2 ~ 5.4, and 5.2, respectively [132-134]. The pI value of BNP is 6.5, numerically calculated with the sequence of BNP and the program of ExPASy. The net charges of those target protein solutions in PBS (pH 7.4) are negative due to the lower pI values than pH 7.4. Based on our biosensing experiments and pI values of target proteins, it is assumed that the negative charges of target proteins resulted in a major carrier accumulation in the PANI nanowire and consequently an increase of conductance. To verify this hypothesis, another cTnI solution in PBS of pH 5 was prepared and tested as shown in Figure 24 (a). cTnI in PBS of pH 5 has positive charges due to pI value of 5.2 ~ 5.4 and the binding to immobilized cTnI mAbs leads to carrier depletion in PANI nanowire. Figure 24 (a) shows that the conductance of PANI nanowire decreased upon the addition of the cTnI solution. The inset of Figure 24 (a) depicts the change of conductive area in nanowire by depletion after binding positive charge of target protein to the mAbs.

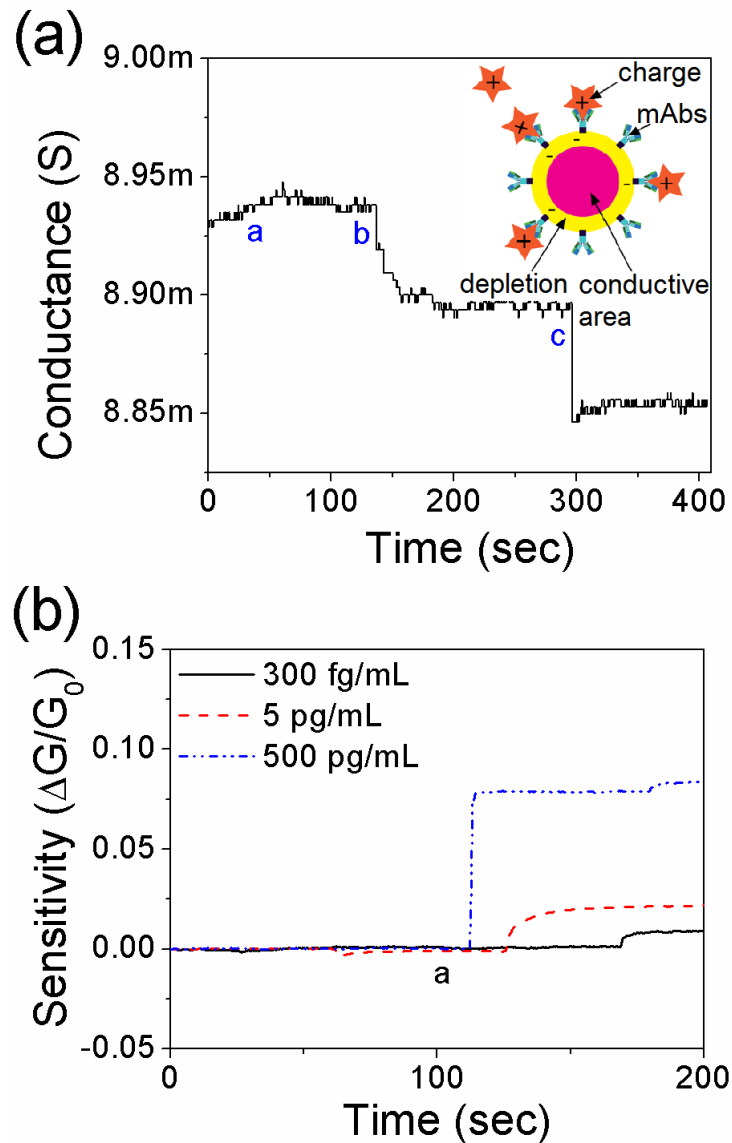


**Figure 24.** Tests of net surface charge effect on the functionalized PANI nanowires. (a) Decreased conductance on the nanowire biosensor during a sensing test with positively charged cTnI protein solutions (a: PBS of pH 5, b: 1 ng/mL, and c: 10 ng/mL). cTnI protein solutions were prepared with PBS of pH 5. (b) Comparison of sensitivity with different concentrations of cTnI detection. The nanowire biosensor shows significantly higher sensitivity according to higher concentration. The mark “a” on black solid line presents the injection of BSA (100 ng/mL). After the injection of BSA, cTnI of 300 fg/mL was injected to the biosensor.

The conductometric biosensing on the single PANI nanowire differentiates significantly signal changes at very low concentrations to high concentrations of target proteins. The different conductance change depending on the concentration of target proteins is determined by the potential strength of net charge in the complex of mAbs and target proteins. The tiny dimension of nanowire can be easily affected by the attached single molecular charge on the nanowire surface [139, 140]. The complex of mAbs and charged proteins of cardiac biomarkers have charge neutralization on the interface between the mAbs and the proteins [141, 142]. Then, the charge neutralization induces the charge re-distribution in the complex; same type of charge to target protein's charge in the mAbs is driven to the bottom of mAbs on the surface of nanowire. The driven charges in the complex of mAbs and proteins affect the accumulation or depletion of major carriers in the nanowire. In addition, the higher concentrations of charged proteins induce the higher sensitivity due to stronger electric field from the complex of mAbs and proteins as compared in Figure 24 (b). In those biosensing, the different concentrations of cTnI are compared with the sensitivity from different single PANI nanowires-based biosensors. Non-response to BSA of 100 ng/mL (mark "a" on black line in Figure 24 (b)) identifies that non-specific proteins do not construct the complex with mAbs or pre-coated BSA on the free-site of nanowire. Therefore, the charge neutralization in complex of mAbs and target proteins drives conductometric biosensing and provides as low as Myo of 100 pg/mL, cTnI of 250 fg/mL, CK-MB of 150 fg/mL, and BNP of 50 fg/mL for detection limits. However, this conjecture includes partial shortcomings, insufficient to support high specificity in biosensing. Those aforementioned sensing mechanism and specificity of the nanowire biosensor have room for further investigation and discussion.

### 5.2.3 Biosensing mechanism

In the nanowire biosensor, a change in physical properties such as electric field, capacitance, or distribution of major carriers may result in the change of conductance in the nanowire. However, the controversial biosensing mechanism in nanowire has been discussed with various suggested theories such as electrostatic gating, changes in gate coupling, carrier mobility changes, and Debye screening effect [104, 143, 144]. It is ambiguous that one suggested theory is dominant to identify the entire sensing mechanism, including the characteristics of high sensitivity, good reproducibility, and specificity on the nanowire biosensor. Therefore, it is important to clarify what kinds of physical or chemical behavior in nanowire dominantly affect on the conductance change in nanowire biosensors.

First, it is necessary to consider the change of conductance in PANI by oxidation and reduction. The oxidation and reduction of PANI result in a change of conductance due to the doping of charge carriers and the transferring of those carriers through polymer chains [74]. A reversible redox process occurs from the direct interaction between adsorbate and PANI. In the structure of functionalized PANI nanowire, the surface of PANI nanowire is coated with immobilized mAbs and blocking agent such as BSA. The coverage of mAbs and BSA on PANI nanowire prevents direct oxidization and reduction of PANI. Therefore, the redox process on PANI nanowire is useful for explaining chemical sensing due to direct interaction between chemical adsorbate and PANI [145]. Another consideration of biosensing mechanism is the work function change between a metal electrode and PANI nanowire [104]. The immobilized mAbs on the metal electrode induces a change of work function from the charged target proteins attaching on the electrodes. In this research, the surface immobilization of mAbs didn't occur on the Au electrode, as shown in the functionalization verification of Figure 16. In the functionalization

development, inorganic nanomaterials based biosensors have been oxidized to build a self-assembled monolayer to couple mAbs on the surface of inorganic nanomaterials including Si, ZnO, In<sub>2</sub>O<sub>3</sub>, Au, and CNT [146]. During the oxidization process, the entire surface of the sample, including the electrodes and the nanomaterials, can be oxidized and be immobilized by mAbs. In order to avoid non-specific binding in biosensing, a passivation layer is generally employed to cover areas other than the nanomaterials. In our single PANI nanowire biosensor, a self-assembled monolayer was not employed due to direct surface immobilization on PANI. Therefore, the consideration of work function change is inappropriate for biosensing mechanism in our single PANI nanowire biosensor.

In the biosensing of cardiac biomarkers, the functionalized PANI nanowires were surrounded by 1× PBS or proteins solutions prepared in 1x PBS. In terms of Debye screening effect for 1× PBS, Debye screening length in 1× PBS is very short, around 0.7 nm, due to the high concentration of NaCl (137 mM). Comparing the approximate size of antibody – target protein complex (~ 15 nm), it seems unlikely that the net charge of target protein would affect the conductance change in nanowire via carrier accumulation or depletion. However, the binding of mAbs and target proteins, which is called antibody – antigen complex (Ab – Ag complex), results in the charge neutralization at the interface between the mAbs and antigen, namely target proteins [147]. In an Ab – Ag complex, binding folds of mAbs recognize target proteins and bind tightly with each other. In a three-dimensional structure, the bound target protein is wrapped by binding site of mAbs. According to the net charge of the target proteins, charge neutralization can be induced by charge complementarity, forming hydrogen bonding between the mAbs and the target proteins at their interface [147, 148]. The charge neutralization at the interface of the Ab – Ag complex distributes countercharges to the charge at the interface at the end of the

mAbs, where is coupled to the surface of a single PANI nanowire as illustrated in Figure 25. Those distributed countercharges at the end of mAbs, which are the same charge as the target proteins, are close enough to induce carrier accumulation or depletion by the surface charge of the PANI nanowire overcoming the limitation of short Debye screening length in 1x PBS. Therefore, the target proteins detected by the immobilized mAbs change the net surface charge on the PANI nanowire. The net surface charge on the PANI nanowire modulates the conductive area of the nanowire depending on the charge value of the target proteins and the doping of nanowire. If the net surface charge of the nanowire is positive or negative, the conductance of p-type PANI nanowire can be depleted or accumulated, respectively. The depletion or accumulation induces a decrease or increase of conductance in nanowire. In the biosensing of single PANI nanowire-based biosensor, the charge neutralization and re-distribution would be dominant biosensing mechanism and result in charge accumulation or depletion in p-type PANI nanowire based on our experiments.

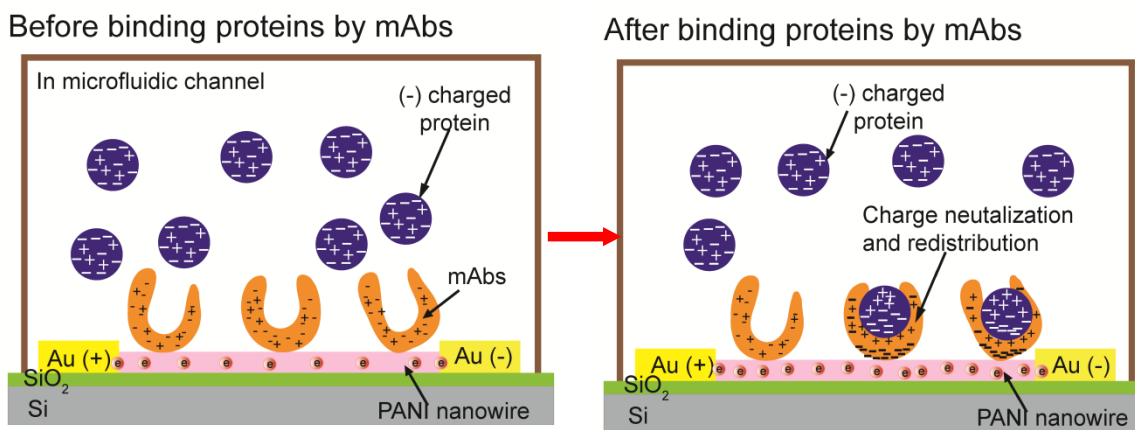


**Figure 25.** An illustration of charge neutralization and re-distribution. The complex of charged proteins and mAbs induce the charge neutralization at the interface, and then charge re-distribution in the mAbs. Those re-distributed charge result in the net surface charge change on the nanowire.

## 5.2.4 FET behavior of single polyaniline nanowires

The fabricated single PANI nanowires can be also applied for a single nanowire FET with a back gate. A single PANI nanowire FET is fabricated via an electrochemical deposition growth method and consists of a single PANI nanowire bridging two Au source/drain electrodes using an Au back gate through  $\text{SiO}_2$  layer to contact Si layer as shown in Figure 26. Each PANI nanowire has the diameter of 100 to 200 nm and typically the length of 5  $\mu\text{m}$  determined by the e-beam patterned nanochannel and the distance between the two Au electrodes. In Figure 27, the measured  $I_{\text{SD}} - V_{\text{SD}}$  data from PANI nanowire FETs are presented with four distinct field effect responses in p-type FET behaviors. It may be caused by the different structure of the nanowire in the width of channel and structure of the PANI nanowire.

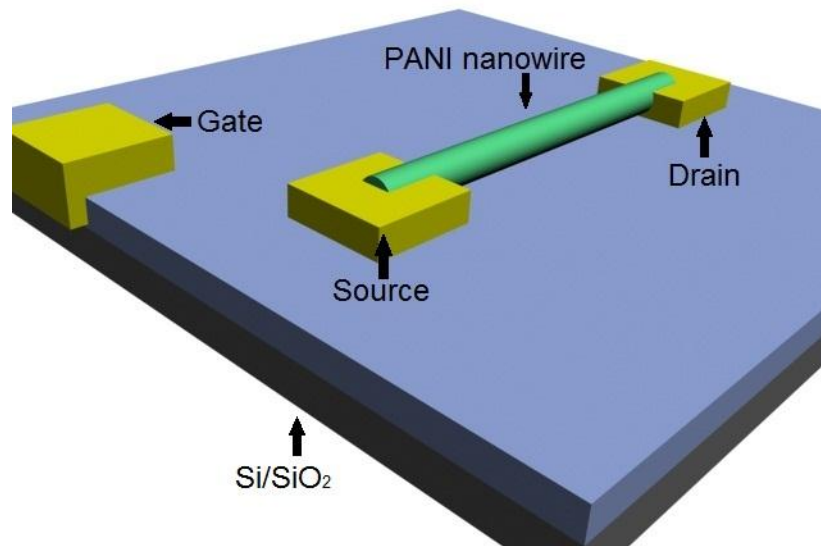


**Figure 26.** A single PANI nanowire FET. The fabricated single PANI nanowire between two Au electrodes works as a channel of FET with a back gate.

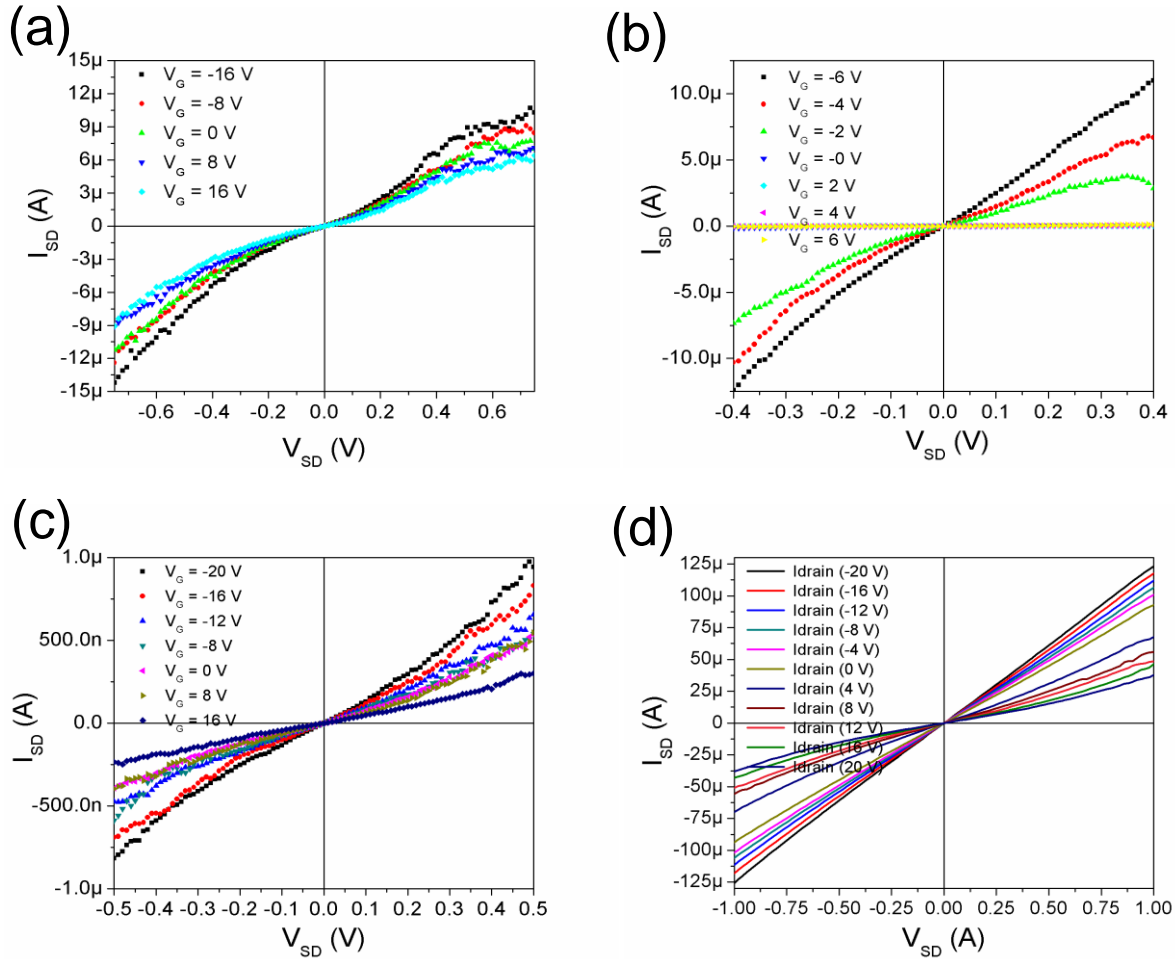


**Figure 27.** The measured  $I_{SD} - V_{SD}$  from PANI nanowire FET. (a) The various  $V_G$  from -16 to 16 V shows slight change of  $I_{SD}$ . (b) The PANI nanowire FET is turned off at  $V_G$  of 0 V. (c) Changing  $V_G$  from -20 to 16 V, the PANI nanowire FET shows clear change of  $I_{SD}$ . (d) The data of PANI nanowire FET scanned by  $V_G$  from -20 to 20 V. This nanowire FET shows very high  $I_{SD}$  and significant change in scanned range of  $V_{SD}$ .

In Figure 27 (a),  $I_{SD}$  shows weak semiconducting behavior with various  $V_G$  stepped by 8 V increments.  $I_{SD}$  intends to saturate on certain values at each different  $V_G$  around  $V_{SD}$  of 0.75 V as shown in Figure 27 (a). However, in Figure 27 (b),  $I_{SD}$  displays a markedly different behavior from Figure 27 (a).  $I_{SD}$  shows clear change by  $V_G$  of 2 V in negative  $V_G$  and turn-off behavior from 0 to positive  $V_G$ . It is important to note that the current range in the turn-on state is similar for both devices in Figure 27 (a) and (b). In Figure 27 (c), we observe a device with lower conductance and weak semiconducting compared to  $I_{SD}$  in Figure 27 (a) and (b), with no sharp turn-off state transition. Finally, Figure 27 (d) displays a device with very high current density, but only weak semiconducting behavior.

The obtained PANI nanowire FET data show p-type characteristics with different levels of channel modulation. To analyze carrier mobility and transconductance, this PANI nanowire FET would be compatible to metal-oxide-insulator FET (MOSFET) theory due to the PANI nanowire, which plays a role of channel between source and drain, on a Si/SiO<sub>2</sub> substrate. In a MOSFET structure,  $I_{SD}$  can be calculated by employing the gradual channel approximation and simplified model as expressed in equation (1) and (2) [149, 150]. This calculation is based on the assumption that the electric charge density varied depending on the electric field along the channel is much smaller than that related to a variation across the channel.

$$I_{SD} = \frac{Z\mu C_{ox}}{L} (-V_G + V_{Th}) \cdot V_{SD} \quad (1)$$

$$V_{Th} = 2\phi_b + \frac{\sqrt{2\varepsilon_s q N_a (\phi_b)}}{C_{ox}} \quad (2)$$

where,  $Z$  is the width of channel.  $\mu$  is the carrier mobility.  $C_{ox}$  is the insulator capacitance.  $V_G$ ,  $V_{Th}$ , and  $V_{SD}$  are gate voltage, threshold voltage and source-drain voltage, respectively.  $\phi_b$  is the

potential difference between the Fermi level and the intrinsic Fermi level in the channel.  $\epsilon_s$  is the semiconductor permittivity.  $q$  is the absolute electron charge.  $N_a$  is the doping level of the p-type substrate.

The other important parameters are channel conductance ( $g_d$ ) the transconductance ( $g_m$ ) to obtain  $\mu$  and  $V_{Th}$  in the linear region of  $I_{SD}$ . The equation (3) and (4) shows the definition of  $g_m$  and  $g_d$ , related with other parameters in MOSFET [151, 152].

$$g_d = \left. \frac{\partial I_{SD}}{\partial V_{SD}} \right|_{V_G=const} = \frac{Z\mu C_{ox}}{L} (V_G - V_{Th}) \quad (3)$$

$$g_m = \left. \frac{\partial I_{SD}}{\partial V_G} \right|_{V_{SD}=const} = \frac{Z\mu C_{ox}}{L} \cdot V_{SD} \quad (4)$$

Using those equations of (1) – (4), the  $\mu$  and  $V_{Th}$  can be calculated for PANI nanowire FETs. The obtained  $\mu$  and  $V_{Th}$  are provided in Table 1.

**Table 1.** The calculated hole mobility and threshold voltage of single PANI nanowire FETs. Sample 1, 2, 3 and 4 is consistent with Figure 27 (a), (b), (c) and (d), respectively.

Sample of PANI FET	Hole mobility ( $\mu$ , $\text{cm}^2/\text{V}\cdot\text{S}$ )	Threshold voltage ( $V_{Th}$ , V)
1	55.98	68.67
2	1362.16	0.89
3	12.26	33.13
4	517.13	62.23

The obtained data of  $\mu$  and  $V_{Th}$  as shown in Table 1 varies from tens to thousands order in hole mobility and an order of magnitude for positive threshold voltages. Based on these experimental data, the various hole mobility would affect on relatively high  $I_{SD}$  and high  $V_{Th}$  in the PANI nanowire FETs comparing to other researches in conducting polymer FET. The transconductance values from sample 2 and 4 in Table 1 have  $1.39 - 1.51 \times 10^{-6}$  S. The other lower hole mobility depends on the transconductance of  $1.78 - 12.22 \times 10^{-8}$  S. As estimated in Figure 27 and Table 1, the gate effect in the PANI nanowire FET works effectively in the samples (Figure 27 (b) and (d)), which shows high hole mobility [153].

The threshold voltage of the PANI nanowire FET is mainly related to the potential difference ( $\phi_b$ ) as could be inferred from equation (2). The potential difference in the PANI nanowire is determined by doping level on the nanowire, which is unstable due to the fabrication methods employed [154]. The doping levels are various according to the condition of the nanowire fabrication. As shown in Table 1, the threshold voltage is distributed in the range of 30 – 40 and 60 – 70 V except one sample. The electrochemical deposition method for PANI nanowire fabrication has provided highly doped PANI nanowire due to high mixture ratio of HCl and Aniline monomer (10:1) and applying static current (350 – 900 nA) as discussed in our previous research.

In this experiment, the saturation behavior of  $I_{SD}$  was not shown. The PANI FET has employed back gate structure. The back gate structure in the MOSFET affects on the bottom surface through insulator. Especially, the back gate structure in the PANI nanowire FET has which produces notably weak channel modulation. It could be presumed that the back gate structure of the nanowire FET causes the weak modulation in the nanowire [155]. The observed FET response is caused by a lower observed hole mobility and larger threshold voltage compared

to inorganic semiconductor nanowire FETs. As well as, the saturation behavior of  $I_{SD}$  would appear for larger  $V_{SD}$ , although when  $V_{SD}$  over 1 V was applied,  $I_{SD} > 1$  mA induces break-down of the nanowire. As shown in Figure 27 (b), the high hole mobility of PANI nanowire indicates that the single PANI nanowire FET can be employed for controllable and useful electric device with distinct turn-on or off behavior as switches in nano-electrical devices.

In these experiments, a single PANI nanowire FET was established easily using bottom up process to build a back gate, Au source/drain electrodes, and PANI nanowire bridging two Au electrodes. This fabrication process provided high density electric device saving efforts to select single nanowires and align electrodes on those nanowires. In addition, the back gate of nanowire FET can be employed for nanowire FET biosensor avoiding reference electrode or interruption from top gate structure. However, various hole mobility of the fabricated nanowire has shown different field effect behavior in the single PANI nanowire FET. In order to apply for a nanowire biosensor, the control of hole mobility in PANI nanowire should be decided first.

Our experimental data of single PANI nanowire FET has demonstrated relatively higher hole mobility in the range of tens to thousands order  $\text{cm}^2/(\text{V}\cdot\text{S})$  than other researches of polymer FET [156]. High mobility provided high current in low operating  $V_{SD}$  as shown in Figure 27. This characteristic is also related to transconductance of nanowire FET and can show high on-off ratio as shown in Figure 27 (b). Therefore, the realization of high and uniform hole mobility of PANI nanowire will be useful for nanowire FET biosensor in the future. In addition, we could establish the single PANI nanowire FET with back gate structure and high density of device via bottom up process.

### 5.2.5 Analysis of nanowire biosensor sensitivity

In biosensors to measure conductance change, the sensor sensitivity is defined as  $\Delta G/G_0$ , where  $G_0$  is initial conductance and  $\Delta G$  is conductance change from the initial value. Therefore, the high sensitivity of biosensor is determined depending on  $\Delta G$ . In this chapter, we analyze and compare the sensitivities of biosensors in a register or nanowire FET structure. In order to compare the conductance changes in FETs and resistor structures, we can develop a simple model of semiconductor nanowires with positive or negative surface charge. In order to study the conductance change by surface charge on a nanowire, a nanowire cross-section schematic is depicted in Figure 28. As shown in Figure 28, the single PANI nanowire is assumed to be p-type, with a constant doping concentration of  $N_A$ . When the nanowire surface is covered by charged molecules with a net surface charge concentration ( $N_s$ ), the mobile charge is depleted by charge neutrality. The total surface charge of the nanowire will be equal to the depleted charge, as described in equation (5) and (6). The depleted region is defined as much smaller than the radius of the nanowire.

$$2\pi RLN_s = \pi(R^2 - (R - \Delta x)^2)LN_A \approx 2\pi R\Delta xLN \quad (5)$$

$$N_s = \Delta xN_A \quad (6)$$

where,  $R$  is the radius of the nanowire.  $L$  is length of the nanowire, and  $\Delta x$  is depletion length in the nanowire.

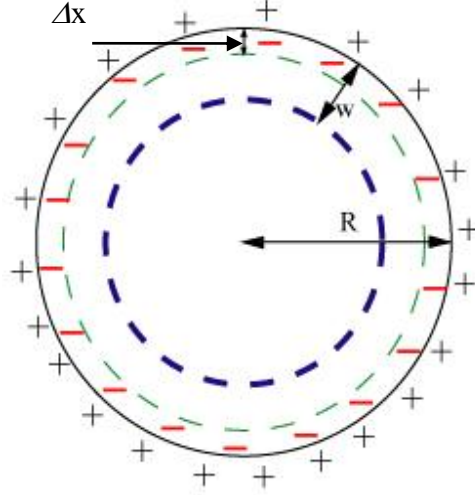


**Figure 28.** The schematic of an effective conductance area in a nanowire. The black solid line is the edge of nanowire. The green dotted line is the edge of the depleted area resulting from surface charge neutrality. The thick blue dotted line is the edge of the effective cross section area after applying  $V_G$ . + and – refer to the surface charge from molecules and immobile charges, respectively.

The conductance of the nanowire is described in terms of conductivity ( $\sigma$ ), length ( $L$ ) and cross section area ( $A$ ) of nanowire as expressed in equation (7). The changed conductance by depletion length  $\Delta x$  can be described with the effective conduction area in equation (8).

$$G_0 = \frac{\sigma A}{L} = \frac{q\mu_p N_A}{L} A = \frac{q\mu_p N_A}{L} \pi R^2 \quad (7)$$

$$G_1 = \frac{\sigma A_1}{L} = \frac{q\mu_p N_A}{L} \pi (R - \Delta x)^2 \quad (8)$$

where,  $q$  is electronic charge.  $\mu_p$  is hole mobility.

The sensitivity of the nanowire in terms of conductance change can then be expressed using equation (6) – (8) as shown in equation (9). The sensitivity of the nanowire increases as the surface charge concentration ( $N_s$ ) increases. In addition, a smaller radius of nanowire forces a higher sensitivity with a larger change in conductance.

$$\frac{\Delta G}{G_0} = \left| \frac{G_1 - G_0}{G_0} \right| = \left| \frac{\frac{q\mu_p N_A}{L} \pi \left\{ (R - \Delta x)^2 - R^2 \right\}}{\frac{q\mu_p N_A}{L} \pi R^2} \right| \approx \frac{2\Delta x}{R} = \frac{2N_s}{RN_A} \quad (9)$$

As derived in equation (9), the high sensitivity of PANI nanowire can be obtained by either long depletion length or small radius of nanowire. Therefore, the nanoscale materials have more advantages than micro- or macro-scale materials in the point of sensitivity. For acquiring higher sensitivity, many researchers have researched also to detect single biomolecules using nanowire FET structure in biosensing area [6, 157]. For a nanowire FET, the applied gate voltage results in a change of additional depletion width ( $w$ ) in the nanowire as depicted in Figure 28. Applying similar way in the nanowire resistor structure to nanowire FET structure, the sensitivity of nanowire FET is as follows (10).

$$\frac{\Delta G_{23}}{G_2} = \left| \frac{G_3 - G_2}{G_2} \right| = \left| \frac{\frac{q\mu_p N_A}{L} \pi \left\{ (R - w - \Delta x)^2 - (R - w)^2 \right\}}{\frac{q\mu_p N_A}{L} \pi (R - w)^2} \right| \approx \frac{2\Delta x}{R - w} = \frac{2N_s}{(R - w)N_A} \quad (10)$$

The depletion by net surface charge is assumed to be same as that of nanowire as expressed in (6). The  $w$  has various values according to the gate voltage. However,  $w$  and  $\Delta x$  have different values in real nanowire FET biosensor from the resistor structure of nanowire biosensor. We assume that the variable  $\Delta x$  is equal in resistor and FET in order to make an analytic comparison. The comparison of sensitivity of a nanowire resistor and nanowire FET can be extracted from (9) and (10), as shown in (11).

$$\frac{\Delta G_{23}/G_2}{\Delta G_{01}/G_0} = \frac{\frac{2N_s}{(R-w)N_A}}{\frac{2N_s}{RN_A}} = \frac{R}{R-w} \geq 1 \quad (11)$$

In (11), the depleted region due to applied gate voltage produces a smaller effective diameter of conduction area in nanowire FETs than in nanowire resistor. Therefore, we conclude that the sensitivity in a nanowire FET is bigger than that in the nanowire resistor structure. In addition, the research nanowire FET will reveal the physical properties of single PANI nanowire such as carrier mobility, doping concentration and threshold voltage. They can be extracted from typical  $I_{\text{Drain}} \text{ vs } V_{\text{Drain}}$  and  $I_{\text{Drain}} \text{ vs } V_{\text{Gate}}$  of nanowire FETs. Obtaining physical properties of PANI nanowire will be useful to analyze quantitatively single PANI nanowire biosensor and to develop high sensitive biosensor with good reliability and switching function.

### 5.3 SUMMARY

The single PANI nanowire-based biosensors show the advantages of single nanowire fabricated using electrochemical deposition growth method, direct surface immobilization of mAbs, free-passivation layer in development of biosensor, and integration of microfluidic device. The single PANI nanowire-based biosensors performed successfully at detecting four different cardiac biomarkers: Myo, cTnI, CK-MB, and BNP. The electrochemical growth method allows the creation of single site-specific nanowire between pre-patterned electrodes. This fabrication method is useful to increase the density of a nanowire array in a unit area with good alignment of nanowires. A well aligned single nanowire between electrodes can improve device reliability as this type of nanowire has uniform dimensions and simple architecture. In the functionalization process, PANI can be coupled with the mAbs of target biomarkers using EDC/NHS, unlikely inorganic materials, where require to form a functional group such as amine or carboxylic to react with the mAbs. The integration of a microfluidic channel allowed us to introduce PBS or a protein solution at a slow flow rate (3 mL/min) to keep laminar flow in the channel for accurate biosensing. The microfluidic channel limited the flow in the nanowire area. Therefore, those advantages of single PANI nanowire-based biosensors help to improve sensitivity and sensing reliability, as we demonstrate in the biosensing of cardiac biomarkers. The detection of cardiac biomarkers on single PANI nanowire biosensor showed ultra-sensitivity with very low detection limits (Myo: 100 pg/mL, cTnI: 250 fg/mL, CK-MB: 150 fg/mL, and BNP: 50 fg/mL) compared to reference values to diagnose cardiac disease and other researches using immunoassay, thin film, and inorganic nanowire and as shown in Table 2.

**Table 2.** Reference values and other research results of cardiac biomarkers

DL: detection limit

Name	Reference values	Other researches
Myo	7 ng/mL [158]	<ol style="list-style-type: none"> <li>1. Ni-CH<sub>3</sub> nanowire (DL: 50 μg/mL) [159]</li> <li>2. Fluorescence technique (DL: 16 ng/mL) [160]</li> <li>3. Micellar electrokinetic chromato-graphy and a cleavable tag immunoassay (DL: 5 ng/mL) [42]</li> </ol>
cTnI	800 pg/mL [37]	<ol style="list-style-type: none"> <li>1. Si nanowire FET (DL: 157 ng/mL) [53]</li> <li>2. fiber optic based SPR (DL: 1.4 ng/mL) [40]</li> <li>3. Fluorimmunoassay using integrated optical waveguide sensing (DL: 15.9 ng/mL) [45]</li> </ol>
CK-MB	5 ng/mL [161]	<ol style="list-style-type: none"> <li>1. Si Nanowire (DL: 1 ng/mL) [162]</li> <li>2. Fluoroimmunoassay using integrated optical waveguide sensing (DL: 2.8 ng/mL) [45]</li> <li>3. Micellar electrokinetic chromato-graphy and a cleavable tag immunoassay (DL: 3 ng/mL) [42]</li> </ol>
BNP	21 pg/mL [163]	<ol style="list-style-type: none"> <li>1. portable SPR (DL: 5 pg/mL) [47]</li> <li>2. Electrical enzyme immunoassay (DL: 10 pg/mL) [164]</li> </ol>

In addition, the specificity of single PANI nanowire was measured from  $10^3$  fold to  $10^6$  fold to high concentration of BSA (100 ng/mL) or other non-target proteins. The nanowire biosensors showed a good linear sensing profile in a wide range, from tens fg/mL to single  $\mu\text{g/mL}$ , with optimization of mAbs' concentration. Those high specificity and wide sensing range of single PANI nanowire-based biosensors provides the feasibility of point-of-care systems for label free detection with fast response in the nanowire biosensor.

In the discussion of biosensing mechanism, we could clarify the charge effect on the biosensing. The positive or negative charge of target proteins showed the contrasting behaviors of conductance increase or decrease. Those conductance changes in biosensing may be caused by the charge neutralization and re-distribution, when the immobilized mAbs on the nanowire surface are bound by the target proteins. This charge neutralization and re-distribution overcome the limit of biosensing from very short Debye screening length ( $\sim 0.7$  nm) in  $1\times$  PBS. In addition, we analyzed the sensitivity of nanowire biosensor in resistor structure and FET structure. Comparing the sensitivity from resistor and FET structure, the high sensitivity in nanowire FET structure enlightens to require the development of nanowire FET biosensor.

This research of cardiac biomarkers' detection on single PANI nanowire biosensors was carried out using purified proteins instead of human serum like a practical case. Those experimental data illustrate the feasibility of developing a practical diagnostic system to test human serum in the future. In addition, this method of developing PANI nanowire biosensors can be applied for the detection of other disease such as cancer and can be further developed in nanowire FET structure for the ultra-high sensitivity and qualitative analysis of biosensing mechanism.

## 6.0 CONCLUSION AND FUTURE WORKS

The current technology of biosensor using nanomaterials such as nanowire, NP, CNT, and nanoscale thin film has been developed in the various architectures of immunoassay, SPR, potentiometric-, amperometric- and conductometric-biosensor [165-167]. The immunoassay biosensor is mostly commercialized presenting good sensitivity, sensing reliability, and well established process. This method requires many processes to immobilize various kinds of antibodies and to react with target biomarkers. The labeled antibodies or target biomarkers with fluorescent or radioactive materials are measured by a specific detector depending on the labeled materials [17]. Although the immunoassay is one of the oldest and most established methods, it has the disadvantages of requiring specialized detector, many process steps, and radiation hazards. The SPR has shown good performance with no-labeling process and detection in small volume of solution. However, this method has difficulty to measure at low concentration of targets or in low molar mass target solution [168]. Potentiometric biosensor measures the potential change of a cell reacting on an electrode at zero current. However, this biosensing method has the disadvantage of lowering potential in the reaction. Amperometric biosensor measure the change of current peak happened by oxidation or reduction between electrode and target. The height of peak is proportional to the concentration of target. Conductometric biosensor measures directly the change of conductance in a sensor. The conductance of a sensor can be various through electron (or hole) transfer between sensor and target or major carrier

accumulation/depletion by the field effect from the detected targets. The change of conductance can be monitored by applying static current or voltage in a sensor. The advantage of conductometric biosensor over other types of biosensor is inexpensive system setup, no reference electrode and noise reduction through differential measurements. The conventional conductometric biosensors are based on the fact that almost all enzymatic reactions involve either consumption or production of charged species and, therefore, lead to a global change in the ionic composition of the target molecules. Biosensors based on the conductometric principle present a number of advantages: a) thin-film electrodes are suitable for miniaturization and large scale production using inexpensive technology, b) they do not require any reference electrode, c) transducers are not light sensitive, and d) the driving voltage can be sufficiently low to decrease significantly the power consumption [20, 169].

In our research, the single PANI nanowire-based biosensors and nanowire FET were established easily using electrochemical deposition growth, surface immobilization, back gate, and microfluidic channels. The nanowire fabrication of electrochemical deposition growth method provided a high density electric device saving efforts to select single nanowires and align electrodes on those nanowires. The single PANI nanowire-based biosensors realize the easy and efficient development of biosensor reducing chemical or physical surface treatment of functionalization and passivation layer for blocking interfered signals. On the functionalized PANI nanowire biosensor, we integrated a microfluidic device for injecting and withdrawing PBS or protein solutions. The microfluidic device limits that the solutions flow onto only nanowire areas. The control of flow rate in microfluidic device can minimize the damage of nanowire in biosensing and protect the hazard from biosensing samples. In addition, the back gate of nanowire FET can be employed for nanowire FET biosensor avoiding reference electrode

or interruption from top gate structure. However, the various hole mobility of the fabricated nanowire has shown different field effect behavior in the single PANI nanowire FET. In order to apply to nanowire biosensor, the control of hole mobility in PANI nanowire should be decided first.

For future works, the single PANI nanowire biosensors show many good experimental results and feasibility of point-of-care diagnostic systems. However, the realization of point-of-care systems require the more advanced and sophisticated development with testing human serum in tough environment. In real diagnosis with human serum, the nanowire biosensor is required to detect target biomarkers in the serum including a lot of non-specific proteins after centrifugation of blood and separation from plasma. Therefore, the single PANI nanowire FET biosensor is one of candidates to develop label-free-detection and miniaturized diagnostic systems. The nanowire FET will increase sensitivity of biosensing and S/N ratio with its current modulation and switching function. In addition, the realization of high and uniform hole mobility of PANI nanowire will be useful for a nanowire FET biosensor, which provide reliable sensing performance, in the future. And then, we could establish the single PANI nanowire FET with back gate structure and high density of device via bottom up process. In order to realize the sophisticated biosensor system, the mass production of PANI nanowire, the employment of aptamer, and the nanowire FET have been studied in our research group. Another chemical synthesis way provides the fabrication and alignment of PANI nanowires between pre-patterned electrodes at a single process in a wafer scale. Aptamer is an attractive candidate substituting for mAbs due to superiority of environmental stability and good sensitivity. In addition, the nanowire fabricated by the chemical synthesis way builds nanowire FET with uniform physical properties such as carrier mobility and doping concentration, because the nanowires are

processed in a same condition. Those researches for our future works will present the sophisticated nanowire biosensor testing in human serum and showing uniform sensing performance.

## APPENDIX A

### MATERIALIZATION OF POLYANILINE

PANI is attractive material in nanotechnology due to its electrical and mechanical properties for electric device application. The electrical conductivity of PANI is controllable with the degree of oxidation states. The general form of polyaniline is consisted with oxidized form and reduced form, as shown in Figure 29. In three different structures of PANI, leucoemeraldine and pernigraniline are fully reduced and oxidized forms of PANI, respectively. They are insulating materials. However, only emeraldine, which is consisted with reduced form and oxidized form, is conducting materials [170].

In application of electric device with PANI, emeraldine form is useful and has been studied frequently. In emeraldine, the electrical conductivity is determined by the degree of oxidation states. The value of  $x$  in Figure 29 can be determined by the degree of oxidation of emeraldine. However, there are not systematic researches the relationship between PANI's electrical conductivity and oxidation states [12, 170, 171]. Here, it will be summarized the story of materialization of PANI through and electrical conductivity of materialized PANI.

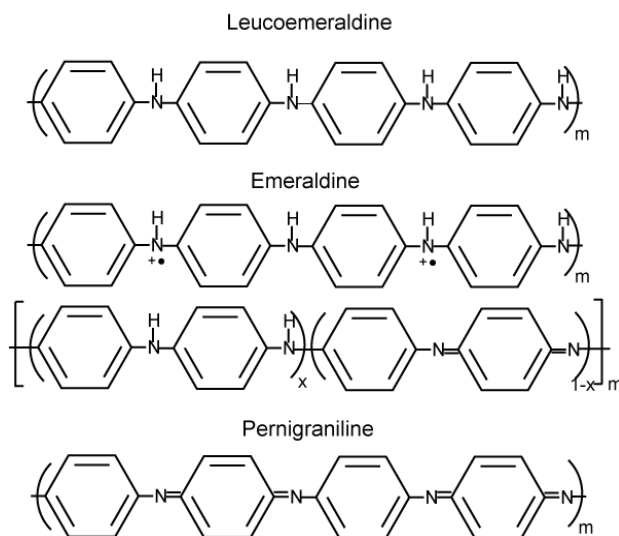


**Figure 29.** The general schemes of polyaniline, Leucoemeraldine and pernigraniline are fully reduced and oxidized forms, respectively. Emeraldine is consisted with reduced and oxidized forms.

Synthesis of polyaniline can be carried out main two methods of chemical polymerization and electrochemical polymerization. In chemical synthesis of PANI, ammonium peroxydisulphate,  $(\text{NH}_4)_2\text{S}_2\text{O}_8$ , which is the most commonly used oxidizing agent, induce the oxidative polymerization of aniline in aqueous acidic media such as aqueous HCl. Oxidation states of polyaniline can be controlled from  $x = 1$  to  $x = 0$ , they are completely reduced and oxidized. The emeraldine oxidation state (in the range from  $x = 1$  to  $x = 0.5$ ) has been developed and verified the conducting property of emeraldine [12, 74, 76]. The chemical polymerization of PANI is carried out three steps of diffusing aniline, adding oxidizing agent and drying in vacuum.

In electrochemical synthesis, aqueous aniline solution with protonic acid such as HCl is polymerized on metal electrode by applied static or cyclic sweeping potential. The electrochemical polymerization setup is consisted with Pt bar as counter electrode, Ag/AgCl reference electrode, Au coating substrate as working electrode and bath with aniline solution. In

that experimental setup, the polymerization of PANI is performed by redox (reduction and oxidation) process from aniline monomer with applied potential. Ionized aniline monomers in aqueous solution form dimeric species and propagate chains stacking aniline monomer to dimeric species, as depicted in Figure 30. The dissolved aniline monomers in aqueous acid transfer two kinds of ionized aniline monomer forms. There are three kinds of transformations for forming dimeric species. According the degree of oxidation potential of dimeric species and aniline monomer, they lose hydrogen and have dangling bond to provide space to stack ionized aniline monomer. That process advances to transfer PANI, eventually [171].

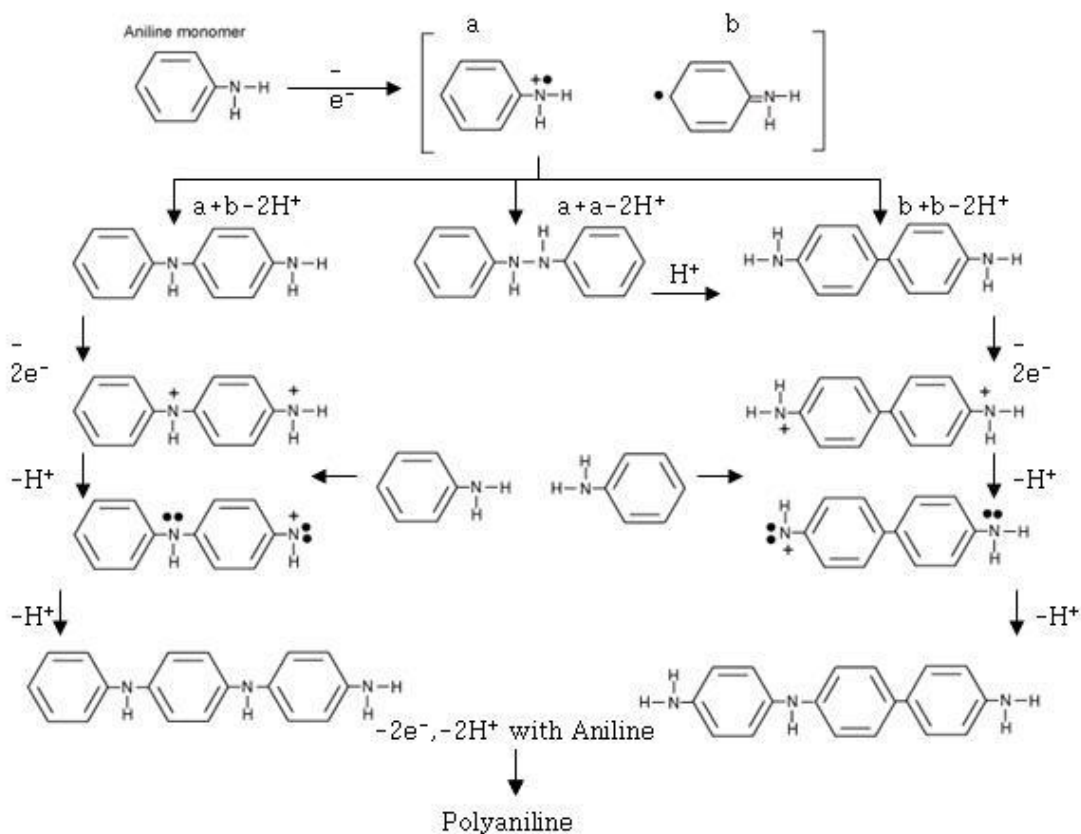


**Figure 30.** The process of polymerization. Aniline monomer transfers into two different kinds of ionized aniline monomer. Ionized aniline monomers combine each other and form dimeric species. Then, polyaniline is synthesized.

In detail, the oxidative polymerization of aniline is mainly carried out by electron loss and de-protonation. Protonation is to provide hydrogen atom to ions, atoms or molecules. De-protonation is the other way to protonation. While protonation and de-protonation, oxidation and reduction processes occur simultaneously in polymerization of PANI. Oxidation and de-protonation in oxidative polymerization provide interim products and PANI from aniline monomer, as shown in Figure 31. Aniline monomers in HCl aqueous solution is ionized on nitrogen or benzene ring by losing electron at applied potential. Ionized aniline monomers make bond each other binding on nitrogen ion and benzene ring. For stabilizing energy of dimeric product, carbon in benzene ring intends to have four covalent bonds and nitrogen transfer to keep tripod structure. This kinematics makes double bonding in benzene ring and nitrogen shift and re-array with de-protonation. Formed dimeric product looks stable. But oxidation and de-protonation continue in HCl aqueous solution. While oxidizing and de-protonating on dimeric products and aniline monomers, they bind each other and make polymerization of aniline. Finally, PANI is resulted in by oxidative polymerization from aniline monomer [76].

The final product of polyaniline is the form of leucoemeraldine form. It is an insulating material. In HCl aqueous solution, the surplus HCl provides the protonic doping in polyaniline. The protonic doping in polyaniline removes electrons from pi bonding of leucoemeraldine. It transfers the leucoemeraldine form to emeraldine form.

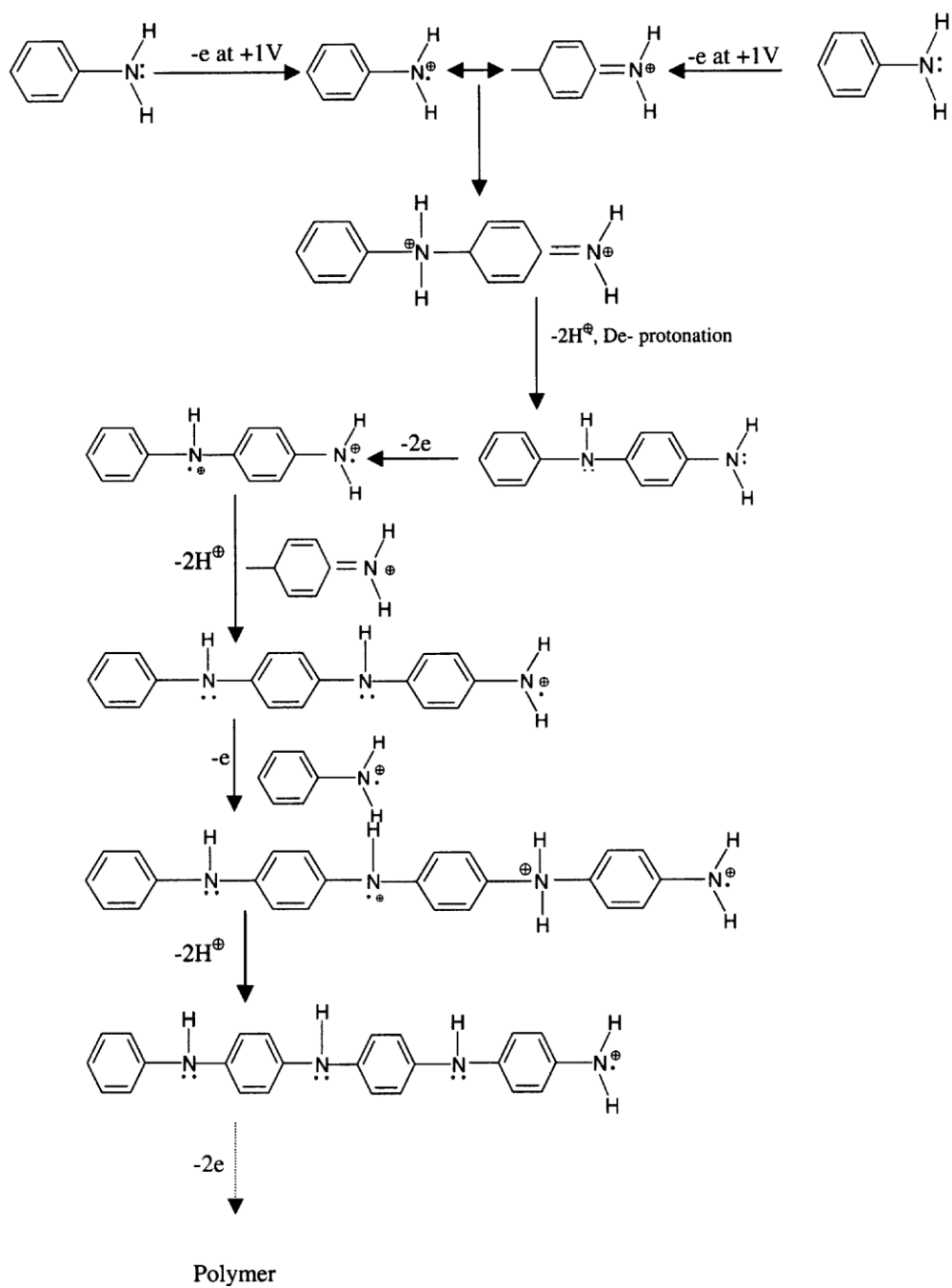


**Figure 31.** Mechanism of oxidative electropolymerization of aniline.

## BIBLIOGRAPHY

- [1] Patolsky, Fernando, and Charles M. Lieber. "Nanowire Nanosensors." *Materials Today* 8, no. 4 (2005): 20-28.
- [2] Liu, Guodong, *et al.* "Aptamer–Nanoparticle Strip Biosensor for Sensitive Detection of Cancer Cells." *Analytical Chemistry* 81, no. 24 (2009): 10013-18.
- [3] Monticone, S., R. Tufeu, and Kanaev. "Complex Nature of the Uv and Visible Fluorescence of Colloidal ZnO Nanoparticles." *The Journal of Physical Chemistry B* 102, no. 16 (1998): 2854-62.
- [4] Ramirez, Arthur P. "Carbon Nanotubes for Science and Technology." *Bell Labs Technical Journal* 10, no. 3 (2005): 171-85.
- [5] Kim, Jun Pyo, *et al.* "Enhancement of Sensitivity and Specificity by Surface Modification of Carbon Nanotubes in Diagnosis of Prostate Cancer Based on Carbon Nanotube Field Effect Transistors." *Biosensors and Bioelectronics* 24, no. 11 (2009): 3372-78.
- [6] Cui, Yi, *et al.* "Nanowire Nanosensors for Highly Sensitive and Selective Detection of Biological and Chemical Species." *Science* 293, no. 5533 (2001): 1289-92.
- [7] Janata, Jiri, and Mira Josowicz. "Conducting Polymers in Electronic Chemical Sensors." *Nat Mater* 2, no. 1 (2003): 19-24.
- [8] Brahim, Sean, *et al.* "Chemical and Biological Sensors Based on Electrochemical Detection Using Conducting Electroactive Polymers." *Microchimica Acta* 143, no. 2 (2003): 123-37.
- [9] Sayed, Wafaa M., and Tousson A. Salem. "Preparation of Polyaniline and Studying Its Electrical Conductivity." *Journal of Applied Polymer Science* 77, no. 8 (2000): 1658-65.

- [10] Meenach, Samantha A, *et al.* "Metal/Conducting-Polymer Composite Nanowires." *Small* 3, no. 2 (2007): 239-43.
- [11] O'Brien, G. A, *et al.* "A Single Polymer Nanowire Photodetector." *Advanced Materials* 18, no. 18 (2006): 2379-83.
- [12] MacDiarmid, Alan G., and Arthur J. Epstein. "Polyanilines: A Novel Class of Conducting Polymers." *Faraday Discussions of the Chemical Society* 88 (1989): 317-32.
- [13] Vivekchand, S. R. C., and *et al.* "Mechanical Properties of Inorganic Nanowire Reinforced Polymer–Matrix Composites." *Nanotechnology* 17, no. 11 (2006): S344.
- [14] Guo, *et al.* "Highly Dispersed Metal Nanoparticles in Porous Anodic Alumina Films Prepared by a Breathing Process of Polyacrylamide Hydrogel." *Chemistry of Materials* 15, no. 22 (2003): 4332-36.
- [15] Okuzaki, Hidenori, and Masayoshi Ishihara. "Spinning and Characterization of Conducting Microfibers." *Macromolecular Rapid Communications* 24, no. 3 (2003): 261-64.
- [16] Pomfret, S. J., *et al.* "Electrical and Mechanical Properties of Polyaniline Fibres Produced by a One-Step Wet Spinning Process." *Polymer* 41, no. 6 (2000): 2265-69.
- [17] Kuo, Chin-Tsou, and Wen-Hong Chiou. "Field-Effect Transistor with Polyaniline Thin Film as Semiconductor." *Synthetic Metals* 88, no. 1 (1997): 23-30.
- [18] Misra, S. C. K., *et al.* "Vacuum-Deposited Metal/Polyaniline Schottky Device." *Applied Physics Letters* 61, no. 10 (1992): 1219-21.
- [19] Curreli, M., *et al.* "Real-Time, Label-Free Detection of Biological Entities Using Nanowire-Based Fets." *IEEE T. Nanotechnol.* 7, no. 6 (2008): 651-67.
- [20] Tang, Juan, *et al.* "Sandwich-Type Conductometric Immunoassay of Alpha-Fetoprotein in Human Serum Using Carbon Nanoparticles as Labels." *Biochem. Eng. J.* 53, no. 2 (2011): 223-28.
- [21] Allen, B. L, P. D Kichambare, and A. Star. "Carbon Nanotube Field-Effect-Transistor-Based Biosensors." *Adv. Mater.* 19, no. 11 (2007): 1439-51.

- [22] Bockrath, Marc, *et al.* "Scanned Conductance Microscopy of Carbon Nanotubes and  $\Lambda$ -DNA." *Nano Lett.* 2, no. 3 (2002): 187-90.
- [23] Gao, Mei, *et al.* "Aligned Coaxial Nanowires of Carbon Nanotubes Sheathed with Conducting Polymers." *Angewandte Chemie International Edition* 39, no. 20 (2000): 3664-67.
- [24] Wang, Joseph. "Nanomaterial-Based Electrochemical Biosensors." *Analyst* 130, no. 4 (2005): 421-26.
- [25] Joo, J., *et al.* "Fabrication and Applications of Conducting Polymer Nanotube, Nanowire, Nanohole, and Double Wall Nanotube." *Synthetic Metals* 153, no. 1-3 (2005): 313-16.
- [26] Dong, B., *et al.* "Fabrication of High-Density, Large-Area Conducting-Polymer Nanostructures." *Advanced Functional Materials* 16, no. 15 (2006): 1937-42.
- [27] Jang, J., and J. H. Oh. "Facile Fabrication of Photochromic Dye-Conducting Polymer Core-Shell Nanomaterials and Their Photoluminescence." *Advanced Materials* 15, no. 12 (2003): 977-80.
- [28] Wang, Joseph, Jinhua Dai, and Travis Yarlagadda. "Carbon Nanotube-Conducting-Polymer Composite Nanowires." *Langmuir* 21, no. 1 (2004): 9-12.
- [29] Chang, Chih-Yang, *et al.* "Electroluminescence from ZnO Nanowire/Polymer Composite P-N Junction." *Applied Physics Letters* 88, no. 17 (2006): 173503-3.
- [30] Li, Yat, *et al.* "Nanowire Electronic and Optoelectronic Devices." *Materials Today* 9, no. 10 (2006): 18-27.
- [31] Banerjee, S., A. Dan, and D. Chakravorty. "Review Synthesis of Conducting Nanowires." *Journal of Materials Science* 37, no. 20 (2002): 4261-71.
- [32] Menke, E. J., *et al.* "Lithographically Patterned Nanowire Electrodeposition." *Nat Mater* 5, no. 11 (2006): 914-19.
- [33] Yun, Minhee, *et al.* "Electrochemically Grown Wires for Individually Addressable Sensor Arrays." *Nano Letters* 4, no. 3 (2004): 419-22.

- [34] Im, Yeonho, *et al.* "Investigation of a Single Pd Nanowire for Use as a Hydrogen Sensor." *Small* 2, no. 3 (2006): 356-58.
- [35] Lee, Innam, *et al.* "Highly Reproducible Single Polyaniline Nanowire Using Electrophoresis Method." *Nano* 3, no. 2 (2008): 75-82.
- [36] Tang, W. H. W., *et al.* "National Academy of Clinical Biochemistry Laboratory Medicine Practice Guidelines: Clinical Utilization of Cardiac Biomarker Testing in Heart Failure." *Circulation* 116, no. 5 (2007): E99-E109.
- [37] Adams, J. E., *et al.* "Cardiac Troponin-I - a Marker with High Specificity for Cardiac Injury." *Circulation* 88, no. 1 (1993): 101-06.
- [38] Etievent, Joseph-Philippe, *et al.* "Use of Cardiac Troponin I as a Marker of Perioperative Myocardial Ischemia." *Ann. Thorac. Surg.* 59, no. 5 (1995): 1192-94.
- [39] NACB WRITING GROUP MEMBERS, *et al.* "National Academy of Clinical Biochemistry and Ifcc Committee for Standardization of Markers of Cardiac Damage Laboratory Medicine Practice Guidelines: Analytical Issues for Biochemical Markers of Acute Coronary Syndromes." *Clin. Chem.* 53, no. 4 (2007): 547-51.
- [40] Masson, J. F., *et al.* "Sensitive and Real-Time Fiber-Optic-Based Surface Plasmon Resonance Sensors for Myoglobin and Cardiac Troponin I." *Talanta* 62, no. 5 (2004): 865-70.
- [41] Adams, JE, 3d, DR Abendschein, and AS Jaffe. "Biochemical Markers of Myocardial Injury. Is Mb Creatine Kinase the Choice for the 1990s?" *Circulation* 88, no. 2 (1993): 750-63.
- [42] Caulum, Meghan M., *et al.* "Detection of Cardiac Biomarkers Using Micellar Electrokinetic Chromatography and a Cleavable Tag Immunoassay." *Anal. Chem.* 79, no. 14 (2007): 5249-56.
- [43] Apple, Fred S., *et al.* "Future Biomarkers for Detection of Ischemia and Risk Stratification in Acute Coronary Syndrome." *Clinical Chemistry* 51, no. 5 (2005): 810-24.
- [44] Darain, Farzana, *et al.* "On-Chip Detection of Myoglobin Based on Fluorescence." *Biosens. Bioelectron.* 24, no. 6 (2009): 1744-50.

- [45] Plowman, T. E., *et al.* "Multiple-Analyte Fluoroimmunoassay Using an Integrated Optical Waveguide Sensor." *Anal. Chem.* 71, no. 19 (1999): 4344-52.
- [46] Masson, Jean-Francois, *et al.* "Quantitative Measurement of Cardiac Markers in Undiluted Serum." *Anal. Chem.* 79, no. 2 (2006): 612-19.
- [47] Kurita, Ryoji, *et al.* "On-Chip Enzyme Immunoassay of a Cardiac Marker Using a Microfluidic Device Combined with a Portable Surface Plasmon Resonance System." *Anal. Chem.* 78, no. 15 (2006): 5525-31.
- [48] Dutra, Rosa Fireman, and Lauro Tatsuo Kubota. "An Spr Immunosensor for Human Cardiac Troponin T Using Specific Binding Avidin to Biotin at Carboxymethyl-dextran-Modified Gold Chip." *Clin. Chim. Acta* 376, no. 1-2 (2007): 114-20.
- [49] Balasubramanian, Kannan. "Challenges in the Use of 1d Nanostructures for on-Chip Biosensing and Diagnostics: A Review." *Biosens. Bioelectron.* 26, no. 4 (2010): 1195-204.
- [50] Gooding, J. Justin. "Nanoscale Biosensors: Significant Advantages over Larger Devices?" *Small* 2, no. 3 (2006): 313-15.
- [51] Ishikawa, Fumiaki N., *et al.* "Label-Free, Electrical Detection of the Sars Virus N-Protein with Nanowire Biosensors Utilizing Antibody Mimics as Capture Probes." *ACS Nano* 3, no. 5 (2009): 1219-24.
- [52] Gao, Zhiqiang, *et al.* "Silicon Nanowire Arrays for Label-Free Detection of DNA." *Anal. Chem.* 79, no. 9 (2007): 3291-97.
- [53] Lin, Tsung-Wu, *et al.* "Label-Free Detection of Protein-Protein Interactions Using a Calmodulin-Modified Nanowire Transistor." *P. Natl. Acad. .Sci.* 107, no. 3 (2010): 1047-52.
- [54] Malhotra, Bansi D., Asha Chaubey, and S. P. Singh. "Prospects of Conducting Polymers in Biosensors." *Analy. Chim. Acta* 578, no. 1 (2006): 59-74.
- [55] Heeger, Peter S., and Alan J. Heeger. "Making Sense of Polymer-Based Biosensors." *P. Natl. Acad. .Sci.* 96, no. 22 (1999): 12219-21.

- [56] Tolani, Sagar, *et al.* "Towards Biosensors Based on Conducting Polymer Nanowires." *Anal. Bioanal. Chem.* 393, no. 4 (2009): 1225-31.
- [57] Gerard, Manju, Asha Chaubey, and B. D. Malhotra. "Application of Conducting Polymers to Biosensors." *Biosens. Bioelectron.* 17, no. 5 (2002): 345-59.
- [58] Adhikari, Basudam, and Sarmishtha Majumdar. "Polymers in Sensor Applications." *Prog. Polym. Sci.* 29, no. 7 (2004): 699-766.
- [59] Ahuja, Tarushee, *et al.* "Biomolecular Immobilization on Conducting Polymers for Biosensing Applications." *Biomaterials* 28, no. 5 (2007): 791-805.
- [60] Briseno, Alejandro L., *et al.* "Introducing Organic Nanowire Transistors." *Mater. Today* 11, no. 4 (2008): 38-47.
- [61] He, Huixin, *et al.* "A Conducting Polymer Nanojunction Switch." *J. Am. Chem. Soc.* 123, no. 31 (2001): 7730-31.
- [62] Arter, Jessica A., *et al.* "Virus-Pedot Nanowires for Biosensing." *Nano Lett.* 10, no. 12 (2010): 4858-62.
- [63] Bangar, Mangesh A., *et al.* "Single Conducting Polymer Nanowire Chemiresistive Label-Free Immunosensor for Cancer Biomarker." *Anal. Chem.* 81, no. 6 (2009): 2168-75.
- [64] Yun, Minhee, *et al.* "Electrochemically Grown Wires for Individually Addressable Sensor Arrays." *Nano Lett.* 4, no. 3 (2004): 419-22.
- [65] Lee, Innam, *et al.* "Highly Sensitive Single Polyaniline Nanowire Biosensor for the Detection of Immunoglobulin G and Myoglobin." *Biosens. Bioelectron.* 26, no. 7 (2011): 3297-302.
- [66] Duffy, David C., *et al.* "Rapid Prototyping of Microfluidic Systems in Poly(Dimethylsiloxane)." *Anal. Chem.* 70, no. 23 (1998): 4974-84.
- [67] Nair, P. R., and M. A. Alam. "Design Considerations of Silicon Nanowire Biosensors." *IEEE T. Electron. Dev.* 54, no. 12 (2007): 3400-08.

- [68] Lee, Innam, *et al.* "Materialization of Single Multicomposite Nanowire: Entrapment of ZnO Nanoparticles in Polyaniline Nanowire." *Nanoscale Research Letters* 6, no. 1 (2011): 393.
- [69] Yushi, Hu, *et al.* "A Single Palladium Nanowire Via Electrophoresis Deposition Used as a Ultrasensitive Hydrogen Sensor." *Nanotechnology, IEEE Transactions on* 7, no. 6 (2008): 693-99.
- [70] Delvaux, Marc, *et al.* "Chemical and Electrochemical Synthesis of Polyaniline Micro- and Nano-Tubules." *Synthetic Metals* 113, no. 3 (2000): 275-80.
- [71] Pouget, J. P., *et al.* "X-Ray Structure of Polyaniline." *Macromolecules* 24, no. 3 (1991): 779-89.
- [72] Huang, Limin, *et al.* "Polyaniline Nanowires by Electropolymerization from Liquid Crystalline Phases." *Journal of Materials Chemistry* 12, no. 2 (2002): 388-91.
- [73] Stejskal, Jaroslav, *et al.* "Polyaniline Prepared in the Presence of Various Acids: A Conductivity Study." *Polymer International* 53, no. 3 (2004): 294-300.
- [74] McManus, Peter M., Richard J. Cushman, and Sze Cheng Yang. "Influence of Oxidation and Protonation on the Electrical Conductivity of Polyaniline." *The Journal of Physical Chemistry* 91, no. 3 (1987): 744-47.
- [75] MacDiarmid, Alan G. "'Synthetic Metals': A Novel Role for Organic Polymers (Nobel Lecture)." *Angewandte Chemie International Edition* 40, no. 14 (2001): 2581-90.
- [76] Hussain, A., and A. Kumar. "Electrochemical Synthesis and Characterization of Chloride Doped Polyaniline." *Bulletin of Materials Science* 26, no. 3 (2003): 329-34.
- [77] Thostenson, Erik T., Zhifeng Ren, and Tsu-Wei Chou. "Advances in the Science and Technology of Carbon Nanotubes and Their Composites: A Review." *Composites Science and Technology* 61, no. 13 (2001): 1899-912.
- [78] Coleman, Jonathan N., *et al.* "Small but Strong: A Review of the Mechanical Properties of Carbon Nanotube-Polymer Composites." *Carbon* 44, no. 9 (2006): 1624-52.
- [79] García, E. J., *et al.* "Fabrication and Nanocompression Testing of Aligned Carbon-Nanotube-Polymer Nanocomposites." *Advanced Materials* 19, no. 16 (2007): 2151-56.

- [80] Stankovich, Sasha, *et al.* "Graphene-Based Composite Materials." *Nature* 442, no. 7100 (2006): 282-86.
- [81] Hong, J. I., *et al.* "Rescaled Electrical Properties of Zn/Low Density Polyethylene Nanocomposites." *Applied Physics Letters* 82, no. 12 (2003): 1956-58.
- [82] Mahamuni, S., *et al.* "Zno Nanoparticles Embedded in Polymeric Matrices." *Nanostructured Materials* 7, no. 6 (1996): 659-66.
- [83] Ajayan, P. M., *et al.* "Single-Walled Carbon Nanotube–Polymer Composites: Strength and Weakness." *Advanced Materials* 12, no. 10 (2000): 750-53.
- [84] Chen, G. Z., *et al.* "Carbon Nanotube and Polypyrrole Composites: Coating and Doping." *Advanced Materials* 12, no. 7 (2000): 522-26.
- [85] Oh, Hyunjoon, and Peter F. Green. "Polymer Chain Dynamics and Glass Transition in Athermal Polymer/Nanoparticle Mixtures." *Nat Mater* 8, no. 2 (2009): 139-43.
- [86] Wu, Tzong-Ming, Yen-Wen Lin, and Chien-Shiun Liao. "Preparation and Characterization of Polyaniline/Multi-Walled Carbon Nanotube Composites." *Carbon* 43, no. 4 (2005): 734-40.
- [87] Wescott, James T., Paul Kung, and Amitesh Maiti. "Conductivity of Carbon Nanotube Polymer Composites." *Applied Physics Letters* 90, no. 3 (2007): 033116-3.
- [88] Olek, M., *et al.* "Nanomechanical Properties of Silica-Coated Multiwall Carbon Nanotubes/poly(Methyl Methacrylate) Composites." *Langmuir* 21, no. 7 (2005): 3146-52.
- [89] Yu, Yijun, *et al.* "Carbon Nanotube/Polyaniline Core-Shell Nanowires Prepared by in Situ Inverse Microemulsion." *Synthetic Metals* 150, no. 3 (2005): 271-77.
- [90] Vivekchand, S. R. C., *et al.* "Electrical Properties of Inorganic Nanowire-Polymer Composites." *Journal of Materials Chemistry* 15, no. 46 (2005): 4922-27.
- [91] Baxter, Jason B., and Charles A. Schmuttenmaer. "Conductivity of ZnO Nanowires, Nanoparticles, and Thin Films Using Time-Resolved Terahertz Spectroscopy†." *The Journal of Physical Chemistry B* 110, no. 50 (2006): 25229-39.

- [92] Schmidt-Mende, Lukas, and Judith L. MacManus-Driscoll. "Zno - Nanostructures, Defects, and Devices." *Materials Today* 10, no. 5 (2007): 40-48.
- [93] Li, Yin-Feng, *et al.* "A Mediator-Free Phenol Biosensor Based on Immobilizing Tyrosinase to Zno Nanoparticles." *Analytical Biochemistry* 349, no. 1 (2006): 33-40.
- [94] Owino, Joseph, *et al.* "Modelling of the Impedimetric Responses of an Aflatoxin B<sub>1</sub> Immunosensor Prepared on an Electrosynthetic Polyaniline Platform." *Analytical and Bioanalytical Chemistry* 388, no. 5 (2007): 1069-74.
- [95] Zhang, Jiaxin, Chen Liu, and Gaoquan Shi. "Raman Spectroscopic Study on the Structural Changes of Polyaniline During Heating and Cooling Processes." *Journal of Applied Polymer Science* 96, no. 3 (2005): 732-39.
- [96] Song, Jinhui, *et al.* "Elastic Property of Vertically Aligned Nanowires." *Nano Letters* 5, no. 10 (2005): 1954-58.
- [97] He, Yongjun. "A Novel Emulsion Route to Sub-Micrometer Polyaniline/Nano-Zno Composite Fibers." *Applied Surface Science* 249, no. 1-4 (2005): 1-6.
- [98] X. Zheng, Z., *et al.* "The Enhanced Photoluminescence of Zinc Oxide and Polyaniline Coaxial Nanowire Arrays in Anodic Oxide Aluminium Membranes." *PhysChemComm* 5, no. 9 (2002): 63-65.
- [99] Wu, H. L., and Philip Phillips. "Polyaniline Is a Random-Dimer Model: A New Transport Mechanism for Conducting Polymers." *Physical Review Letters* 66, no. 10 (1991): 1366.
- [100] Stru'mpler, R., and J. Glatz-Reichenbach. "Feature Article Conducting Polymer Composites." *Journal of Electroceramics* 3, no. 4 (1999): 329-46.
- [101] Capozzi, C. J, and R. A Gerhardt. "Novel Percolation Mechanism in Pmma Matrix Composites Containing Segregated Ito Nanowire Networks." *Advanced Functional Materials* 17, no. 14 (2007): 2515-21.
- [102] Bozano, L., *et al.* "Temperature- and Field-Dependent Electron and Hole Mobilities in Polymer Light-Emitting Diodes." *Applied Physics Letters* 74, no. 8 (1999): 1132-34.

- [103] Matyjaszewski, Krzysztof, and Nicolay V. Tsarevsky. "Nanostructured Functional Materials Prepared by Atom Transfer Radical Polymerization." *Nat Chem* 1, no. 4 (2009): 276-88.
- [104] Tang, Xiaowu, *et al.* "Carbon Nanotube DNA Sensor and Sensing Mechanism." *Nano Letters* 6, no. 8 (2006): 1632-36.
- [105] Luo, Xiliang, *et al.* "Enhancement of a Conducting Polymer-Based Biosensor Using Carbon Nanotube-Doped Polyaniline." *Analytica Chimica Acta* 575, no. 1 (2006): 39-44.
- [106] Adhikari, Basudam, and Sarmishtha Majumdar. "Polymers in Sensor Applications." *Progress in Polymer Science* 29, no. 7 (2004): 699-766.
- [107] Muhammad-Tahir, Zarini, and Evangelyn C. Alocilja. "A Conductometric Biosensor for Biosecurity." *Biosensors and Bioelectronics* 18, no. 5-6 (2003): 813-19.
- [108] Wang, Wayne U., *et al.* "Label-Free Detection of Small-Molecule-Protein Interactions by Using Nanowire Nanosensors." *Proceedings of the National Academy of Sciences of the United States of America* 102, no. 9 (2005): 3208-12.
- [109] Dong, Hua, *et al.* "An in Situ Electrochemical Surface Plasmon Resonance Immunosensor with Polypyrrole Propyllic Acid Film: Comparison between Spr and Electrochemical Responses from Polymer Formation to Protein Immunosensing." *Biosensors and Bioelectronics* 23, no. 7 (2008): 1055-62.
- [110] Ruben, L. N., B. F. Edwards, and J. Rising. "Temperature Variation and the Function of Complement and Antibody of Amphibia." *Cellular and Molecular Life Sciences* 33, no. 11 (1977): 1522-24.
- [111] Balamurugan, Subramanian, *et al.* "Surface Immobilization Methods for Aptamer Diagnostic Applications." *Analytical and Bioanalytical Chemistry* 390, no. 4 (2008): 1009-21.
- [112] Peluso, Paul, *et al.* "Optimizing Antibody Immobilization Strategies for the Construction of Protein Microarrays." *Analytical Biochemistry* 312, no. 2 (2003): 113-24.
- [113] Lo, Young-Seop, *et al.* "Oriented Immobilization of Antibody Fragments on Ni-Decorated Single-Walled Carbon Nanotube Devices." *ACS Nano* 3, no. 11 (2009): 3649-55.

- [114] Sam, S., *et al.* "Semiquantitative Study of the Edc/Nhs Activation of Acid Terminal Groups at Modified Porous Silicon Surfaces." *Langmuir* 26, no. 2 (2009): 809-14.
- [115] Gao, Yuan, and Ilias Kyratzis. "Covalent Immobilization of Proteins on Carbon Nanotubes Using the Cross-Linker 1-Ethyl-3-(3-Dimethylaminopropyl)Carbodiimide—a Critical Assessment." *Bioconjugate Chemistry* 19, no. 10 (2008): 1945-50.
- [116] Ban, N, *et al.* "Crystal Structure of an Idiotype-Anti-Idiotype Fab Complex." *Proceedings of the National Academy of Sciences* 91, no. 5 (1994): 1604-08.
- [117] Murphy, R. M., *et al.* "Size and Structure of Antigen-Antibody Complexes. Electron Microscopy and Light Scattering Studies." *Biophysical Journal* 54, no. 1 (1988): 45-56.
- [118] Kwon, Oh Seok, Seon Joo Park, and Jyongsik Jang. "A High-Performance Vegf Aptamer Functionalized Polypyrrole Nanotube Biosensor." *Biomaterials* 31, no. 17 (2010): 4740-47.
- [119] Hsiao, Cheng-Yun, *et al.* "Novel Poly-Silicon Nanowire Field Effect Transistor for Biosensing Application." *Biosensors and Bioelectronics* 24, no. 5 (2009): 1223-29.
- [120] Prina-Mello, Adriele, *et al.* "Comparative Flow Cytometric Analysis of Immunofunctionalized Nanowire and Nanoparticle Signatures." *Small* 6, no. 2 (2010): 247-55.
- [121] Katz, Eugenii, and Itamar Willner. "Integrated Nanoparticle–Biomolecule Hybrid Systems: Synthesis, Properties, and Applications." *Angewandte Chemie International Edition* 43, no. 45 (2004): 6042-108.
- [122] Luo, Xiliang, *et al.* "Ultrasensitive Protein Detection Using an Aptamer-Functionalized Single Polyaniline Nanowire." *Chem. Commun.* 47, no. 22 (2011): 6368-70.
- [123] Painter, Paul C., and J. L. Koenig. "Raman Spectroscopic Study of the Structure of Antibodies." *Biopolymers* 14, no. 3 (1975): 457-68.
- [124] Danczyk, R., *et al.* "Comparison of Antibody Functionality Using Different Immobilization Methods." *Biotechnology and Bioengineering* 84, no. 2 (2003): 215-23.

- [125] Herrwerth, S., *et al.* "Covalent Coupling of Antibodies to Self-Assembled Monolayers of Carboxy-Functionalized Poly(Ethylene Glycol): Protein Resistance and Specific Binding of Biomolecules†." *Langmuir* 19, no. 5 (2003): 1880-87.
- [126] Lee, Woonchang, *et al.* "Fabrication of Self-Assembled Protein a Monolayer and Its Application as an Immunosensor." *Biosensors and Bioelectronics* 19, no. 3 (2003): 185-92.
- [127] Bangar, Mangesh A., *et al.* "Single Conducting Polymer Nanowire Chemiresistive Label-Free Immunosensor for Cancer Biomarker." *Analytical Chemistry* 81, no. 6 (2009): 2168-75.
- [128] Tolani, Sagar, *et al.* "Towards Biosensors Based on Conducting Polymer Nanowires." *Analytical and Bioanalytical Chemistry* 393, no. 4 (2009): 1225-31.
- [129] García-Aljaro, Cristina, *et al.* "Conducting Polymer Nanowire-Based Chemiresistive Biosensor for the Detection of Bacterial Spores." *Biosensors and Bioelectronics* 25, no. 10 (2010): 2309-12.
- [130] Lei, B., *et al.* "Tuning Electronic Properties of  $\text{In}_2\text{O}_3$  Nanowires by Doping Control." *Applied Physics A: Materials Science & Processing* 79, no. 3 (2004): 439-42.
- [131] Gao, Xuan P. A., Gengfeng Zheng, and Charles M. Lieber. "Subthreshold Regime Has the Optimal Sensitivity for Nanowire Fet Biosensors." *Nano Letters* 10, no. 2 (2009): 547-52.
- [132] Mizel, SB, and D Mizel. "Purification to Apparent Homogeneity of Murine Interleukin 1." *J. Immunol.* 126, no. 3 (1981): 834-37.
- [133] Peronnet, Estelle, *et al.* "Isoelectric Point Determination of Cardiac Troponin I Forms Present in Plasma from Patients with Myocardial Infarction." *Clin. Chim. Acta* 377, no. 1-2 (2007): 243-47.
- [134] Wevers, R. A., R. J. Wolters, and J. B. J. Soons. "Isoelectric Focusing and Hybridisation Experiments on Creatine Kinase (Ec 2.7.3.2)." *Clin. Chim. Acta* 78, no. 2 (1977): 271-76.
- [135] Huang, S., *et al.* "Sequential Detection of Salmonella Typhimurium and Bacillus Anthracis Spores Using Magnetoelastic Biosensors." *Biosen. Bioelectron.* 24, no. 6 (2009): 1730-36.

- [136] Mire-Sluis, Anthony R., *et al.* "Recommendations for the Design and Optimization of Immunoassays Used in the Detection of Host Antibodies against Biotechnology Products." *J. Immunol. Methods* 289, no. 1-2 (2004): 1-16.
- [137] Maraldo, David, and Raj Mutharasan. "Optimization of Antibody Immobilization for Sensing Using Piezoelectrically Excited-Millimeter-Sized Cantilever (Pemc) Sensors." *Sensor. Actuat. B-Chem.* 123, no. 1 (2007): 474-79.
- [138] Nyamsi Hendji, A. M., *et al.* "Enzyme Biosensor Based on a Micromachined Interdigitated Conductometric Transducer: Application to the Detection of Urea, Glucose, Acetyl- Andbutyrylcholine Chlorides." *Sensor. Actuat. B-Chem.* 21, no. 2 (1994): 123-29.
- [139] Rowe, Chris A., *et al.* "Array Biosensor for Simultaneous Identification of Bacterial, Viral, and Protein Analytes." *Anal. Chem.* 71, no. 17 (1999): 3846-52.
- [140] Elfström, Niklas, *et al.* "Surface Charge Sensitivity of Silicon Nanowires: Size Dependence." *Nano Lett.* 7, no. 9 (2007): 2608-12.
- [141] Rini, JM, U Schulze-Gahmen, and IA Wilson. "Structural Evidence for Induced Fit as a Mechanism for Antibody-Antigen Recognition." *Science* 255, no. 5047 (1992): 959-65.
- [142] Sheriff, S, *et al.* "Three-Dimensional Structure of an Antibody-Antigen Complex." *P. Natl. Acad. .Sci.* 84, no. 22 (1987): 8075-79.
- [143] Stern, Eric, *et al.* "Importance of the Debye Screening Length on Nanowire Field Effect Transistor Sensors." *Nano Letters* 7, no. 11 (2007): 3405-09.
- [144] Heller, Iddo, *et al.* "Identifying the Mechanism of Biosensing with Carbon Nanotube Transistors." *Nano Letters* 8, no. 2 (2007): 591-95.
- [145] Liu, Haiqing, *et al.* "Polymeric Nanowire Chemical Sensor." *Nano Letters* 4, no. 4 (2004): 671-75.
- [146] Wink, Th, *et al.* "Self-Assembled Monolayers for Biosensors." *Analyst* 122, no. 4 (1997): 43R-50R.
- [147] Davies, D R, S Sheriff, and E A Padlan. "Antibody-Antigen Complexes." *Journal of Biological Chemistry* 263, no. 22 (1988): 10541-4.

- [148] Sheriff, S, *et al.* "Three-Dimensional Structure of an Antibody-Antigen Complex." *Proceedings of the National Academy of Sciences* 84, no. 22 (1987): 8075-79.
- [149] Prost, Werner, *et al.* "Modeling the Carrier Mobility in Nanowire Channel Fet." *MRS Online Proceedings Library* 1017 (2007): null-null.
- [150] Ho-Young, Cha, and *et al.* "Fabrication and Characterization of Pre-Aligned Gallium Nitride Nanowire Field-Effect Transistors." *Nanotechnology* 17, no. 5 (2006): 1264.
- [151] Greytak, A. "Growth and Transport Properties of Complementary Germanium Nanowire Field-Effect Transistors." *Appl. Phys. Lett.* 84, no. 21 (2004): 4176.
- [152] Horowitz, Gilles. "Organic Field-Effect Transistors." *Advanced Materials* 10, no. 5 (1998): 365-77.
- [153] Wang, D. "Germanium Nanowire Field-Effect Transistors with SiO<sub>2</sub> and High- $\kappa$  HfO<sub>2</sub> Gate Dielectrics." *Appl. Phys. Lett.* 83, no. 12 (2003): 2432.
- [154] Kuo, Chin-Tsou, *et al.* "Field-Effect Transistor with the Water-Soluble Self-Acid-Doped Polyaniline Thin Films as Semiconductor." *Synthetic Metals* 93, no. 3 (1998): 155-60.
- [155] Katz, O., and *et al.* "Charge Carrier Mobility in Field Effect Transistors: Analysis of Capacitance-Conductance Measurements." *Semiconductor Science and Technology* 20, no. 1 (2005): 90.
- [156] Babel, Amit, *et al.* "Electrospun Nanofibers of Blends of Conjugated Polymers: Morphology, Optical Properties, and Field-Effect Transistors." *Macromolecules* 38, no. 11 (2005): 4705-11.
- [157] Hahm, Jong-in, and Charles M. Lieber. "Direct Ultrasensitive Electrical Detection of DNA and DNA Sequence Variations Using Nanowire Nanosensors." *Nano Letters* 4, no. 1 (2003): 51-54.
- [158] Hofmann, Denis, *et al.* "Prognostic Value of Serum Myoglobin in Patients after Cardiac Surgery." *Journal of Anesthesia* 21, no. 3 (2007): 304-10.

- [159] Fond, Amanda M., *et al.* "Preferential Noncovalent Immunoglobulin G Adsorption onto Hydrophobic Segments of Multi-Functional Metallic Nanowires." *Journal of Photochemistry and Photobiology A: Chemistry* 186, no. 1 (2007): 57-64.
- [160] Darain, Farzana, *et al.* "On-Chip Detection of Myoglobin Based on Fluorescence." *Biosensors and Bioelectronics* 24, no. 6 (2009): 1744-50.
- [161] McLaurin, Mary D., *et al.* "Cardiac Troponin I, Cardiac Troponin T, and Creatine Kinase Mb in Dialysis Patients without Ischemic Heart Disease: Evidence of Cardiac Troponin T Expression in Skeletal Muscle." *Clin Chem* 43, no. 6 (1997): 976-82.
- [162] Guo-Jun, Zhang, *et al.* "Highly Sensitive and Selective Label-Free Detection of Cardiac Biomarkers in Blood Serum with Silicon Nanowire Biosensors." Paper presented at the Electron Devices Meeting (IEDM), 2009 IEEE International, 7-9 Dec. 2009 2009.
- [163] Wang, Thomas J., *et al.* "Impact of Age and Sex on Plasma Natriuretic Peptide Levels in Healthy Adults." *The American journal of cardiology* 90, no. 3 (2002): 254-58.
- [164] Matsuura, Hiroaki, *et al.* "Electrochemical Enzyme Immunoassay of a Peptide Hormone at Picomolar Levels." *Analytical Chemistry* 77, no. 13 (2005): 4235-40.
- [165] Star, Alexander, *et al.* "Electronic Detection of Specific Protein Binding Using Nanotube Fet Devices." *Nano Letters* 3, no. 4 (2003): 459-63.
- [166] Turner, A.P.F., I. Karube, and G.S. Wilson. *Biosensors: Fundamentals and Applications*: Oxford University Press, 1987.
- [167] Bergveld, Piet. "Development, Operation, and Application of the Ion-Sensitive Field-Effect Transistor as a Tool for Electrophysiology." *Biomedical Engineering, IEEE Transactions on BME-19*, no. 5 (1972): 342-51.
- [168] Neumann, T., *et al.* "Spr-Based Fragment Screening: Advantages and Applications." *Current Topics in Medicinal Chemistry* 7, no. 16 (2007): 1630-42.
- [169] Nyamsi Hendji, A. M., *et al.* "Enzyme Biosensor Based on a Micromachined Interdigitated Conductometric Transducer: Application to the Detection of Urea, Glucose, Acetyl- Andbutyrylcholine Chlodes." *Sensors and Actuators B: Chemical* 21, no. 2 (1994): 123-29.

- [170] Alan G, MacDiarmid. "Polyaniline and Polypyrrole: Where Are We Headed?" *Synthetic Metals* 84, no. 1-3 (1997): 27-34.
- [171] Gospodinova, N., and L. Terlemezyan. "Conducting Polymers Prepared by Oxidative Polymerization: Polyaniline." *Progress in Polymer Science* 23, no. 8 (1998): 1443-84.